IMPROVING WIND VELOCITY MEASUREMENTS ON SHIPS

Industrial Training year at the James Rennell Centre for Ocean Circulation

12 Aug 1993 - 9 Sept 1994

B. I. Moat

1994

Gamma House
Chilworth Research Park
Chilworth
Southampton
S01 7NS
Tele: (0703) 766184
Facsimile: (0703) 767507

ABSTRACT

Accurate wind speed measurements are required from Research vessels for satellite validation and climate research, but the results have been shown to differ significantly from ship to ship. This report discusses an attempt to find the cause of the discrepancies and, if possible, to correct for them.

A study on wind speed errors was undertaken to study the airflow distortions around a ship using numerical modelling. Simple potential models were used to study the airflow distortions around an idealised cylindrical mast to find the effect of the ship's mast on anemometers positioned close to it. The wake potential model was applied to wind speed data from R.R.S. Charles Darwin cruise 43 and partially corrected the wind speed measurements from anemometers at 5 to 6 mast diameters. The airflow distortions over the ship's hull and superstructure were then investigated to try to account for these remaining wind speed errors. Wind speed errors were calculated using a Computational Fluid Dynamics (C.F.D.) package and computer generated ship models. The study is in a preliminary stage and the C.F.D. package has been validated against a wind tunnel study for the C.S.S. Dawson and wind speed corrections agree to within 2 %.

IMPROVING WIND VELOCITY MEASUREMENTS ON SHIPS

1. INTRODUCTION

Accurate wind measurements at sea are required for satellite validation and climate research. The anemometers on Natural Environment Research Council, N.E.R.C., ships are very accurate, but the results differ from ship to ship. For example wind speed differences of up to 10 % appear in the results from the R.R.S. Charles Darwin when compared with the R.R.S. Discovery. The Meteorology team at the James Rennell Centre[1] also uses data from other sources, such as the French Research ship, the Suroit, and the Ocean Weather Ship Cumulus, both of which display possible systematic errors in wind speed. Section 2 discuses the quality of the data sets used in this study.

There are two possible causes of error in wind speed measurements; 1) the anemometer itself, and 2) disturbance of the flow of air at the anemometer site. The first of these was investigated by testing a typical anemometer in a wind tunnel (section 3). This approach could not be used to study the airflow since it would be too time consuming and extremely costly to build and wind tunnel test a model of every ship. Instead numerical modelling was used and the airflow distortions treated in two parts. In section 4, the airflow disturbance caused by the proximity of the ships mast to the anemometer is investigated using two potential flow models applied to an idealised mast (an infinitely long cylinder). The problem has been studied by many people such as (Kondo and Naito, 1972) and (Dabberdt, 1968). They compare their wind speed measurements to a simple potential model (section 4.2), and not to the realistic wake model of (Wucknitz, 1977), (section 4.3). The second cause of air flow disturbance is the effect of the ship itself, e.g. the air may lifted or accelerated over the bows of the ship, or may be blocked by the ships superstructure. This approach has been investigated using two dimensional numerical modelling by (Kahma and Lepparanta, 1981) on the Research Vessel Aranda and wind speed estimates where made to within 5% of those measured by an accurate bowsprit anemometer. This complex airflow problem is examined in greater detail using a three dimensional commercial Computational Fluid Dynamics package (section 5).

2. QUALITY CONTROL OF WIND SPEED DATA

2.1 Introduction

Wind speed data has been obtained from three six week R.R.S.. Discovery cruises, two cruises on R.R.S. Charles Darwin and one cruise on Le Suroit. All of these cruises used the fast

[1] A summary of the work of the James Rennell Centre is attached in Appendix A.

sampling Solent Sonic anemometer, plus other standard meteorological instrumentation, which are mounted on the foremast, which is situated in the bows of the ship. The data from R.R.S. Discovery is considered to be the best since the anemometer site has the best exposure, and because more cruises have been performed. The measurements made are therefore used as the standard in comparisons with other ships.

All research cruise data have already been processed. Figure 1 shows friction velocity, U* (the square root of wind stress), vs wind speed normalised to 10 m and reveal a possible 5% underestimate of wind speed by Le Suroit and an over estimate of 10% by R.R.S. Charles Darwin in comparison, to our R.R.S. Discovery standard. The friction velocity, U*, can be measured very accurately which leads us to believe that the errors occurring are due to errors in wind speed.

The O.W.S. Cumulus is situated at station LIMA (57 N 20 W), in the North Atlantic, which it holds four weeks in every five returning to Greenoch in Scotland to refuel and take on supplies. The Meteorological team has had instrumentation on board since 1987 which logs wind speed and direction via a Solent Sonic Anemometer and a Young Propeller Vane, pressure, position via a G.P.S. receiver and heading via a flux gate compass, and sea state information from a Ship Borne Wave Recorder. Cumulus experiences all weathers and logs data in two situations; 1) in moderate conditions it drifts with the port side exposed to the wind, and 2) in high wind speeds it 'hoves-to', were it steams slowly into the developing seas to ride out storms.

2.2 Method

The O.W.S. Cumulus data sets are received every month and are processed, checked and archived for future use. The processing is a standard procedure taken from the Cumulus data transfer/Processing instructions, refer to (Birch et al., 1993).

2.3 Quality of Data sets

Figure 2 shows friction velocity vs wind speed normalised to 10m for when Cumulus is drifting and hove to and it can clearly be seen that discrepancies of up to 30 % in wind speed occur. Although a lot of the Cumulus data is of lower quality than the research ships, it will be useful in future for testing the C.F.D. package, since the wind speed errors are larger than those experienced on other research ships. The Cumulus data set is also unique as measurements have been taken almost continuously at the same position for over seven years. In comparison to the data sets made on other research ships we have a large archived store of data with slightly larger wind speed errors, which will be reduced by the C.F.D. study, section 5, producing a large accurate data set.

Results from the wake potential model, sections 4.3, and wind speed errors found from the C.F.D. study of the C.S.S. Dawson, section 5, have been used in a paper, entitled 'The accuracy of wind observations from ships[2] , written for the COADS Winds Workshop presented in Kiel between

---

[2] Taylor, P. K., E. C. Kent, M. J. Yelland and B. I. Moat, 1994: The accuracy of wind observations from ships. *COADS Winds Workshop*, Kiel. Is included in Appendix C.

31st May till 2nd June 1994. The paper covers the accuracy of the O.W.S. Cumulus observations and the use of the O.W.S. Cumulus to validate wind estimates from the VOS Observing Programme - North Atlantic (VSOP-NA).

3. WIND TUNNEL STUDY OF AN ANEMOMETER

3.1 Introduction

All James Rennell Centre Cruises have a Solent Sonic Fast sampling Anemometer logging data. The Sonic anemometer is very accurate, around ± 1.5 % error for wind speeds < 30 m/s, but it is believed that the anemometer is designed to be mounted on stable platforms as the vertical axis calibration is not as thorough as the horizontal axis calibration. It was therefore decided to perform a wind tunnel study on a Solent Sonic anemometer that would soon be deployed on a Meteorological buoy in an experiment off the Welsh coast.

The anemometer was tested in the wind tunnel of Southampton University using a bracket that allowed the anemometer to be moved to all headings and elevations that could be encountered on a ship or buoy. The Solent sonic produced velocity readings in the x, y and z directions for each 10 degree angle and elevation over a 30 second period.

3.2 Method

This logged data was transferred onto the James Rennell Centre Sun network where it was converted into Pexec format which allows it to be easily manipulated using a library of over 200 Fortran routines. Areas of spurious data occurred as the anemometer was moved in the wind tunnel and these where removed by taking out data of a large standard deviation. The clean data was then averaged over each orientation for each elevation producing wind speed and directional errors.

3.3 Results

The results from the wind tunnel studies showed that the Solent Sonic anemometer was defective and was sent back to the suppliers to be re-calibrated.

4. AIR FLOW DISTORTIONS AROUND CYLINDRICAL MASTS

4.1 Introduction

It is well known that anemometers mounted close to towers or cylindrical mast can produce inaccuracies in wind speed measurements, therefore the position of an anemometer relative to this obstruction is critical in producing accurate wind speed measurements. R.R.S. Charles Darwin cruise 43 was undertaken to accurately measure wind stress using a number of fast sampling anemometers. The comparison of the wind speeds, (Yelland et al., 1991) , shows up discrepancies, some of which depend upon relative wind direction. This implies that the anemometers may feel the influence of the mast. The same problem has influenced the Royal Navy to undertake air flow trials on aircraft carriers. A large wind speed, or especially directional, error could mean that during night operations an aircraft could be launched from the wrong side of the ship causing the aircraft engine/transmission system to be over torqued. Increasing engine maintenance time, wasting fuel and increasing cost Wind speed errors were calculated from measurements made at an anemometer site and compared to a reference anemometer mounted on a 60 meter mast in an exposed position. These wind speed errors are available to us and could be used to validate the following two models.

The following section investigates the airflow distortion around an idealised cylindrical mast using two numerical models. The models are developed to show if wind speed errors can be explained by the air flow distortions found around the mast they are mounted on or are due to other effects such as the ships hull and superstructure. The two models developed are; 1) a simple potential flow model found in most fluid dynamics books (section 4.2), and 2) a realistic wake potential model built up from single complex equation, section 4.3 equation 11, given by (Wucknitz, 1977). The first model is too simple to model physical conditions and is used to form the basis of the second more relevant wake model. Section 4.4 applies wind speed corrections from the potential flow models to wind speed measurements made by R.R.S. Charles Darwin cruise 43.

4.2 Simple Potential Model

4.2.1 Introduction

This is a purely theoretical model of an ideal fluid which has zero viscosity. In this case the velocity potential ϕ and the stream function φ are defined as $\nabla^2\phi = 0$ and $\nabla^2\varphi = 0$ where ∇^2 is the Laplacian operator.

The flow field is symmetrical on either side of the cylindrical mast and it agrees closely with a flow of Reynolds number $Re < 10^{-1}$ and cylinder drag coefficient of about 50, which is entirely due to skin friction. This is known as a creeping flow and as the inertia forces are negligible the flow remains attached over the entire cylinder surface. Such flows occur in, for example, water seepage through a porous medium around a pipe.

It is hoped that some physical insight can be gained from this simple model with respect to the more complicated viscous flow.

4.2.2 The model

Velocity, direction and pressure are calculated in polar co-ordinates from a Cartesian grid of resolution (0.1,0.1) based on a mast diameter of one unit, which gave 10,251 grid points. The equations where built up using Pexec routines. Each addition and multiplication had to be applied to the grid points using a single Pexec routine. This was very slow, but gave an insight into the development of the more complex potential model.

The model is developed from a complex potential in three stages; 1) the velocity potential and stream function, 2) the velocity field, and 3) the pressure field.

As is well-known (e.g.. (Ditsworth and Allen, 1972)), the solution for the case of a static infinitely long cylinder of radius r_0 with undisturbed free stream velocity V_∞ is given by the complex potential

$$F(z) = V_\infty\left[z + \frac{r_0}{z}\right] \text{ where } z = x + iy \qquad (1)$$

$$\therefore F(z) = V_\infty\left[\text{Cos}\theta\left(r + \frac{r_0^2}{r}\right) + i\text{Sin}\theta\left(r - \frac{r_0^2}{r}\right)\right] \qquad (2)$$

which leads to a velocity potential of

$$\phi = V_\infty\left(\text{Cos}\theta\left(r + \frac{r_0^2}{r}\right)\right) \qquad (3)$$

and a stream function of

$$\varphi = V_\infty\left(\text{Sin}\theta\left(r - \frac{r_0^2}{r}\right)\right) \qquad (4)$$

see figure 3 which shows the equipotentials for velocity and stream lines.

where

V_∞ = free stream velocity. φ = stream function.

r = distance from cylinder centre. ϕ = velocity potential.

θ = angle to the flow. r_0 = mast radius.

refer to figure 5 which shows the model variables.

The velocities normal and tangential to the cylinder are calculated from the gradient of the velocity potential

$$V_n = \frac{\partial \phi}{\partial r} = V_\infty \mathrm{Cos}\theta\left(1 - \frac{r_0^2}{r^2}\right) \tag{5}$$

$$V_t = \frac{1}{r}\frac{\partial \phi}{\partial \theta} = -V_\infty \mathrm{Sin}\theta\left(1 + \frac{r_0^2}{r^2}\right) \tag{6}$$

and resolving the velocity into x and y components gives

$$V_x = V_\infty\left[\mathrm{Cos}^2\theta\left(1 - \frac{r_0^2}{r^2}\right) + \mathrm{Sin}^2\theta\left(1 + \frac{r_0^2}{r^2}\right)\right] \tag{7}$$

$$V_y = V_\infty\left[\mathrm{Sin}\theta\mathrm{Cos}\theta\left(1 - \frac{r_0^2}{r^2}\right) - \mathrm{Sin}\theta\mathrm{Cos}\theta\left(1 + \frac{r_0^2}{r^2}\right)\right] \tag{8}$$

$$Vel_C = V_\infty\sqrt{V_x^2 + V_y^2} \tag{9}$$

This model predicts that the flow is decreased both upwind and downwind of the cylinder. To either side the flow is increased, with a maximum occurring at 90 degrees to the free flow direction. On the cylinder surface at θ = 90 degrees the free stream velocity is doubled, decreasing to 4 % error at 5 mast radii and then decreasing to less than 1% at 10 mast radii. The percentage change from the free stream velocity is shown in figure 7 and the directional errors are shown in figure 9.

The ideal position for an anemometer in this model is at approximately θ = 45 and 135 degrees, where the calculated velocity is equal to the undisturbed free stream velocity.

The pressure field can be calculated from Bernoulli's equation.

$$\frac{P}{\rho} + \Phi_B + \frac{V^2}{2} - \frac{\partial \phi}{\partial t} = g(t)$$

Body forces (Φ_B) are neglected, $\frac{\partial \phi}{\partial t}$ = 0 for a constant velocity field and $g(t)$ becomes a constant.

ρ = density

P = pressure

V= Velocity

Leading to

$$P = P_\infty - \rho\frac{V_\infty^2}{2}\left[\frac{2r_0^2}{r^2}\left(\mathrm{Sin}^2\theta - \mathrm{Cos}^2\theta\right) + \frac{r_0^4}{r^4}\right] \tag{10}$$

where

P_∞ = Pressure at large distances from cylindrical mast

It can be shown that the flow has two stagnation points, where the velocity is zero, which are located on the surface of the cylinder upwind at θ = 180 degrees and downstream at θ = 0 degrees. These stagnation points correspond to maximum in the pressure field, whilst the minimum pressure is found on the cylinder surface at θ = 90 where the free stream velocity is doubled.

4.2.3 Summary

A velocity maximum is found at 90 degrees to the flow and a velocity decrease is shown upwind and downwind of the cylindrical body. The region of zero velocity error, or the ideal anemometer position, is located at 45 and 135 degrees to the flow. The model doesn't give a realistic interpretation of a physical atmospheric flow, because it uses a high drag coefficient (giving a very low Reynolds number) and is laminar everywhere within the flow.. Therefore the better airflow model will be the realistic turbulent wake region model described in section 4.3.

4.3 Wake Potential Model

4.3.1 Introduction

The following model was developed from a complex potential given by (Wucknitz, 1977).. It uses a point source near the centre of the mast and a point sink at a distance a downstream of the mast. This model differs from the simple potential model in that a wake is developed down stream of the mast, for a given cylindrical drag coefficient. This gives a more realistic interpretation of a flow for an atmospheric Reynolds number ($10^4 < Re < 10^7$). A theoretical treatment of the turbulent flow around a two dimensional cylindrical bodies has been given by (Hunt, 1973) and (Parkinson and Jandali, 1970).

4.3.2 The model

The velocity, direction and pressure fields are calculated and based on the same method as the simple potential model, except it is only possible to calculate the fields outside the mast and wake region. The model excludes all calculations within the wake because this region is known to exhibit turbulence and vortex shedding, which is chaotic in behaviour. The calculations are performed on the same grid and using the same resolution as the simple potential model. The equations where found too large to be manipulated using Pexec routines so both sets of model equations where written into a single Pexec routine giving repeated use and the same visualisation capabilities.

The only equations that exists for this model are the complex potential, equation 11, from (Wucknitz, 1977), the approximation to the mast and wake body, equation 14, and the relationship

$a = \frac{R}{2}$ which are both taken from (Wucknitz, 1980). The remaining equations have been developed during the duration of this project.

The complex potential for this model is

$$F(z) = V_\infty\left[z + \frac{Y_1}{\pi}\ln(z) - \frac{Y_2}{\pi}\ln(z-a)\right] \qquad (11)$$

$$= V_\infty\left[\phi + i\varphi\right]$$

where $z = x + iy$

which leads to a Velocity potential of

$$\phi = V_\infty\left[r_1 Cos\theta_1 + \frac{Y_1}{\pi}\ln(r_1) - \frac{Y_2}{\pi}\ln(r_3)\right] \qquad (12)$$

and a Stream Function of

$$\varphi = V_\infty\left[r_1 Sin\theta_1 + \frac{Y_1}{\pi}\theta_1 - \frac{Y_2}{\pi}\theta_3\right] \qquad (13)$$

see figure 4 which shows the equipotentials for velocity and stream lines.

where

$$r_1^2 = x^2 + y^2$$

$$\theta_1 = Tan^{-1}\left(\frac{y}{x}\right)$$

$$r_3^2 = (x-a)^2 + y^2 = r_1^2 + a(a - 2r_1 Cos\theta_1)$$

$$\theta_3 = Tan^{-1}\left(\frac{y}{x-a}\right) = Tan^{-1}\left(\frac{r_1 Sin\theta_1}{r_1 Cos\theta_1 - a}\right)$$

Source intensity = $2V_\infty Y_1$ Sink intensity = $2V_\infty Y_2$ where $Y_1 > Y_2$

Refer to figure 6 which shows the model variables.

A better approximation to the mast and wake body is given by (Wucknitz, 1980) where

$$\varphi = Y_1 - Y_2 = R.C_D \qquad (14)$$

Y_1 and Y_2 are calculated from solving

$$\varphi = V_\infty\left[r_1 Sin\theta_1 + \frac{Y_1}{\pi}\theta_1 - \frac{Y_2}{\pi}\theta_3\right] = 0 \qquad (15)$$

substituting $Y_1 = R.C_D + Y_2$ from equation 14

gives

$$Y_2 = \frac{-\left(R.C_D.\theta_1 + \pi.r_1 Sin\left(\theta_1\right)\right)}{\left(\theta_1 - \theta_3\right)} \qquad (16)$$

Which gives a formula for calculating the value Y_2 along the contour $\varphi = R.C_D$.

The velocities normal and tangential to the cylinder are calculated from the gradient of the velocity potential

$$V_n = \frac{\partial\phi}{\partial r_1} = V_\infty\left[Cos\theta_1 + \frac{Y_1}{\pi r_1} - \frac{Y_2\left(r_1 - aCos\theta_1\right)}{\pi r_3^2}\right] \qquad (17)$$

$$V_t = \frac{1}{r_1}\frac{\partial\phi}{\partial\theta_1} = -V_\infty\left[Sin\theta_1\left(1 + \frac{Y_2 a}{\pi r_3^2}\right)\right] \qquad (18)$$

The source sink separation $a = \frac{R}{2}$ moves the centre of approximated cylinder downstream a distance a_0 (where $a_0 \propto C_D$) away from the origin of the co-ordinate system. To reduce this error in the velocity field the polar co-ordinate system must be calculated from this approximated mast centre using

$$V_n = \frac{\partial\phi}{\partial r_2} = V_\infty\left[Cos\theta_2 + \frac{Y_1}{\pi r_2} - \frac{Y_2\left(r_2 - aCos\theta_2\right)}{\pi r_3^2}\right] \qquad (19)$$

$$V_t = \frac{1}{r_2}\frac{\partial\phi}{\partial\theta_2} = -V_\infty\left[Sin\theta_2\left(1 + \frac{Y_2 a}{\pi r_3^2}\right)\right] \qquad (20)$$

where

$$r_2^2 = \left(x - a_0\right)^2 + y^2 = r_1^2 + a_0\left(a_0 - 2r_1 Cos\theta_1\right) \qquad (21)$$

$$\theta_2 = Tan^{-1}\left(\frac{y}{x - a_0}\right) = Tan^{-1}\left(\frac{r_1 Sin\theta_1}{r_1 Cos\theta_1 - a_0}\right) \qquad (22)$$

Refer to figure 6 which shows the model variables..

The velocity can be resolved into x and y components using

$$V_x = V_n Cos\theta_2 - V_t Sin\theta_2 \qquad (23)$$

$$V_y = V_n Sin\theta_2 + V_t Cos\theta_2 \qquad (24)$$

The region of maximum velocity is located downstream at 60 degrees to flow. The contour of the calculated wind velocity equal to the free stream velocity (i.e.. no velocity error) is located close to 100 degrees in the upstream region of the flow. This contour of the ideal anemometer location moves towards 90 degrees for decreasing drag cylindrical coefficient (C_D). Figures 8 and 10 show the percentage change from the free stream velocity and directional errors for a C_D of 1.0.

The contours of the wake region for varying cylindrical drag coefficient are shown in figure 11. The offset variable, a_0, can be approximated from this diagram and is shown, with corresponding Y_1 and Y_2 values, in table 1.

The pressure field can be calculated from

$$P = \left(\left(\frac{P_\infty}{\rho} + \frac{V_\infty^2}{2} \right) - \frac{\left(V_n^2 + V_t^2 \right)}{2} \right) \rho \qquad (25)$$

where

ρ = density

P_∞ = Pressure at large distances from the cylindrical mast.

Only one stagnation point occurs and is located upwind of the mast at θ = 180 degrees, where the velocity is zero and the pressure at a maximum.

4.3.3 Summary

The region of maximum velocity is moved downstream, from 90 degrees in the simple potential model to approximately 60 degrees in the wake potential model.

In comparison to the simple model the velocity decrease found upwind is approximately doubled when compared with the simple model and the contour of no velocity error moves from 135 degrees to close to 90 degrees to the flow. The wake potential model exhibits a realistic wake profile that is dependent on cylindrical drag coefficient and gives a more physical interpretation of airflow around a cylindrical mast.

4.4 Potential Models applied to R.R.S. Charles Darwin Cruise 43

4.4.1 Introduction

This study hopes to explain the wind speed discrepancies between measurements taken from research vessels and attribute these discrepancies to the anemometers proximity to a cylindrical mast. This section applies the wind speed corrections calculated from the potential models to wind speed measurements made on R.R.S. Charles Darwin cruise 43.

Charles Darwin cruise 43 was a joint Institute of Oceanographic Sciences Deacon Laboratory (I.O.S.D.L.) and the University of Manchester Institute of Science and Technology (U.M.I.S.T.) project to measure wind stress using a number of fast sampling wind sensors. The anemometers used were two fast sampling Sonic anemometers, the Solent Sonic and the Kaijo Denki Sonic, and three propeller anemometers, the RM Young Propeller vane, the RM Young Bi - Vane and the RM Young Tri - Axis anemometer. The only wind speed and direction data used are from those winds within $\pm$ 30 degrees of the Charles Darwin's bow. The anemometers are mounted close to a mast of 0.4 m

in diameter and situated in a well exposed position the bows of the ship. Refer to figure 12 and table 2 for their positions. No data is available for the Young Tri - Axis anemometer as one axis failed during the cruise.

4.4.2 Potential models applied to wind speed data from Charles Darwin Cruise 43

This study assumes that the anemometers do not to disturb the flow and are considered to be in the same plane (i.e.. vertical distortions are ignored). The model wind speed correction factors are produced for each anemometer from a Pexec program that calculates percentage wind speed error, percentage directional error and a scalar wind speed correction factor. These values are calculated for every one degree of relative wind direction and based on an input of cylindrical drag coefficient and distance to the anemometer. The wind speed data from Charles Darwin, normalised to 10 meters, is sorted on relative wind direction and the wind speed correction factors are applied. The comparisons of none model corrected wind speeds between different pairs of anemometers are plotted and a best line of fit is calculated for each pair. This is repeated for the model corrected wind speeds at different drags and the regression lines and regression coefficients are compared. The results are in three sections; 1) the model wind speed errors for each anemometer are shown, 2) the comparisons of none corrected wind speed to the model corrected wind speed for each anemometer are examined, and 3) the findings are discussed.

4.4.3 Results

The model wind speed and directional errors are shown in figures 13 to 22 and are discussed below.

The wind speed and directional errors are larger and more sensitive to change at those anemometer sites closest to the mast such as the Young Propeller Vane anemometer (figures 15 and 16) and the Young Bi Vane anemometer (figures 17 and 18). The Kaijo Denki Sonic anemometer (figures 21 and 22) is not so sensitive to change and shows a -4 % wind speed error, whilst the Solent Sonic anemometer (figures 13 and 14) and Tri - Axis anemometer (figures 19 and 20) show the lowest wind speed errors, between $\pm$ 2%. The largest errors are found at the Young Propeller Vane site, -10 % wind speed error and $\pm$ 4% directional error. The smallest errors are found at the Young Tri axis anemometer site, $\pm$ 2% wind speed error.

Table 3 shows the wind speed comparisons of the Solent Sonic and Young Propeller Vane. The gradient of the regression line for all the model corrected data, except for the simple potential model, has increased towards one and the offset has increased for all drag coefficients. This could imply that the model corrections give a good interpretation of the flow with an unexplained offset. The best gradient increase is in the comparisons of wind speed data at a drag of 1.2, see figure 21. The regression coefficient for the corrected wind speeds drops in comparison to the original data showing an increase in scatter which gives the impression the model isn't correcting the measurements.

The wind speed comparisons of the Solent Sonic and Kaijo-Denki Sonic are shown in table 4. The regression lines for all model corrected wind speeds are improved in comparison to the original

measured wind speed. The gradients are increased, the offsets are reduced and more significantly the regression coefficients are increased. The best line of fit is in the comparisons of wind speed data at a drag of 1.2, see figure 22. The potential model has improved the wind speed and has accounted for some of the errors.

The comparisons of the Kaijo-Denki and the Young Propeller Vane, refer to table 5, show worse regression lines for all model corrected data, an example is shown in figure 23. The model corrections have increased the wind speed errors and could imply that the Young Propeller Vane is being affected by objects not used in this study. For example, like railings and the open frame that runs the length of the mast.

The Solent Sonic and the Young Propeller Vane are mounted at different distances, the Solent Sonic at 2.4083 m and the Young Propeller Vane at 1.1180 m. The Young Propeller Vane is the closest anemometer to the mast and is considerably more sensitive to the mast and objects mounted on the mast. Which could explain the models inability to explain the errors in comparisons made using the Young Propeller Vane. The distances from the mast of the Solent Sonic anemometer and the Kaijo-Denki are large and quite similar, Solent Sonic at 2.4083 m and the Kaijo Denki at 2.3345 m, giving both good exposure. The model accounts some wind speed errors in these comparisons and attributes them to the airflow distortion around the mast. There are still unexplained wind speed errors in the data which could be explained by the airflow modelling in section 5.

4.5 Conclusions

From the potential flow study of Charles Darwin cruise 43 it becomes clear that the airflow distortion around the mast doesn't explain all the errors in the comparisons. The potential models don't take into account the effect of the anemometers on the flow and they also don't take into account the vertical distortion in the flow. The wake potential model is realistic in it's behaviour, but it only considers the air flow in a horizontal plane around an idealised mast. This could prove significant, possibly accounting for some more of the errors in the comparisons, and is measured in studies by (Mollo-Christensen, 1979) and (Kondo and Naito, 1972), but I believe that the major unexplained errors are due to the airflow over ships hull and superstructure and section 5 will give us the corrections needed to produce even higher quality wind speed data sets.

5. AIR FLOW DISTORTIONS OVER THREE DIMENSIONAL SHIP MODELS

5.1 Introduction

This study proposes to produce a quantitative error for the wind speed measurements from a simulated boundary layer flow within a Computational Fluid Dynamics package.

We are considering eight vessels. The N.E.R.C. research vessels, R.R.S. Charles Darwin, R.R.S. Discovery and R.R.S. Challenger, which measurements have been taken from. The French

vessel Le Suriot, which has also been used, and the Canadian research vessels C.S.S. Dawson and C.S.S. Hudson which we have wind tunnel results for. The O.W.S. Cumulus and lastly the M.O.D. buoy deploying vessel The Warden. All the Ship models are shown in appendix B.

A number of Computational fluid Dynamics (C.F.D.) packages have been researched and Ricardo Engineering agreed to do a preliminary study of the C.S.S. Dawson. This gave us the opportunity to evaluate the Ricardo C.F.D. wind tunnel results of the C.S.S. Dawson using the wind tunnel study carried out by (Thiebaux, 1990).

5.2 The ship models

From initial consultation with Ricrado Engineering it was decided to create our ship models using a pre-processor called Femgen. The Ricardo Finite element code, Vetis, has an interface with this pre-processor and also possesses an automatic mesh generating technique which is directly applicable to Femgen models. The Femgen package was installed at the James Rennell Centre and each model took approximately three weeks to make, starting from the two dimensional ship plans. The Vectis code uses a numerical three dimensional fluid dynamics model to calculate velocity vectors, pressure, temperature, turbulent velocity. It displays these results in colour shaded planes.

Two dimensional information for each ship was obtained and was digitised into auto-cad and saved in IGES format. The digitised two dimensional plans were read into Femgen and then each point could be easily be manipulated to the correct height, either by moving a whole section of points vertically or as was the case, each in turn. The information from the plans only contained horizontal sections at the deck level, main deck level and at the lower deck level, no information was available for the waterline section. This had to be interpolated from the two adjacent sections. The hulls of the vessels are symmetrical, whilst the superstructures are generally asymmetrical. This means that the hulls can be simply mirror imaged in Femgen to produce the whole hull, therefore only half the ships hull was digitised in Auto-Cad to save time.

In this way a line structure of the ship was built up until the meshing staged was reached. The Vectis code needs a three noded triangular mesh to be applied to the surface of the ship. This is achieved by defining surfaces using three or four points and then mesh generating these surfaces using the relevant mesh type. The mirroring process tended to double up points down the mirroring plane causing some surfaces to overlap. This was spotted by Ricardo when the finished model of the C.S.S. Dawson was sent to them for evaluation.

The accuracy of the ships generated within Femgen are dependent on the ship plans they have been generated from and at the time of writing this report the only results available are those carried out by Ricardo on the C.S.S. Dawson, refer to (Ricardo, 1994).

5.3 C.S.S. Dawson

The C.S.S. Dawson has two anemometer sites, one situated on a mast in the bows in a well exposed position and the other above the superstructure. Figure 26 shows the surface geometry and locations of the anemometer sites.

The bow anemometer is situated 1m back from the bow and 12.5 meters above the water line whilst the main anemometer is located 38.58 m from the bow, offset to port by 1.8 m and is 18.8 m above the water line. The study by (Thiebaux, 1990) also includes two test anemometer positions at heights of 2 m and 1 m above and below the bow anemometer site. At the time of writing this report the Vetis code didn't incorporate multiple monitoring locations so no results are available from these test anemometer locations.

5.4 Results

The results obtained by Ricardo with the C.S.S. Dawson head to wind show errors of 1% for the bow anemometer and 7.6% for the main anemometer. These results are very accurate in comparison to a bow anemometer wind speed error of -1% and a main anemometer wind speed error of 7% found by (Thiebaux, 1990). The wind speeds and directions over the C.S.S. Dawson are shown in Figure 27 taken from (Ricardo, 1994). This is at only one heading as the C.P.U. time needed to obtain this result is about a week. An over all processing time of around 12 weeks is needed to obtain a set of wind speed corrections every five degrees at $\pm$ 30 of a ships bow.

6. SUMMARY

The wake potential model used by J. Wucknitz and developed in this study can describe realistic velocity fields around a cylindrical mast. The model has been used to partially corrected wind speed errors for anemometers mounted close to a mast of 0.4m in diameter mounted on Charles Darwin cruise 43. The remaining wind speed errors have been attributed to the potential models inability take into account the air flow distortions caused by the anemometers themselves, the vertical airflow distortions around the mast and the effect of the ships hull and superstructure. This has been undertaken by using a commercial Computational Fluid Dynamics package to calculate wind speed errors from three dimensional computer generated ship models, and results from the C.S.S. Dawson model show an agreement to within 2% of wind tunnel studies.

The C.F.D. code is being installed at the James Rennell Centre and will be used to finish of the correction errors for the C.S.S. Dawson and calculate the wind speed correction errors for the Natural Environment Research Councils research vessels R.R.S. Discovery, R.R.S. Charles Darwin, R.R.S. Challenger, O.W.S. Cumulus, C.S.S. Hudson, Le Suriot and M.O.D. The Warden.

Future work is to compare the potential models to Navy data for further validation. Interest has been also shown in the James Rennell Centre creating ship models of the VOS Observing Programme - North Atlantic (VSOP-NA) fleet and using a Computational Fluid Dynamics package to study airflow distortions at the anemometer sites.

7. ACKNOWLEDGEMENTS

Dr. P.K. Taylor, Margaret Yelland, Vic Cornell.

8. REFERENCES

Birch, K. G., M. J. Yelland and S. K. Ward, 1993: *Cumulus data transfer/processing instructions (Unpublished Report).* , James Rennell Centre, Southampton, U.K., pp. .

Dabberdt, W. F., 1968: Wind disturbance by a vertical cylinder in the atmospheric surface layer. *J. Appl. Meteorol.*, 7, 367-371.

Ditsworth, R. L. and T. Allen, 1972: *Fluid mechanics*, .McGraw-Hill, Kogakusha, pp. 415.

Gill, G. C., L. E. Olsson, J. Sela and M. Suda, 1967: Accuracy of wind measurments on Towers or Stacks. *Bulletin American Meteorological Society*, 48, 665-674.

Hunt, J. C. R., 1973: A theory of turbulent flow round two-dimensional bluff bodies. *J. Fluid Mech.*, 61, 625-706.

Kahma, K. K. and M. Lepparanta, 1981: On errors in wind speed observations on R/V Aranda. *Geophysica*, 17(1-2), 155-165.

Kondo, J. and G. Naito, 1972: Disturbed Wind Fields around the Obsticle in Sheared Flow near the Ground Surface. *J. Meteorol. Soc Japan*, 50(2), 346-354.

Mollo-Christensen, E., 1979: Upwind distorsion due to probe support in Boundary-Layer observation. *J. Appl. Meteorol.*, 18, 367-370.

Parkinson, G. V. and T. Jandali, 1970: A wake source model for bluff body potential flow. *J. Fluid Mech.*, 40, 577-594.

Ricardo, 1994: *CFD analysis of airflow over the C.S.S. Dawson. (Unpublished Report).* , Ricardo Consulting Engineers. Shoreham, U.K., pp. .

Thiebaux, M. L., 1990: *Wind tunnel experiments to determine correction functions for shipboard Anemometers.* , Canadian Contractor Report of Hydrography an Ocean sciences, Bedford Institute of Oceanography, Dartmouth, Novia Scotia, pp. .

Wucknitz, J., 1977: Disturbance of wind profile measurements by a slim mast. *Boundary layer Meteorology*, 11, 155-169.

Wucknitz, J., 1980: Flow distortion by Supporting Structures. : *Air sea Interaction. Instruments and Methods*, F. Dobson, L. Hasse and R. Davis, Ed., Plenum Press, 605 - 626.

Yelland, M. J., P. K. Taylor, K. G. Birch, R. W. Pascal and A. L. Williams, 1991: *Evaluation of a Solent Sonic anemometer on R.R.S. Charles Darwin Cruise 43.* , Institute of Oceanographic Sciences Deacon Laboratory, pp. .

8. REFERENCES

Birch, K. G., M. J. Yelland and S. K. Ward, 1993: Cumulus data transfer/processing instructions (Unpublished Report). , James Rennell Centre, Southampton, U.K., pp. .

Dabberdt, W. F., 1968: Wind disturbance by a vertical cylinder in the atmospheric surface layer. J. Appl. Meteorol., 7, 367-371.

Ditsworth, R. L. and T. Allen, 1972: Fluid mechanics, .McGraw-Hill, Kogakusha, pp. 415.

Gill, G. C., L. E. Olsson, J. Sela and M. Suda, 1967: Accuracy of wind measurements on Towers or Stacks. Bulletin American Meteorological Society, 48, 665-674.

Hunt, J. C. R., 1973: A theory of turbulent flow round two-dimensional bluff bodies. J. Fluid Mech., 61, 625-706.

Kahma, K. K. and M. Lepparanta, 1981: On errors in wind speed observations on R/V Aranda. Geophysica, 17(1-2), 155-165.

Kondo, J. and G. Naito, 1972: Disturbed Wind Fields around the Obstacle in Sheared Flow near the Ground Surface. J. Meteorol. Soc Japan, 50(2), 346-354.

Mollo-Christensen, E., 1979: Upwind distortion due to probe support in Boundary-Layer observation. J. Appl. Meteorol., 18, 367-370.

Parkinson, G. V. and T. Jandali, 1970: A wake source model for bluff body potential flow. J. Fluid Mech., 40, 577-594.

Ricardo, 1994: CFD analysis of airflow over the C.S.S. Dawson. (Unpublished Report). , Ricardo Consulting Engineers. Shoreham, U.K., pp. .

Taylor, P. K., E. C. Kent, M. J. Yelland and B. I. Moat, 1994: The accuracy of wind observations from ships. To be published in Proceedings of COADS Winds Workshop, May 1994, Kiel.

Thiebaux, M. L., 1990: Wind tunnel experiments to determine correction functions for shipboard Anemometers. , Canadian Contractor Report of Hydrography an Ocean sciences, Bedford Institute of Oceanography, Dartmouth, Novia Scotia, pp. .

Wucknitz, J., 1977: Disturbance of wind profile measurements by a slim mast. Boundary layer Meteorology, 11, 155-169.

Wucknitz, J., 1980: Flow distortion by Supporting Structures. : Air sea Interaction. Instruments and Methods, F. Dobson, L. Hasse and R. Davis, Ed., Plenum Press, 605 - 626.

Yelland, M. J., P. K. Taylor, K. G. Birch, R. W. Pascal and A. L. Williams, 1991: Evaluation of a Solent Sonic anemometer on R.R.S. Charles Darwin Cruise 43., Institute of Oceanographic Sciences Deacon Laboratory, 55 pp.

9. FIGURES

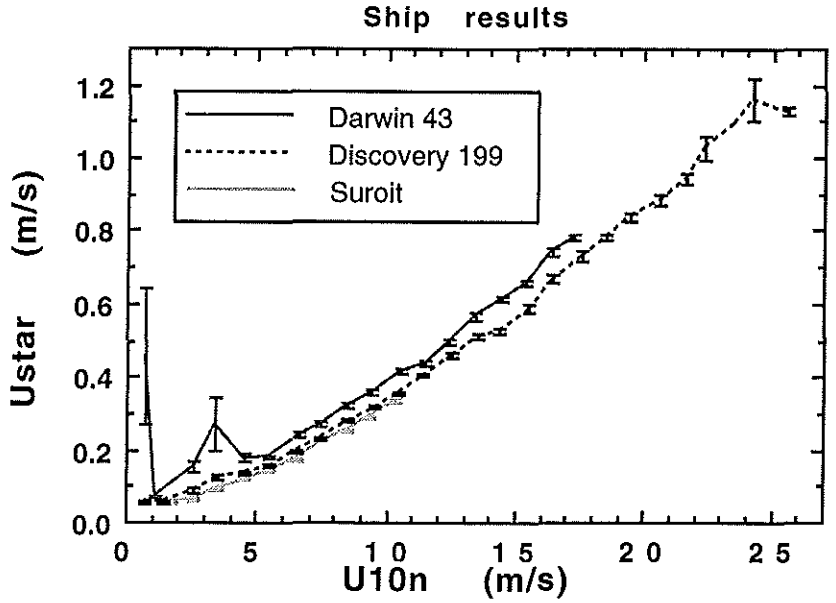

Figure 1 Comparison of friction velocity (U*) against normalised wind speed (U10n) showing wind speed discrepancies between R.R.S Charles Darwin, R.R.S. Discovery and Le Suroit.

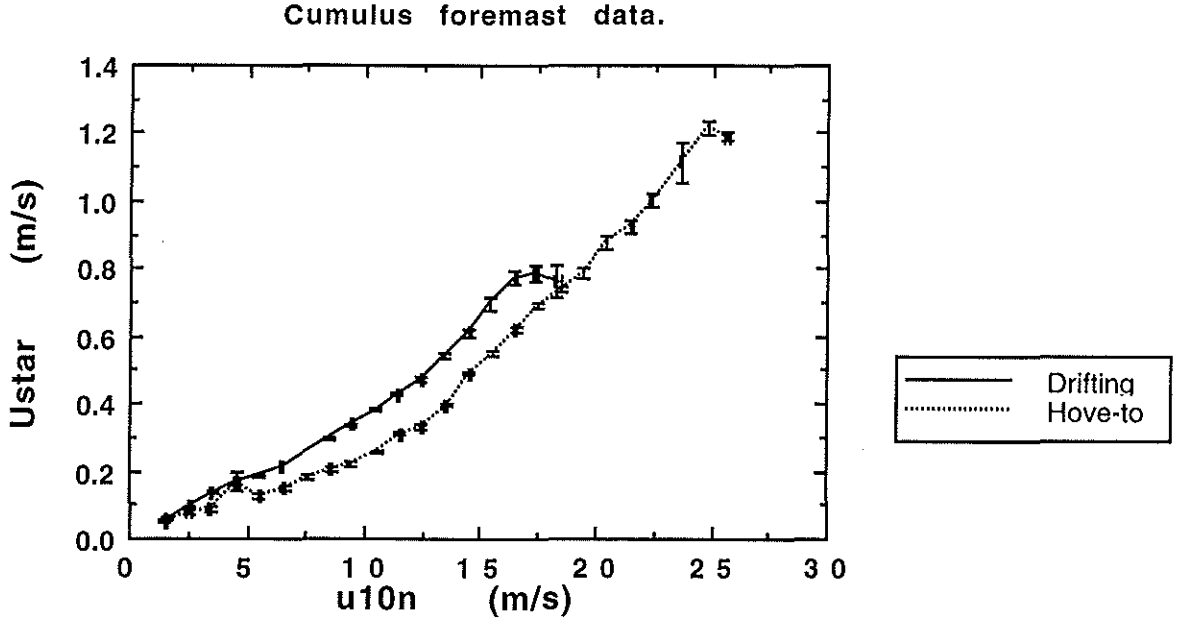

Figure 2 Comparison of friction velocity (Ustar) against normalised wind speed to 10 meters (U10n) showing wind speed discrepancies when the O.W.S. Cumulus is drifting and hove-to.

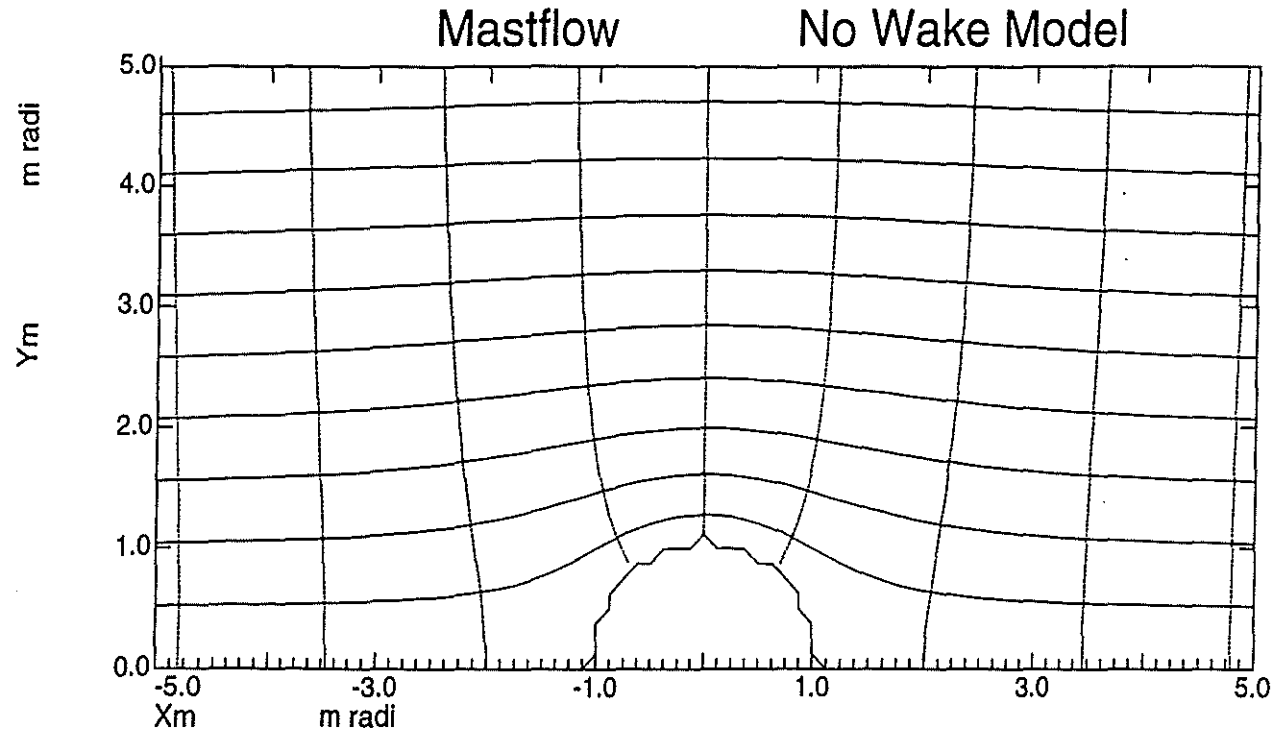

Figure 3 The solid and dashed lines respectively show the stream lines and equipotentials (for the no wake solution) around a mast of unit radius with the free stream entering from the left.

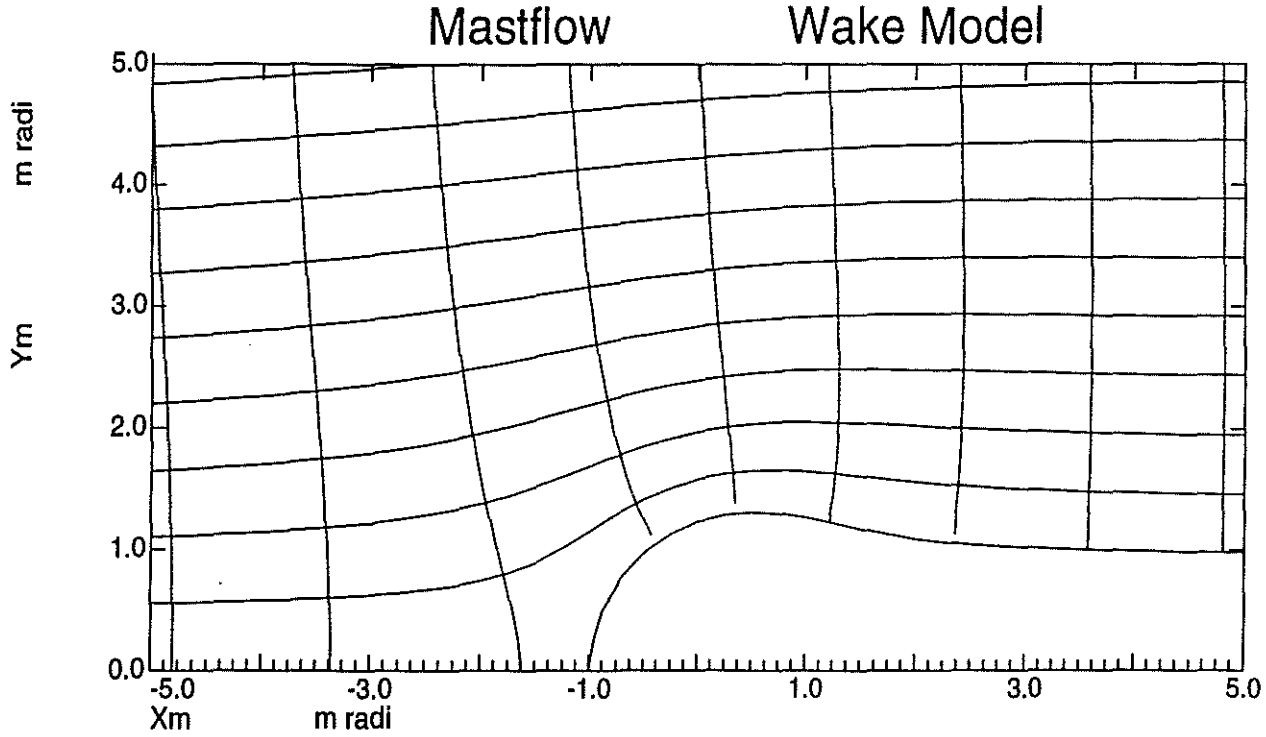

Figure 4 The solid and dashed lines respectively show the stream lines and equipotentials (for the wake solution where C_D=1.0) around a mast of unit radius with the free stream entering from the left..

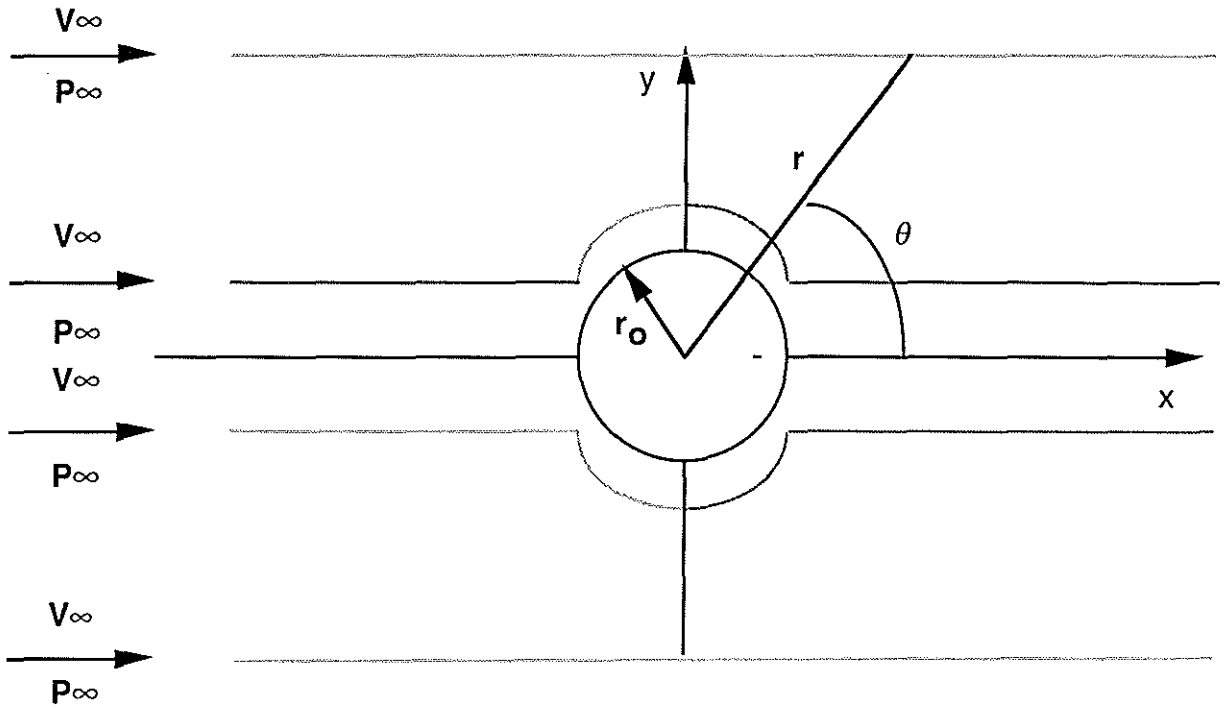

Figure 5 The variables in calculating the simple potential solution of an airflow around a cylindrical mast.

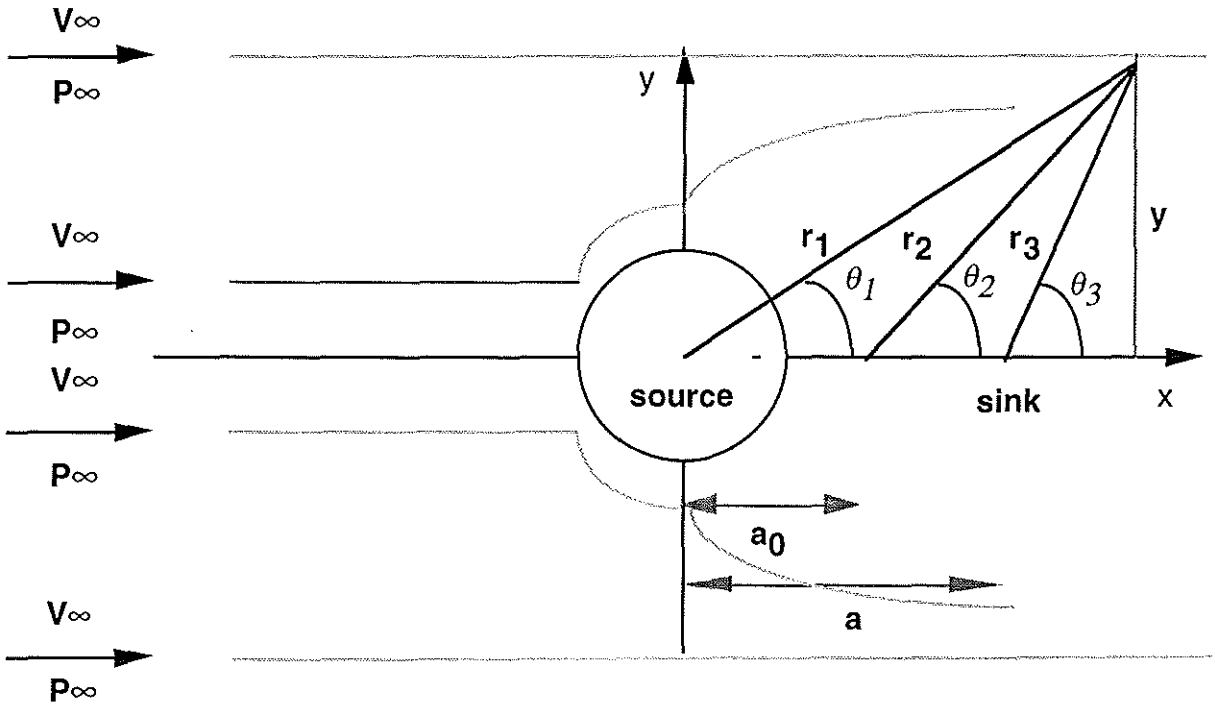

Figure 6 The variables used in calculating the potential solution of an airflow around a cylindrical mast with wake region downstream.

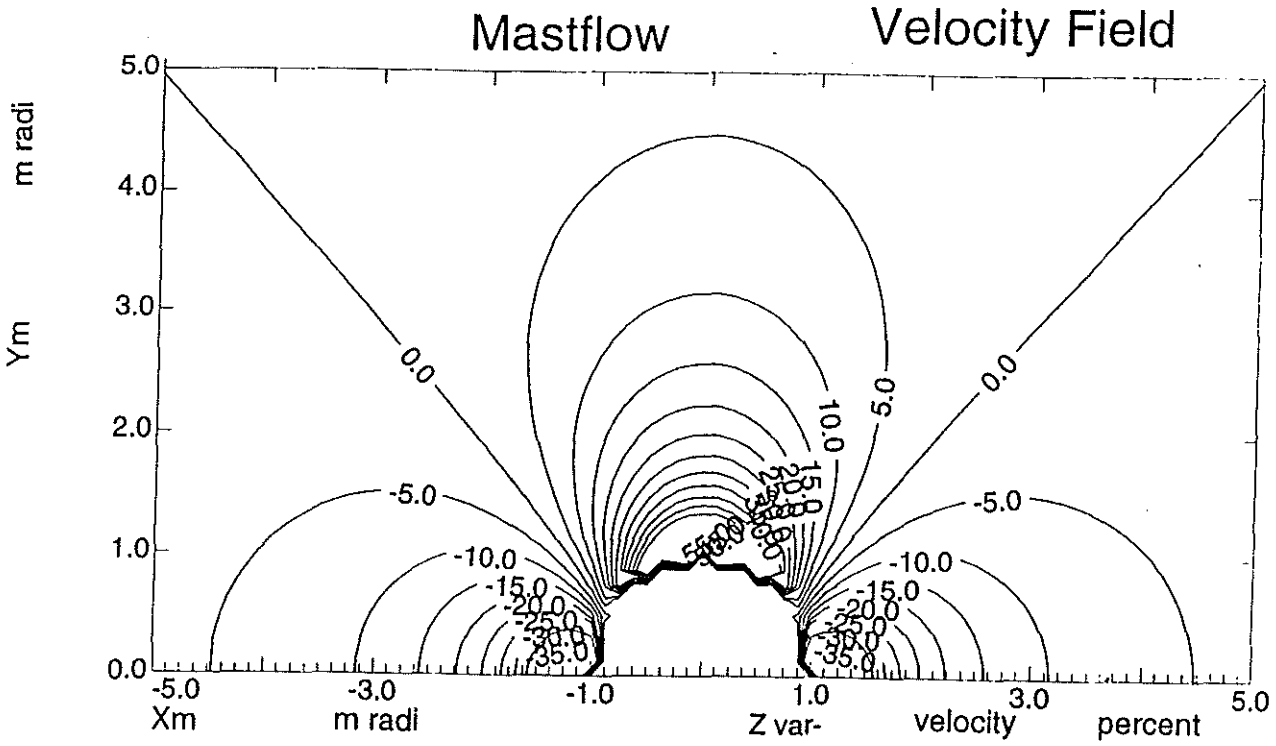

Figure 7 The Percentage change from the free stream velocity for the no wake solution around a cylindrical mast of unit radius. This shows a symmetric profile with error free contours at approx. 45 and 135 degrees, and maximum velocity region at 90 degrees to the flow

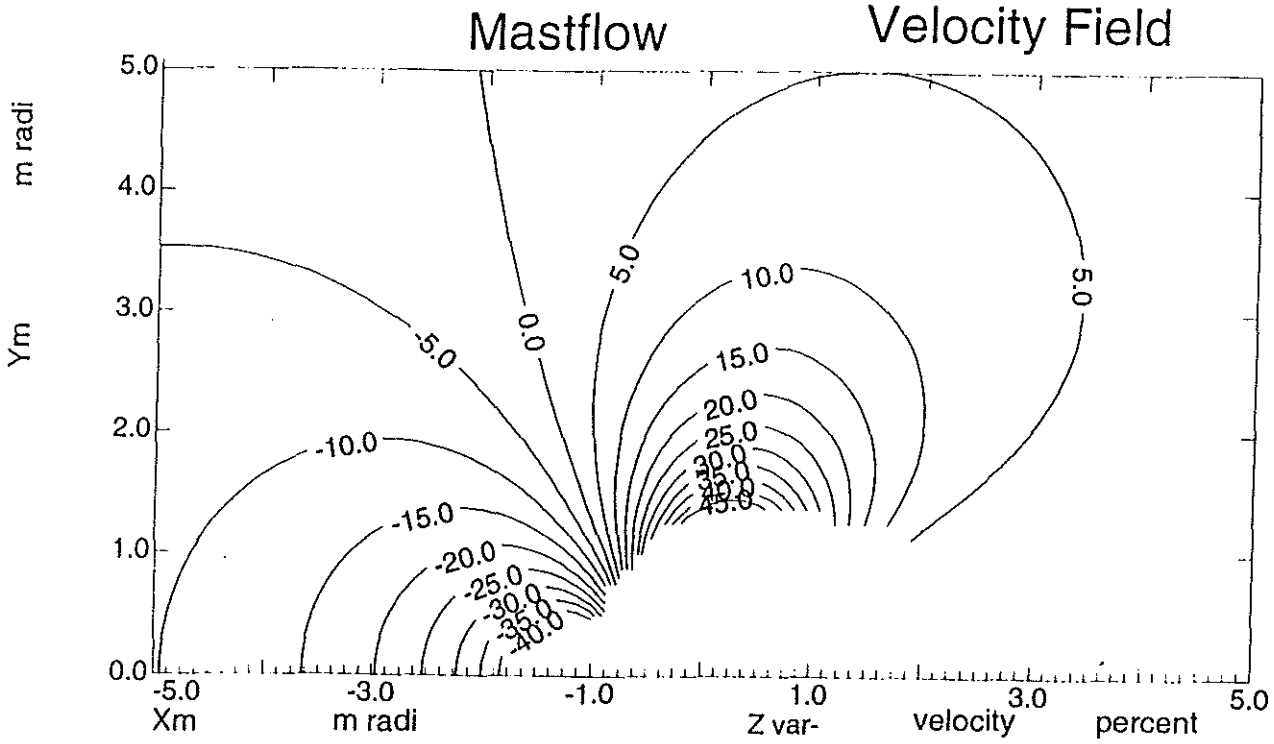

Figure 8 The Percentage change from the free stream velocity for wake potential solution around a cylindrical mast of unit radius. This shows a non-symmetric profile with an error free contour approaching 90 degrees, and maximum velocity region downstream of the flow.

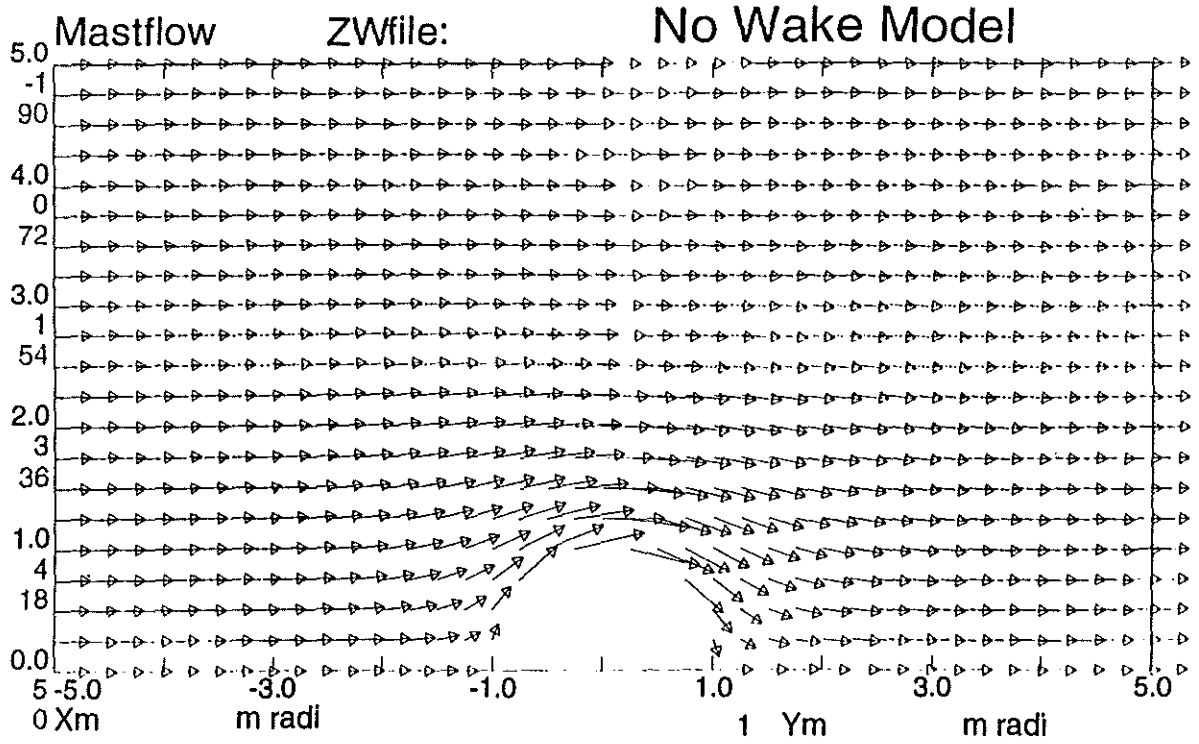

Figure 9 Flow distortion around a cylindrical mast of unit radius for the simple potential solution where the cylindrical drag coefficient = 1.0.

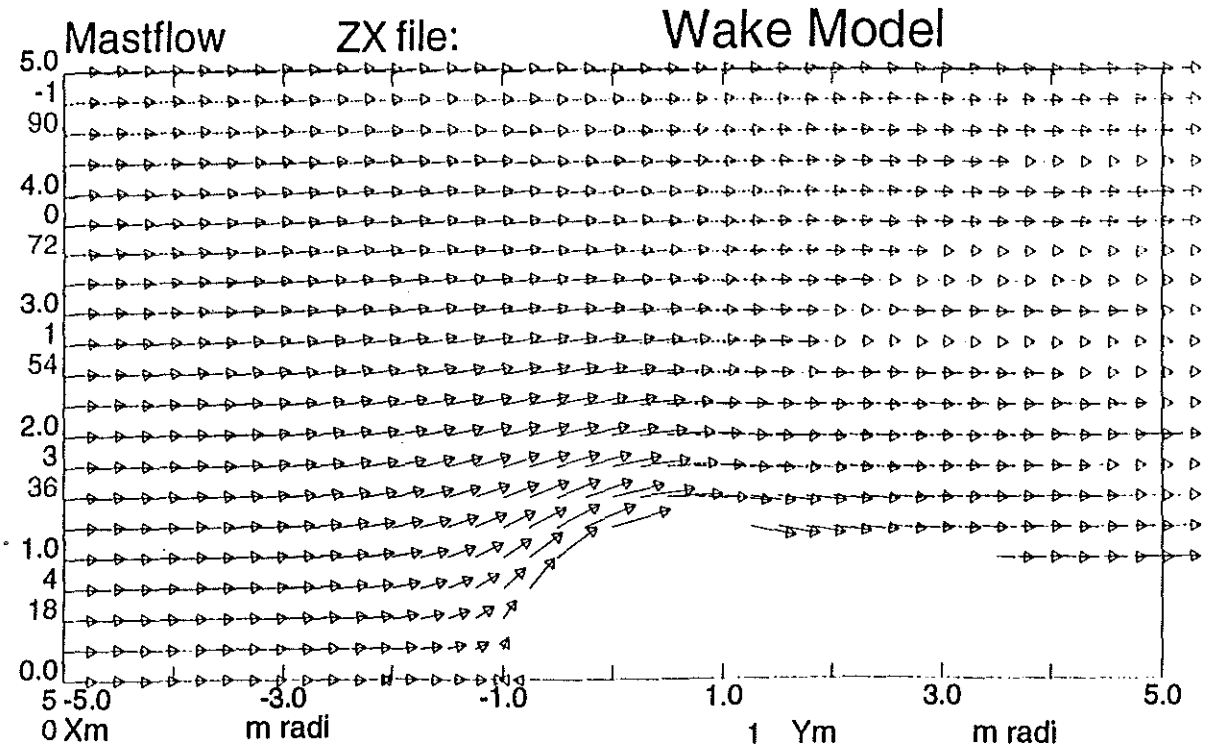

Figure 10 The flow distortion around a cylindrical mast of unit radius for the wake potential solution where C_D=1.0.

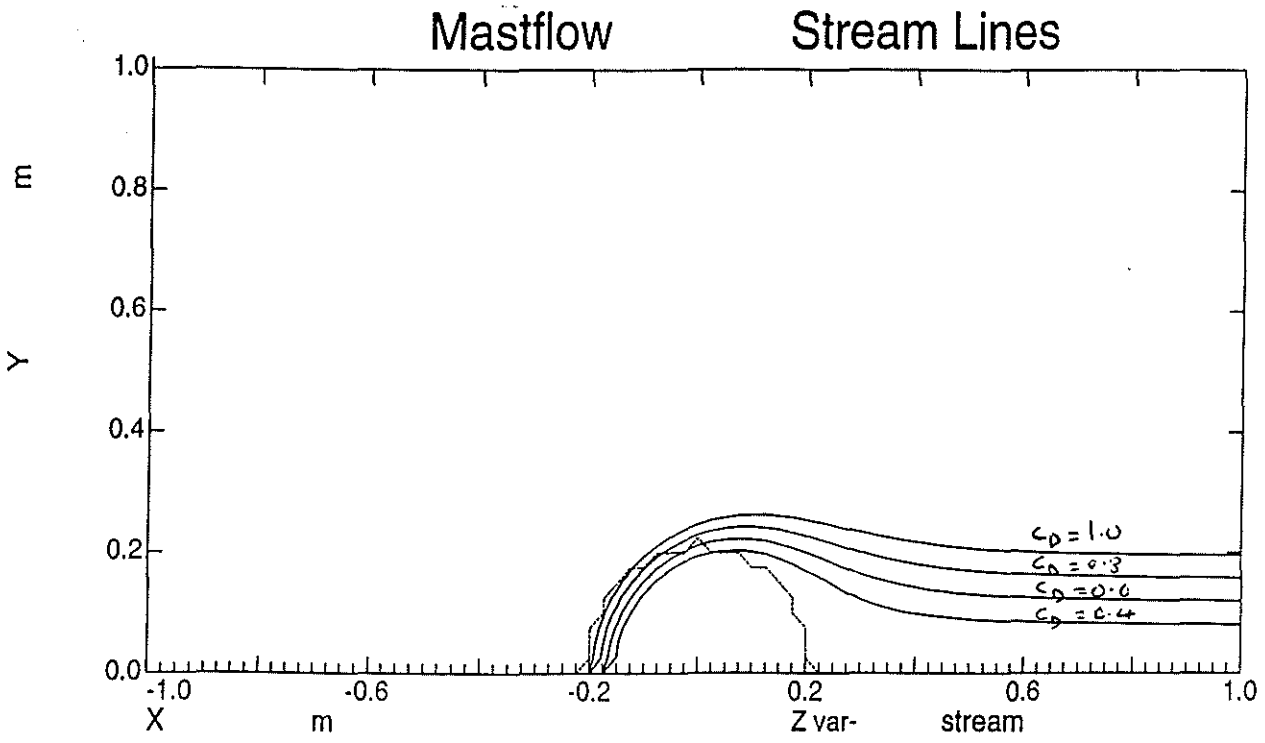

Figure 11 The wake region contours and offsets calculated by the wake potential model for a varying cylindrical drag coefficient.

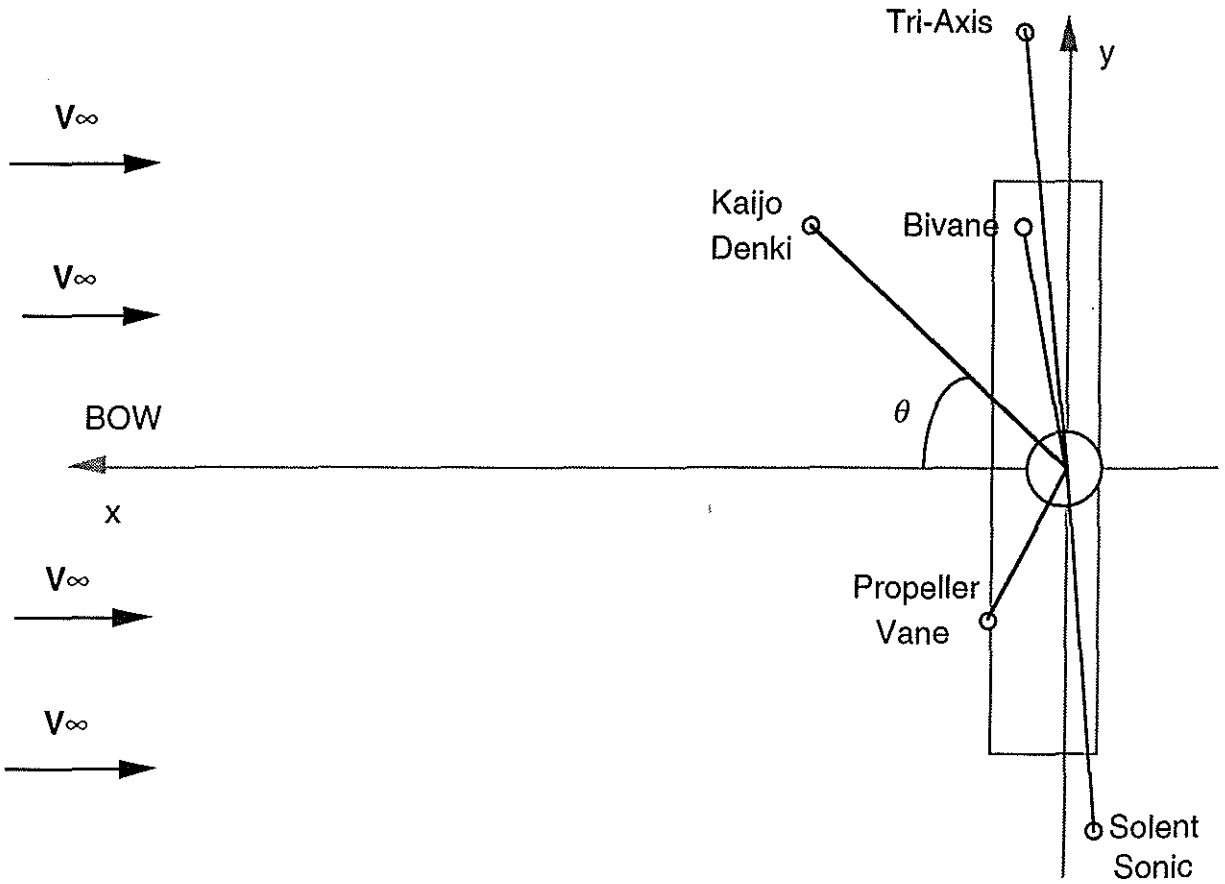

Figure 12 Anemometer positions on R.S.S. Charles Darwin Cruise 43.

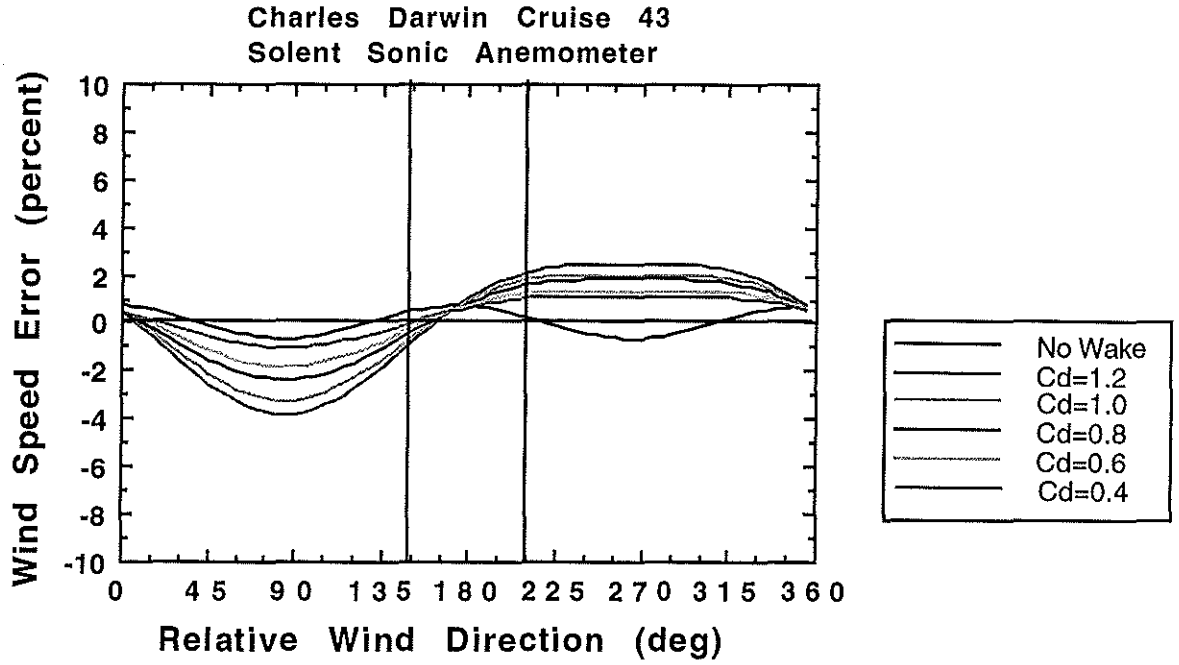

Figure 13 Wind speed errors for the Solent Sonic Anemometer.

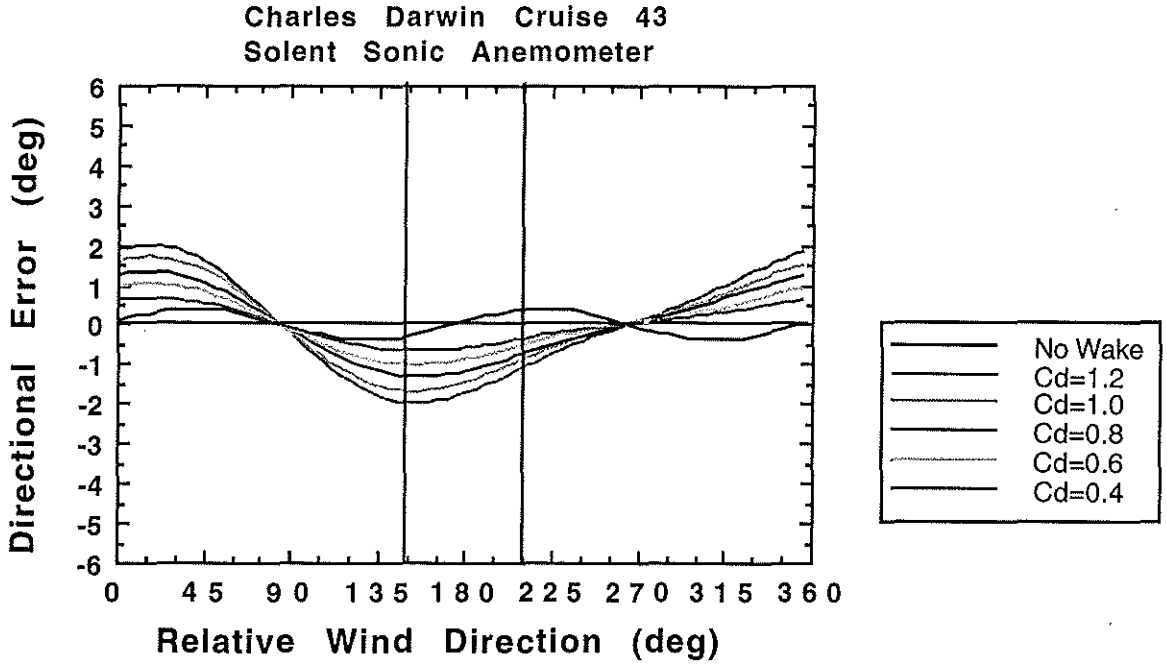

Figure 14 Directional errors for the Solent Sonic Anemometer.

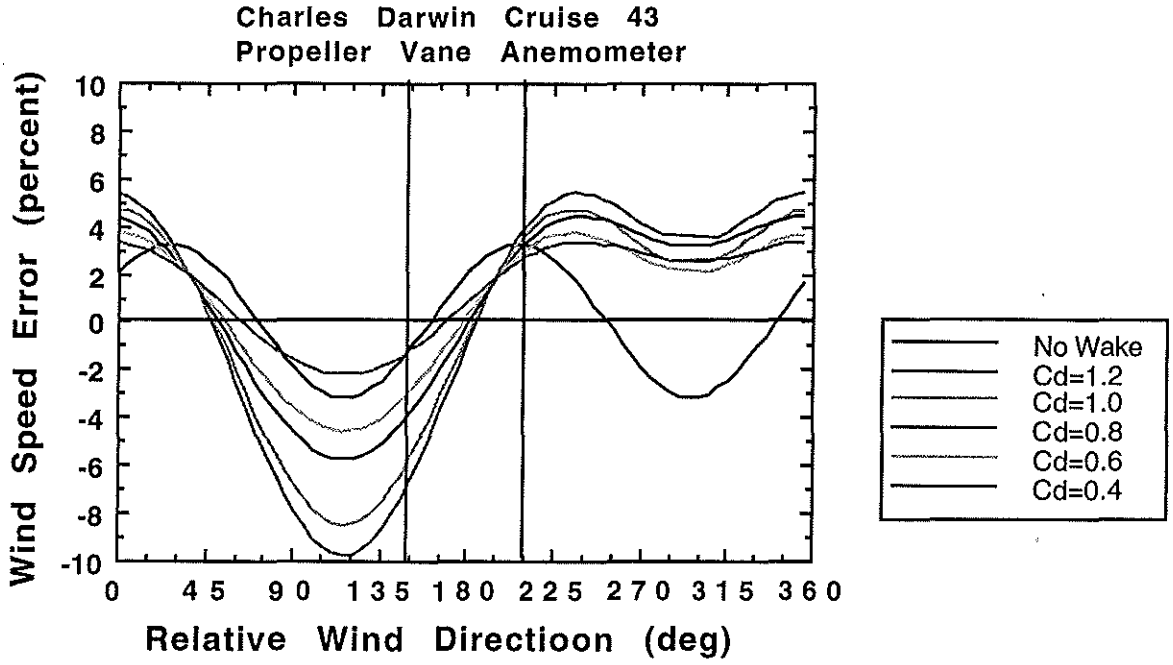

Figure 15 Wind speed errors for the Young Propeller Vane Anemometer.

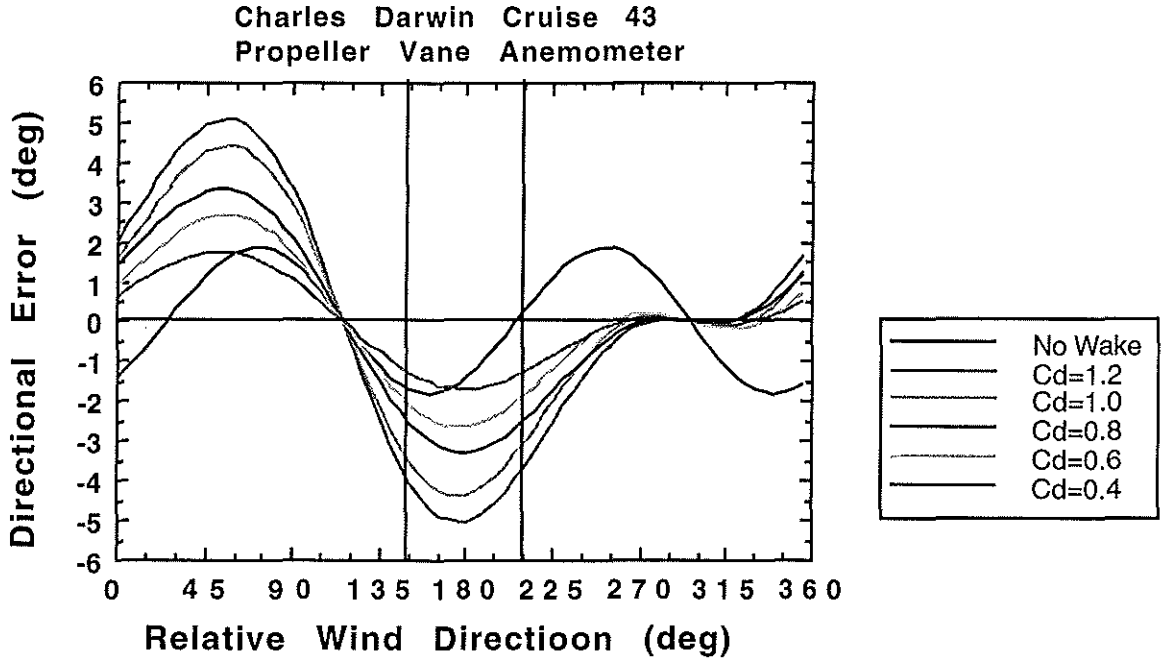

Figure 16 Directional errors for the Young Propeller Vane Anemometer.

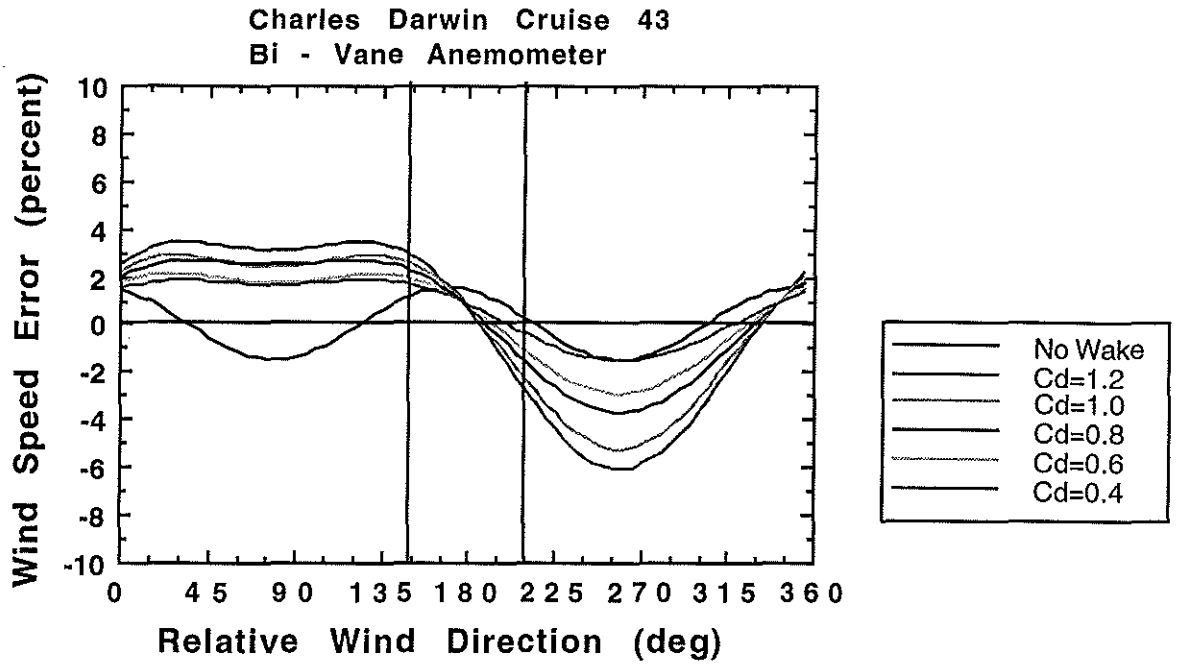

Figure 17 Wind speed errors for the Young Bi - Vane Anemometer.

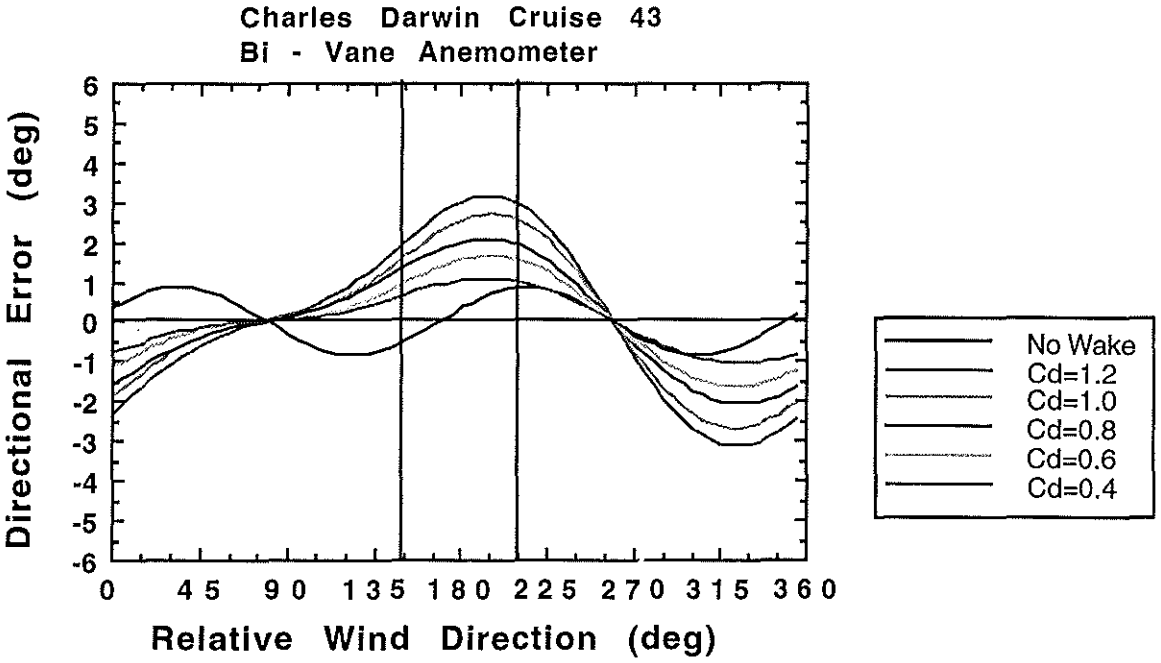

Figure 18 Directional errors for the Young Bi - Vane Anemometer.

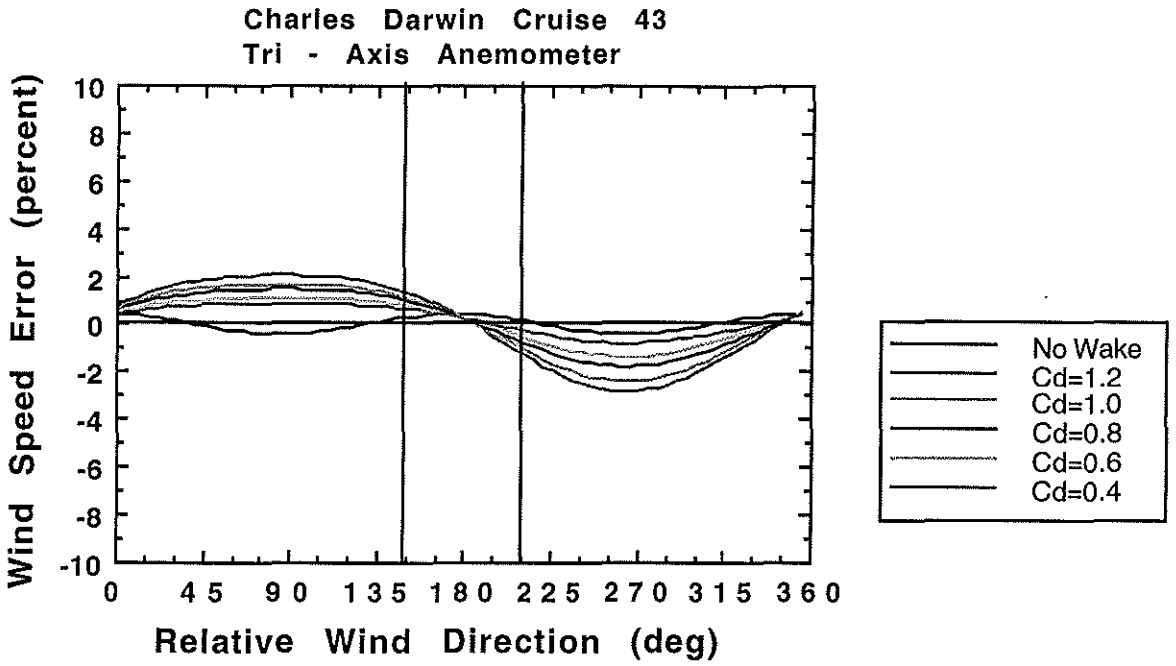

Figure 19 Wind speed errors for the Young Tri - Axis Anemometer.

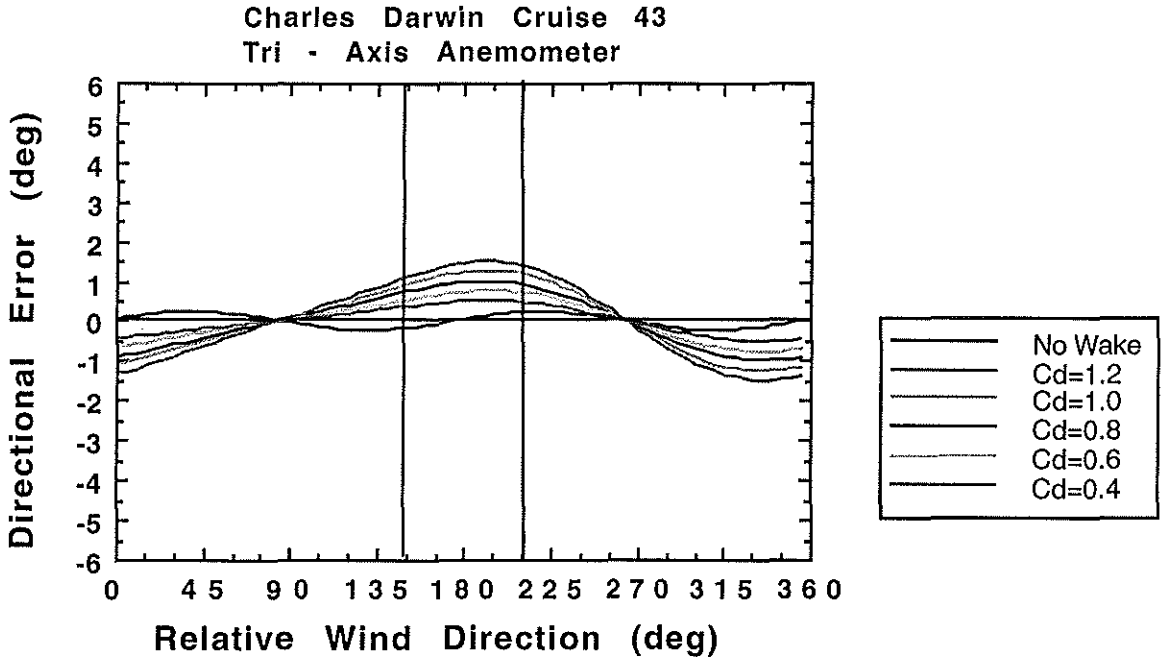

Figure 20 Directional errors for the Young Tri - Axis Anemometer.

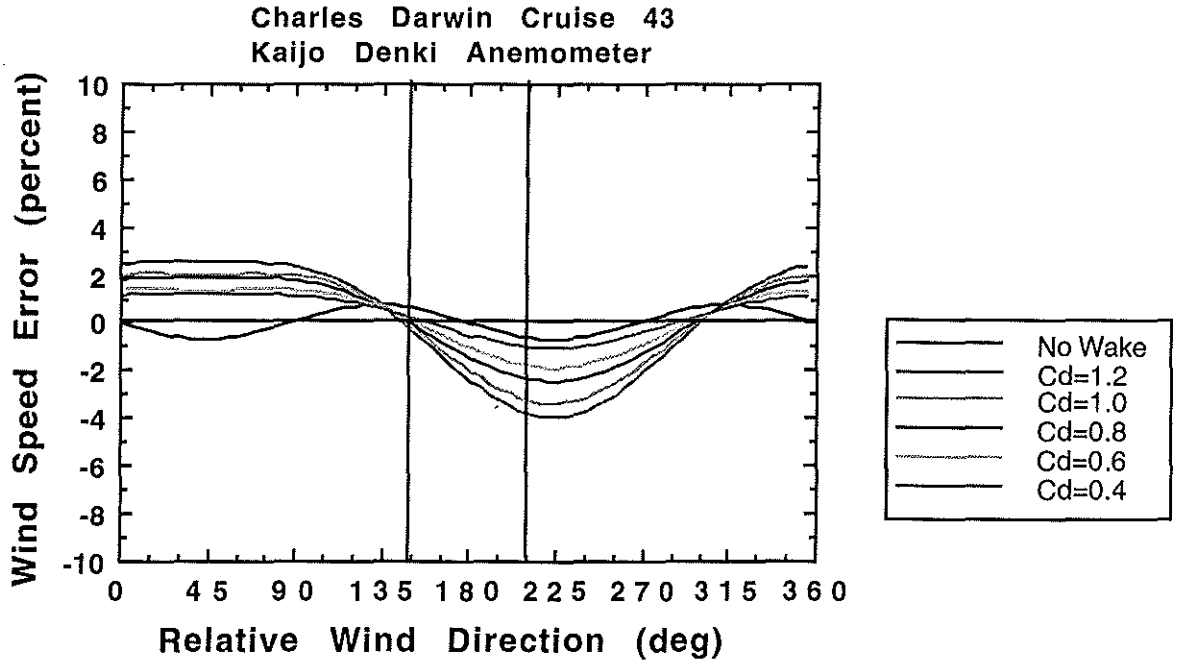

Figure 21 Wind speed errors for the Kaijo Denki Anemometer.

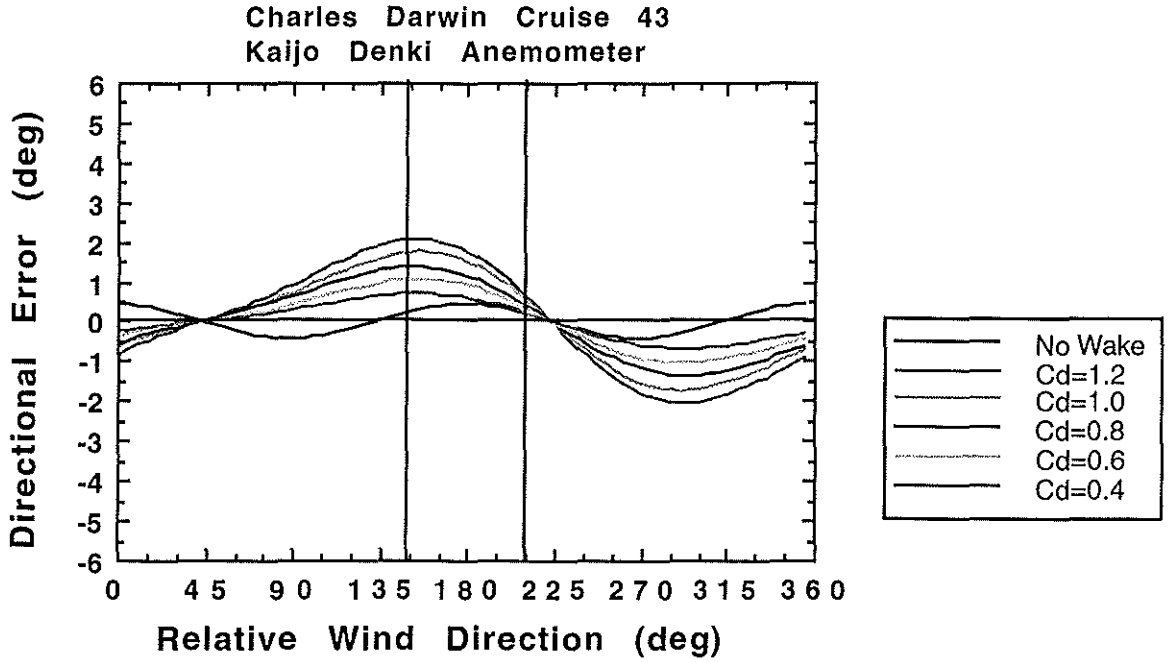

Figure 22 Directional errors for the Kaijo Denki Anemometer.

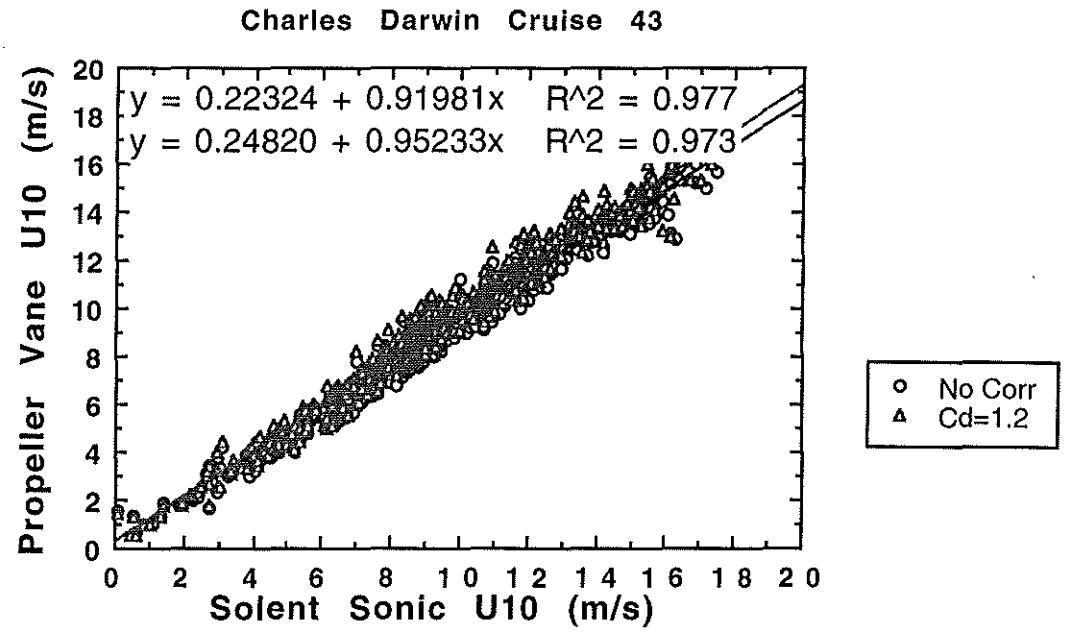

Figure 23 The Solent Sonic vs the Young Propeller for none corrected and model corrected normalised wind speed showing a drop in correlation for the corrected data.

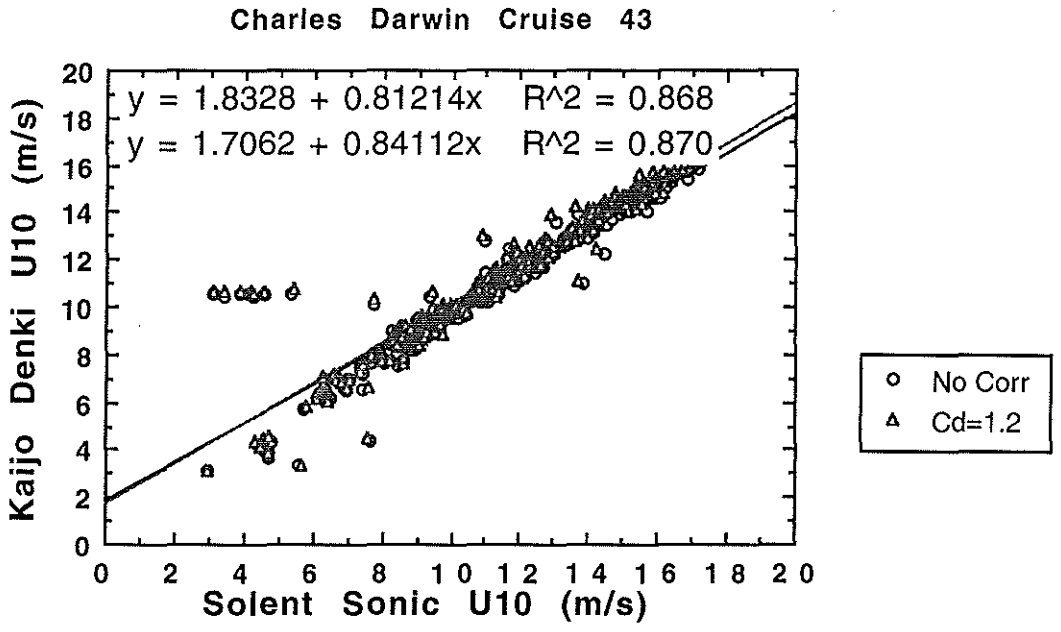

Figure 24 The Solent Sonic vs Kaijo Denki Sonic for none corrected and model corrected normalised wind speed showing an increase in correlation for the corrected data.

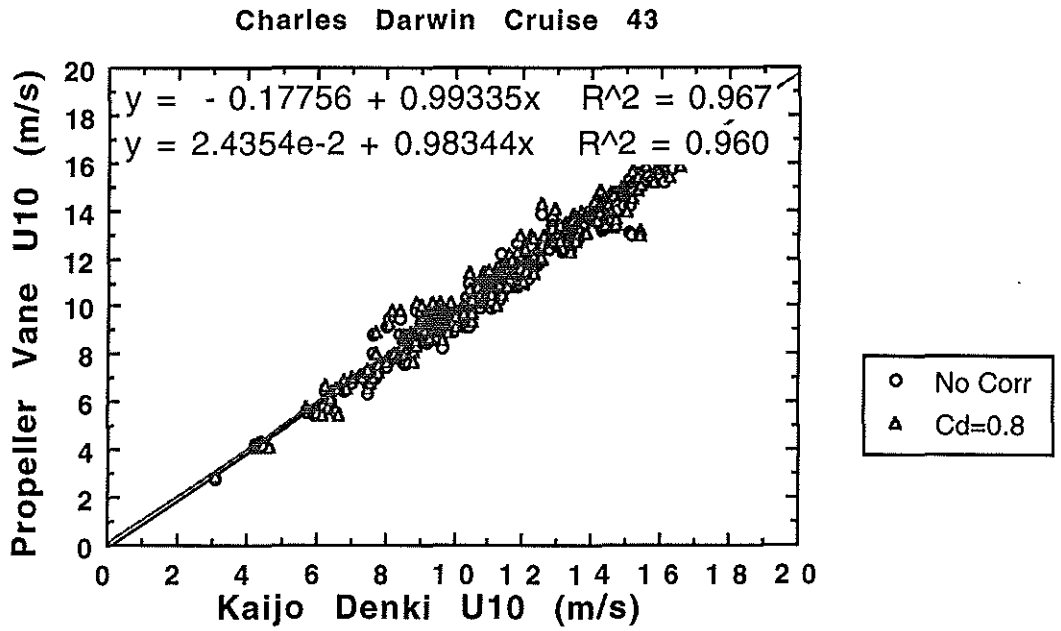

Figure 25 The Kaijo Denki Sonic vs The Young Propeller Vane for none corrected and model corrected normalised wind speed showing a drop in correlation for the corrected data.

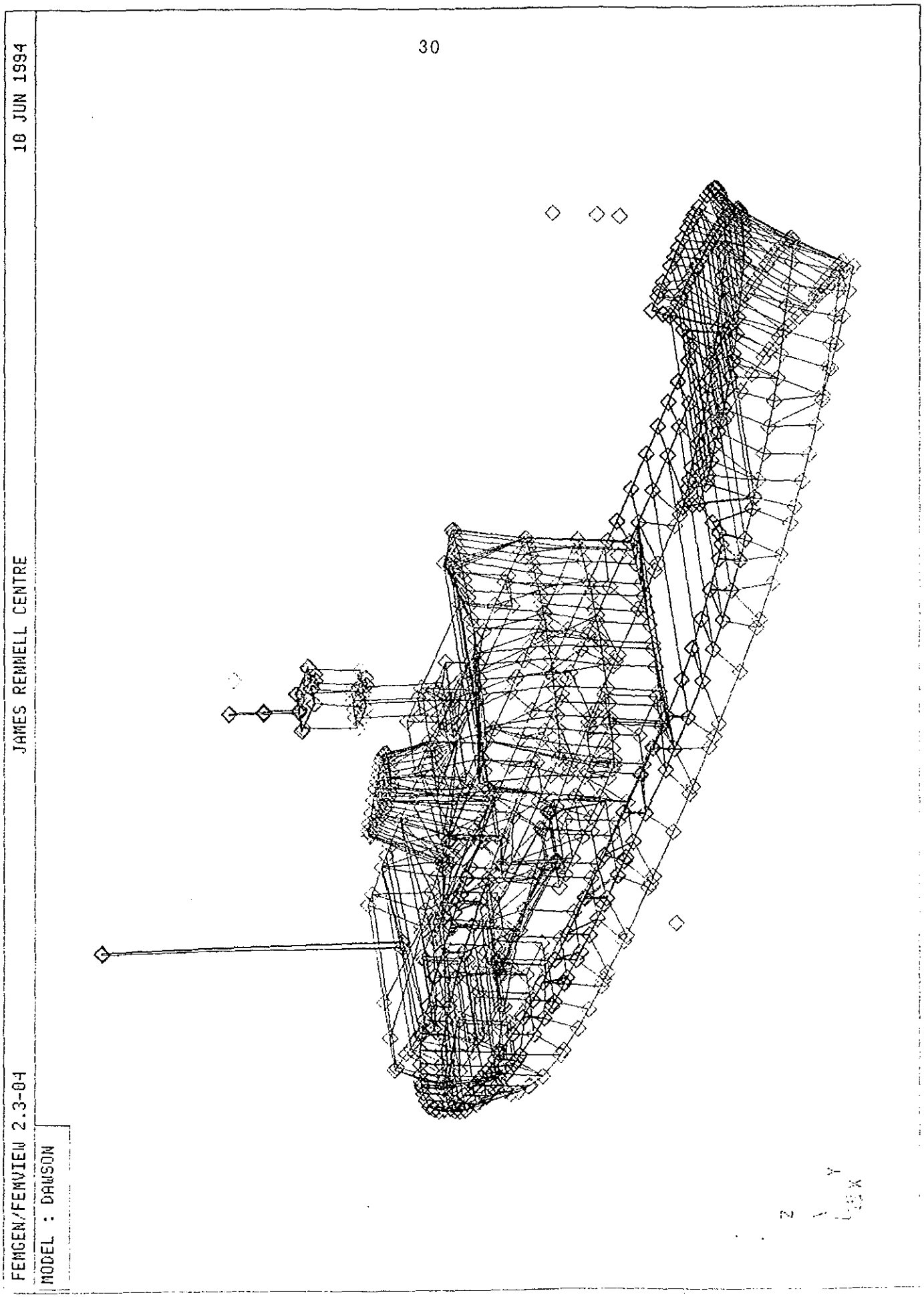

Figure 26 Surface Geometry and Anemometer sites of C.S.S. Dawson produced by the Finite element pre-processor Femgen.

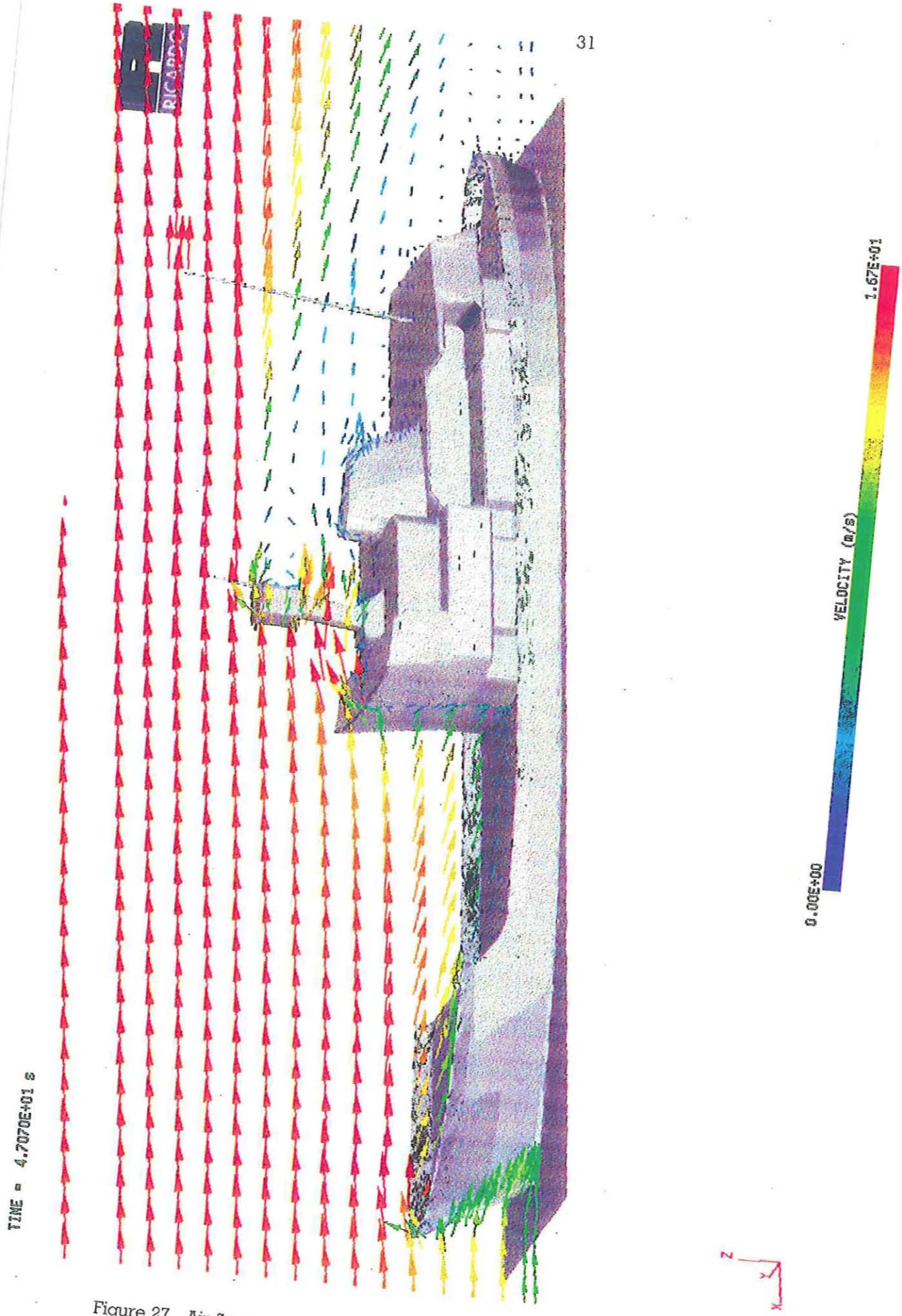

Figure 27 Air flow over the C.S.S. Dawson determined by C.F.D. modelling.

10. TABLES

Charles Darwin Cruise 43				
Drag Coefficient C_D	Mast radius r_o (m)	Source Y_1	Sink Y_2	Offset a_0 (m)
1.0	0.2	1.4012265	1.2012265	0.0
0.8	0.2	1.2984665	1.1384665	0.025
0.6	0.2	1.1957064	1.0757064	0.025
0.4	0.2	1.0929464	1.0129464	0.05

Table 1 The estimated offset, Y_1 and Y_2 for varying cylindrical drag coefficients.

Anemometer	X (m)	Y (m)	Distance (m)	Distance (mast diam)	Theta (deg)
Solent Sonic	-0.2	2.4	2.4083	6.0208	94.7636
Propeller Vane	0.5	1.0	1.1180	2.7950	63.4349
Bi - Vane	0.3	-1.6	1.6279	4.0698	79.3803
Tri - Axis	0.3	-3.1	3.1145	7.7863	84.4725
Kaijo Denki	1.7	-1.6	2.3345	5.8363	43.2643

Table 2 Anemometer positions in relation to mast centre.

Drag Coefficient	Solent Sonic vs Young Propeller Vane		
	m	c	R^2
Raw	0.91981	0.22324	0.977
No Wake	0.91513	0.26551	0.974
1.2	0.95233	0.26551	0.973
1.0	0.94682	0.24820	0.973
0.8	0.93791	0.23772	0.975
0.6	0.93235	0.23840	0.975
0.4	0.92337	0.23013	0.976

Table 3 Regression lines for Solent Sonic Anemometer vs the Young Propeller Vane Anemometer

Drag Coefficient	Solent Sonic vs Kaijo Denki Sonic		
	m	c	R^2
Raw	0.81214	1.8328	0.868
No Wake	0.81857	1.7916	0.869
1.2	0.84112	1.7062	0.870
1.0	0.83715	1.7217	0.870
0.8	0.83155	1.7442	0.869
0.6	0.82763	1.7598	0.869
0.4	0.82228	1.7814	0.896

Table 4 Regression lines for Solent Sonic vs Kaijo Denki Sonic.

Drag Coefficient	Kaijo Denki Sonic vs Young Propeller Vane		
	m	c	R^2
None Corrected	0.99335	-0.17756	0.967
No Wake	0.97541	$-2.6650*10^{-2}$	0.963
1.2	0.98242	0.14377	0.952
1.0	0.98300	0.10316	0.955
0.8	0.98344	$2.4354*10^{-2}$	0.960
0.6	0.98335	$-9.5225*10^{-3}$	0.962
0.4	0.98225	$-7.2240*10^{-2}$	0.964

Table 5 Regression lines of wind speed for Kaijo Denki Sonic anemometer vs Young Propeller Vane anemometer.

11. APPENDIX A - THE JAMES RENNELL CENTRE

1. THE NEED FOR OCEANOGRAPHIC RESEARCH

Oceanography is influencing our everyday lives; not only is it useful for seamen to possess detailed knowledge of the oceans, surface currents and winds but it is evident that the oceans are an integral part of the world climate system. The oceans can transport and store vast amounts of energy and can therefore determine the time scale and regional patterns of climate change. Solar energy is absorbed at the equator and warms the water which is transported towards the poles, were it cools and sinks, and flows back towards the equator. The heat from this process is distributed into the atmosphere, which influences the winds, rainfall patterns and regional temperatures.

1.1 THE JAMES RENNELL CENTRE FOR OCEAN CIRCULATION

The Natural Environment Research Council (N.E.R.C.) was formed in 1965. Its purpose was to combine all the different environment agencies under the management and funding of one central body. The National Institute of Oceanography combined with the Institute of Coastal Oceanography and Tides and the Unit of Coastal Sedimentation in 1973, to become the Institute of Oceanographic Sciences Deacon Laboratory (I.O.S.D.L.), which remains in Surrey to this day. In the spring of 1990 it was announced that the James Rennell Centre for Ocean Circulation (J.R.C.) was to be established at Southampton as a component of the I.O.S.D.L. It opened in December 1990, and is now being managed independently to I.O.S.D.L. Its purpose is to manage and support the U.K. contribution to the World Ocean Circulation Experiment (W.O.C.E.). The W.O.C.E. is part of the World Climate Research Programme. It is the largest ever international study of the physics of the ocean and its role in the climate of our planet. It involves scientists from over forty nations using satellites, ships, buoys and floats.

The J.R.C. has a staff of about fifty, some of whom are based at the I.O.S.D.L., who are split up into six scientific teams with support from an administrative team. The Survey team enables frequent cruises to be supported and undertakes acquisition and processing of data to high standards both at sea and at the J.R.C. The Tracer Chemistry team concentrates on the measurement and distribution of oxygen, silicate, phosphate, nitrate; the chlorofluorocarbons CFC-10, CFC-11, CFC-12 and CFC-13, and plant pigments within the oceans. The Biological team is producing models with the aim of predicting nitrogen and carbon cycles from plankton and zooplankton activity in the upper ocean. The Satellite team is developing techniques for processing images of the oceans taken from satellites such as ERS - 1 and TOPEX/POSIDEN. The satellites can measure sea surface temperature, wind velocity, wave height and slopes in sea level, which relate to ocean currents. The Physical Modelling team is developing the Atlantic Isopycnic Model (A.I.M.), which is being used to examine the coupling between the upper ocean and the ocean interior and the role of eddies in ocean circulation.

The James Rennell Centre, I.O.S.D.L., Southampton University Department of Oceanography and Research Vessel Services are going to be combined into one new dockside centre, in Southampton in 1995, called the Southampton Oceanography Centre.

1.2 THE SURFACE METEOROLOGY TEAM

Until April 1994 the Surface Meteorology team was split into the Ocean Instrumentation Group, based at the I.O.S.D.L., whilst the data analysis group is situated at the J.R.C. The Ocean Instrumentation group is now known as the Centre for Ocean Technology Development (C.O.T.D.), leaving five members in the Meteorological team at the J.R.C.

The Surface Meteorology teams primary role is to understand how the ocean controls and responds to the weather in the atmosphere. Values for the transfers (or fluxes) of heat, water, and momentum between the ocean and the atmosphere are calculated and used to verify climate models of the coupled ocean atmosphere system.

12. APPENDIX B - SHIP MODELS

The following Appendix contains the ship models created using the Finite Element pre-processor Femgen. The models included are the R.R.S. Challenger, O.W.S. Cumulus, R.R.S. Charles Darwin, C.S.S. Dawson, R.R.S. Discovery, C.S.S. Hudson, Le Suroit and The Warden.

DEL: CHALAL

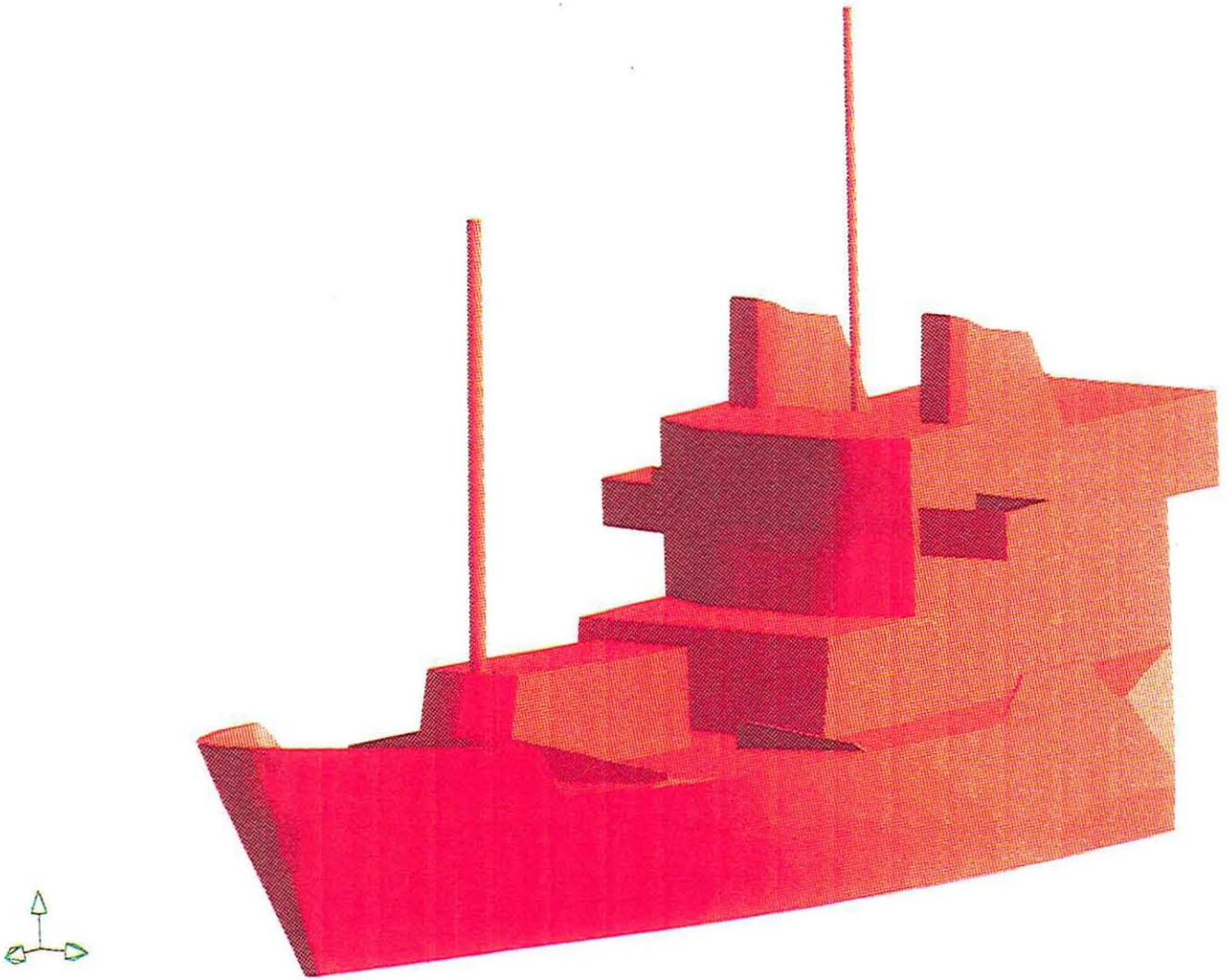

R.R.S. Challenger

DEL: CUMULU

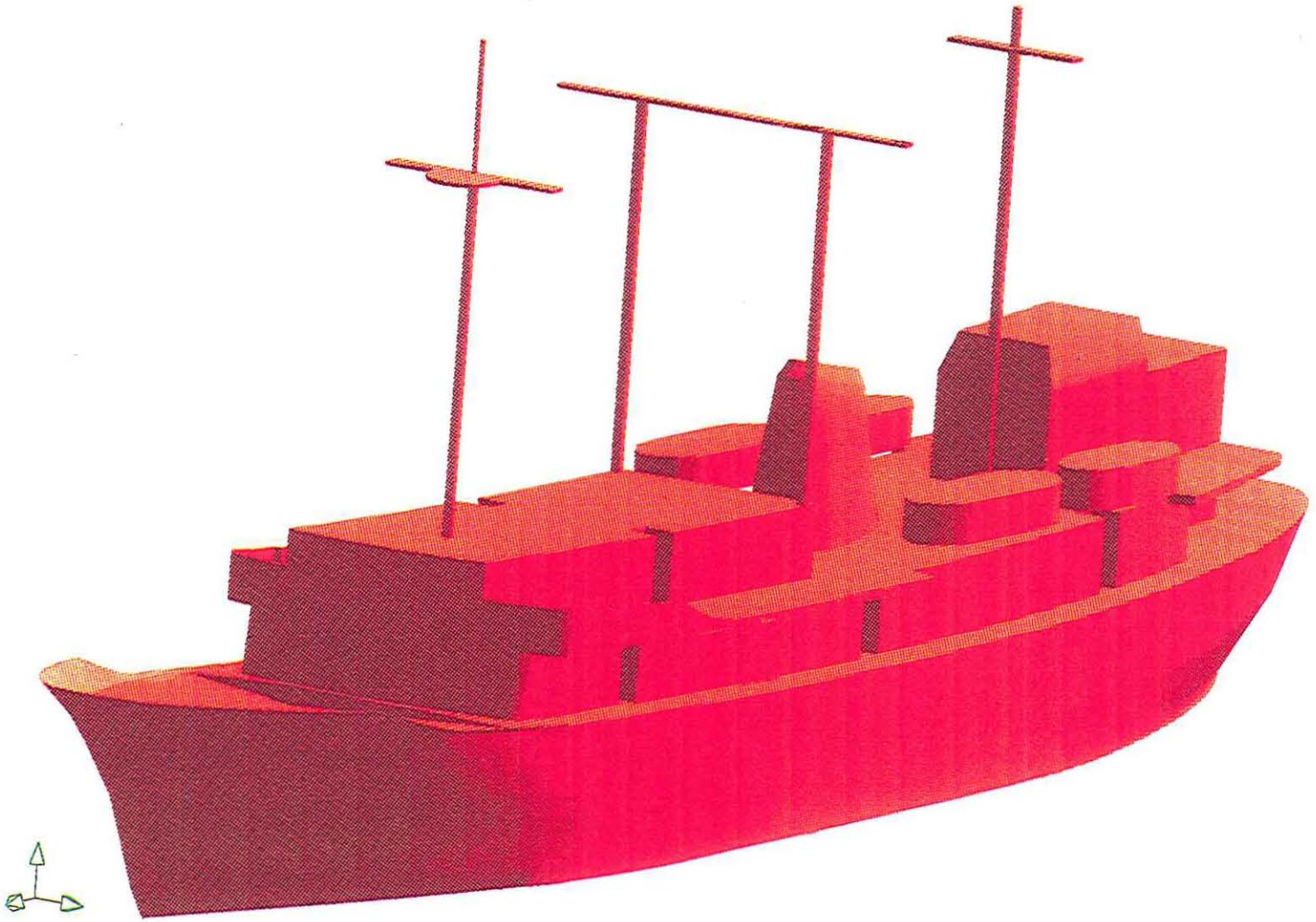

O.W.S. Cumulus

DEL: NEW1

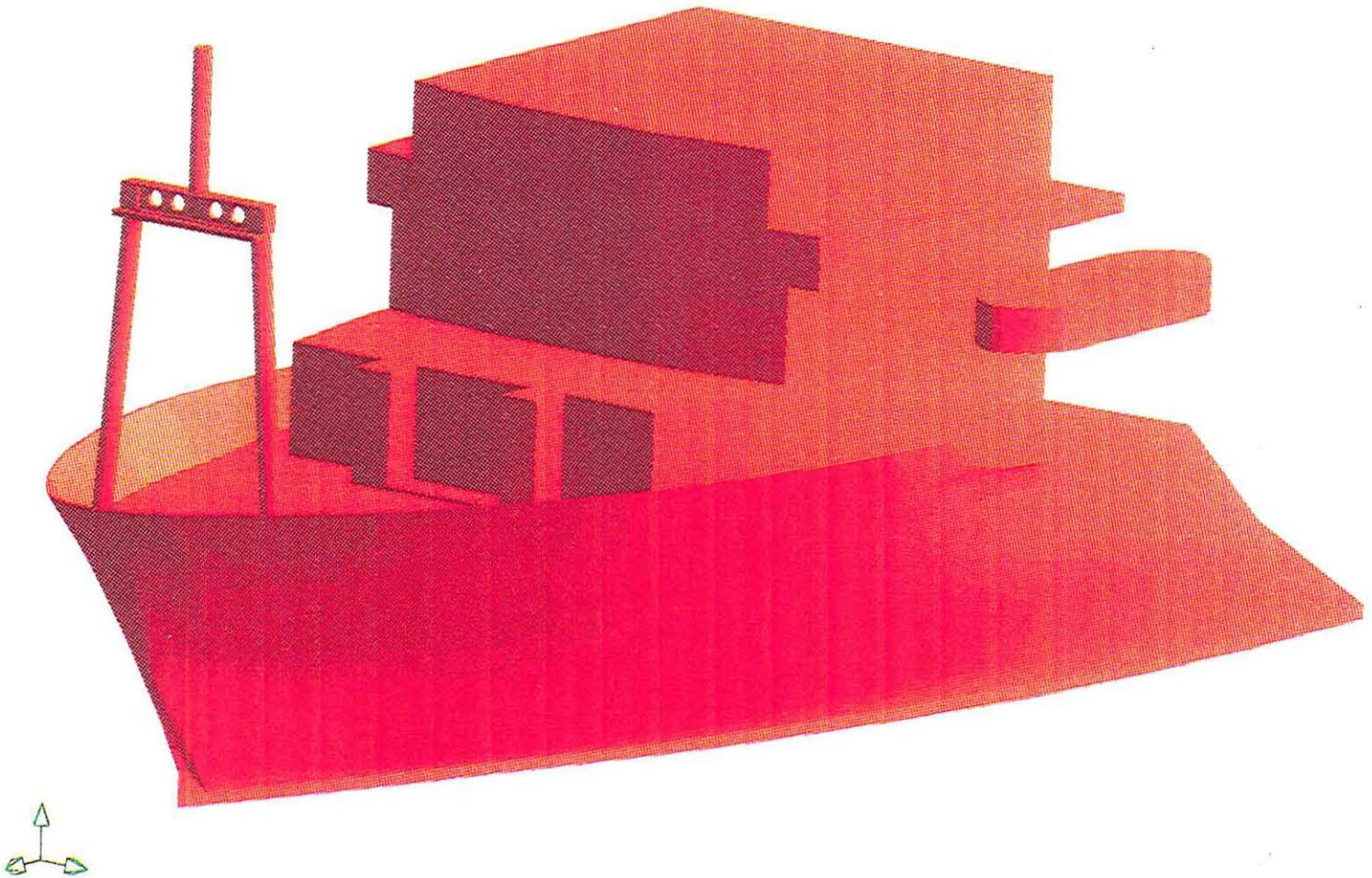

R.R.S. Charles Darwin

DEL: DAWSON

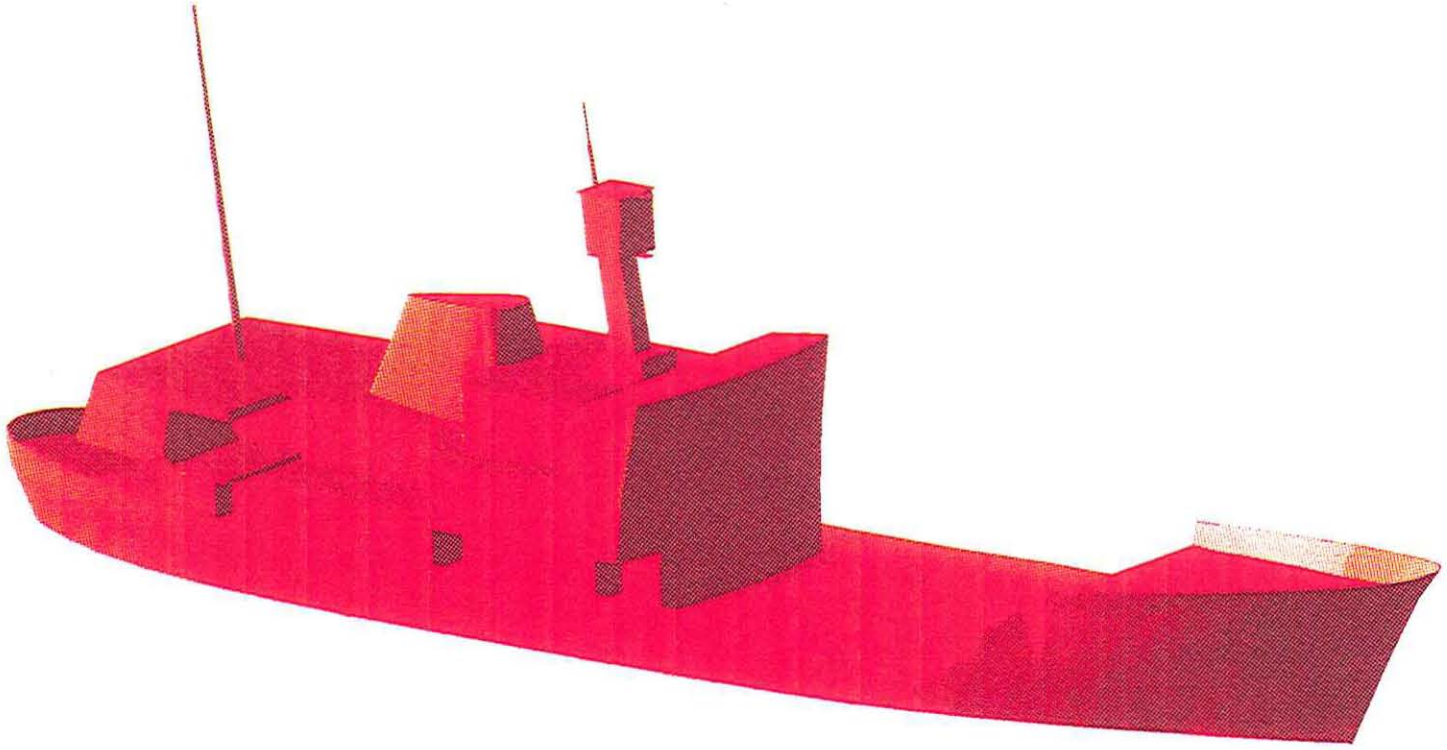

C.S.S. Dawson

DEL: DISCAL

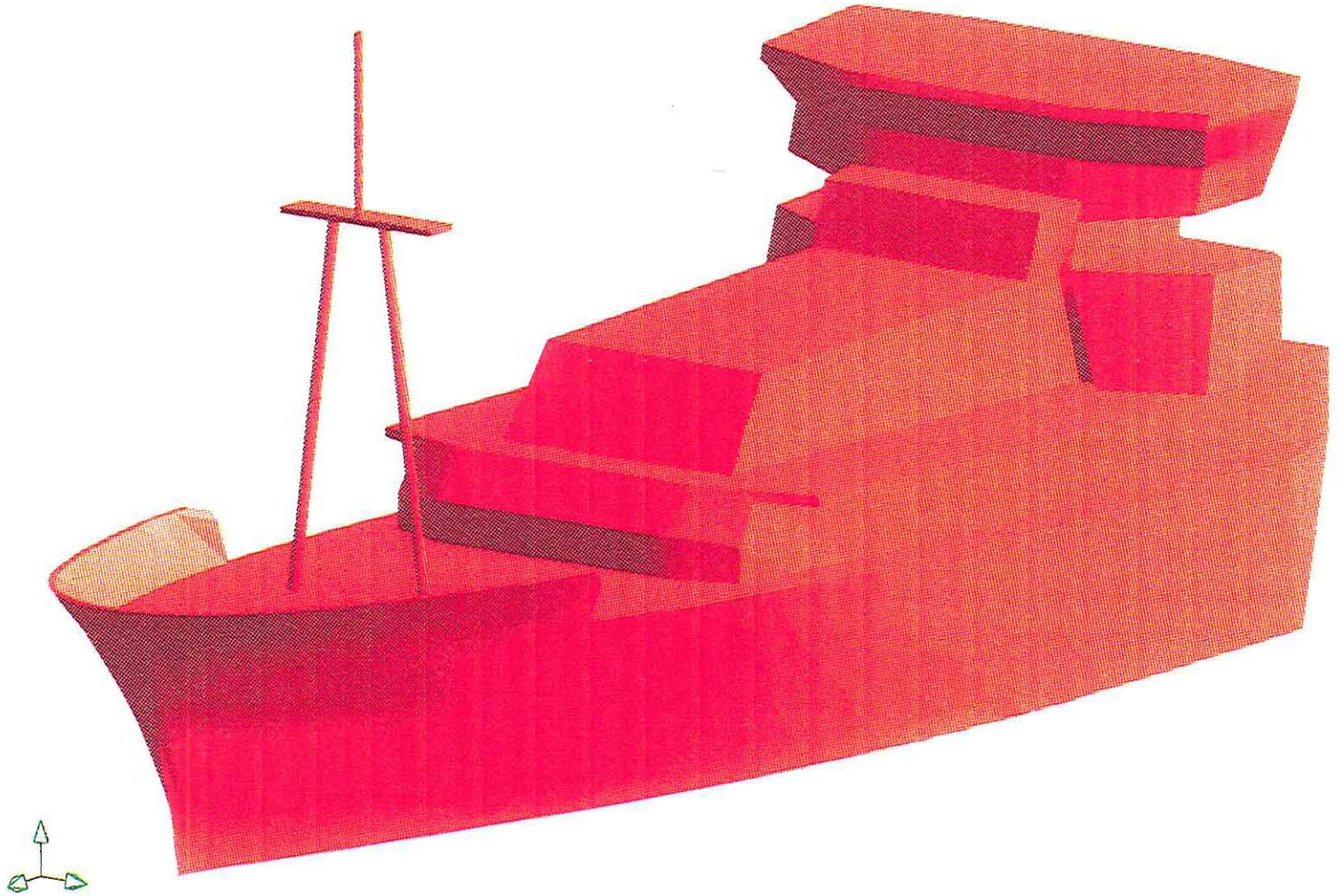

R.R.S. Discovery

HUDALL

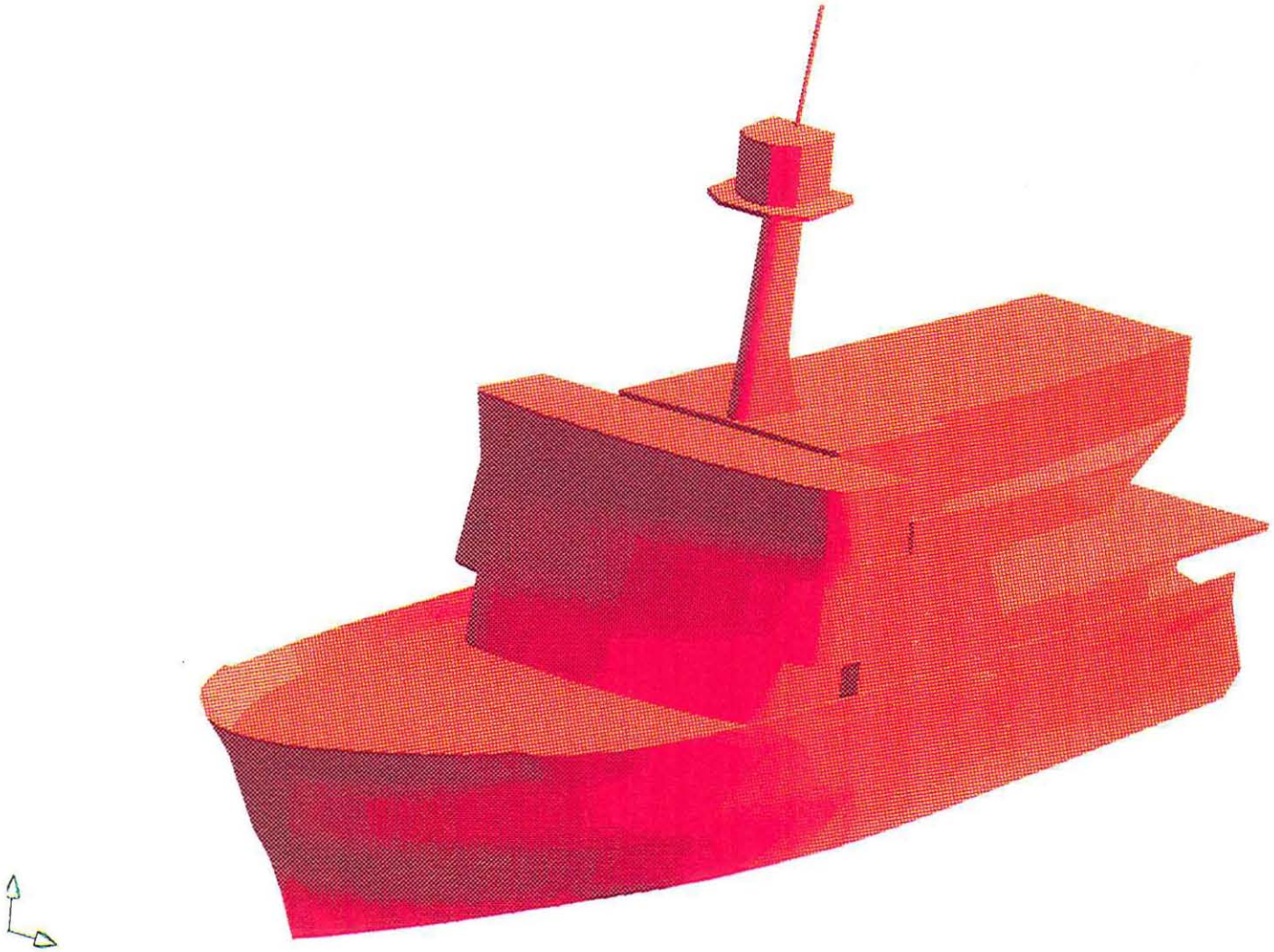

C.S.S. Hudson

DEL: SUROIT

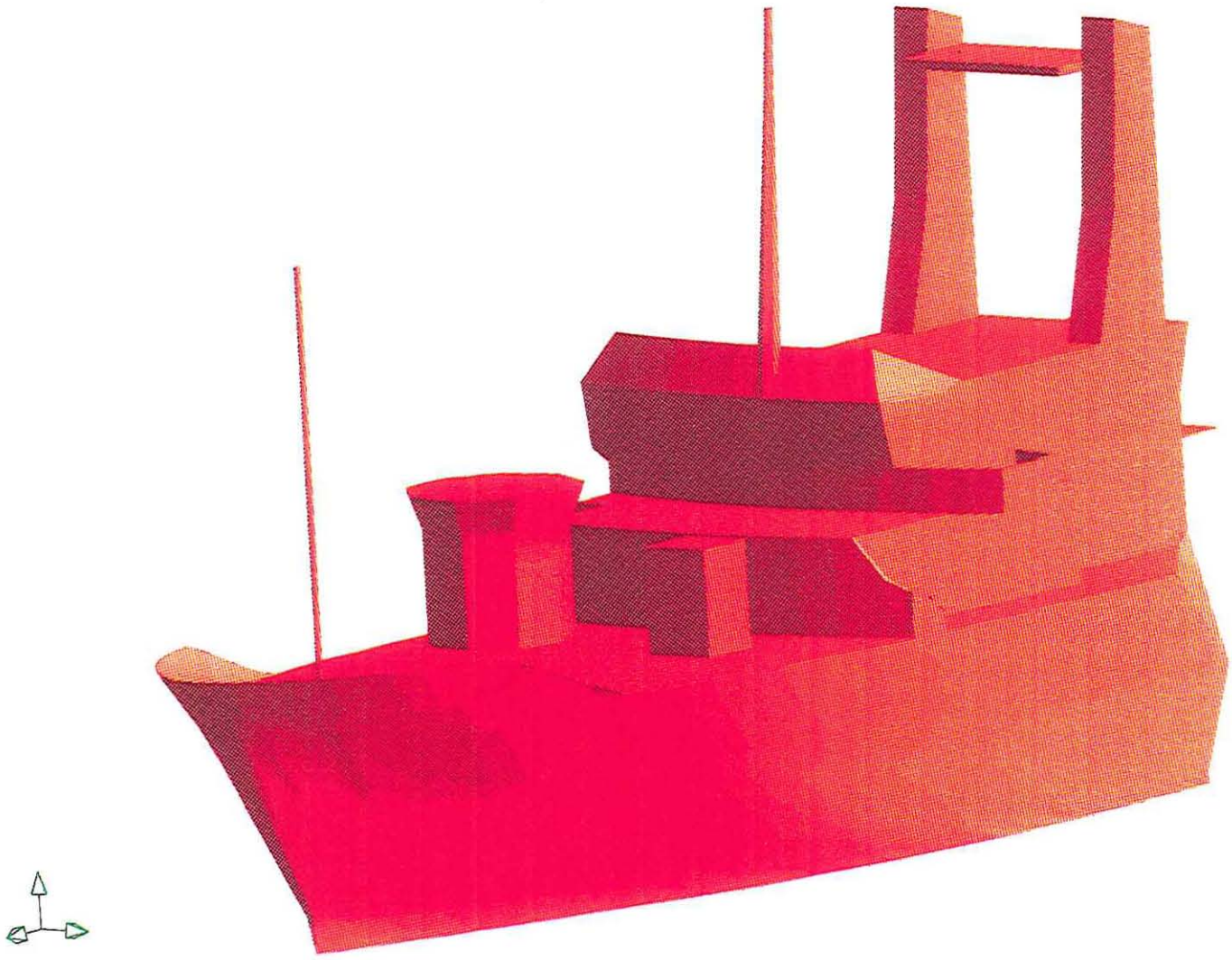

Le Suroit

DEL: WARDSE

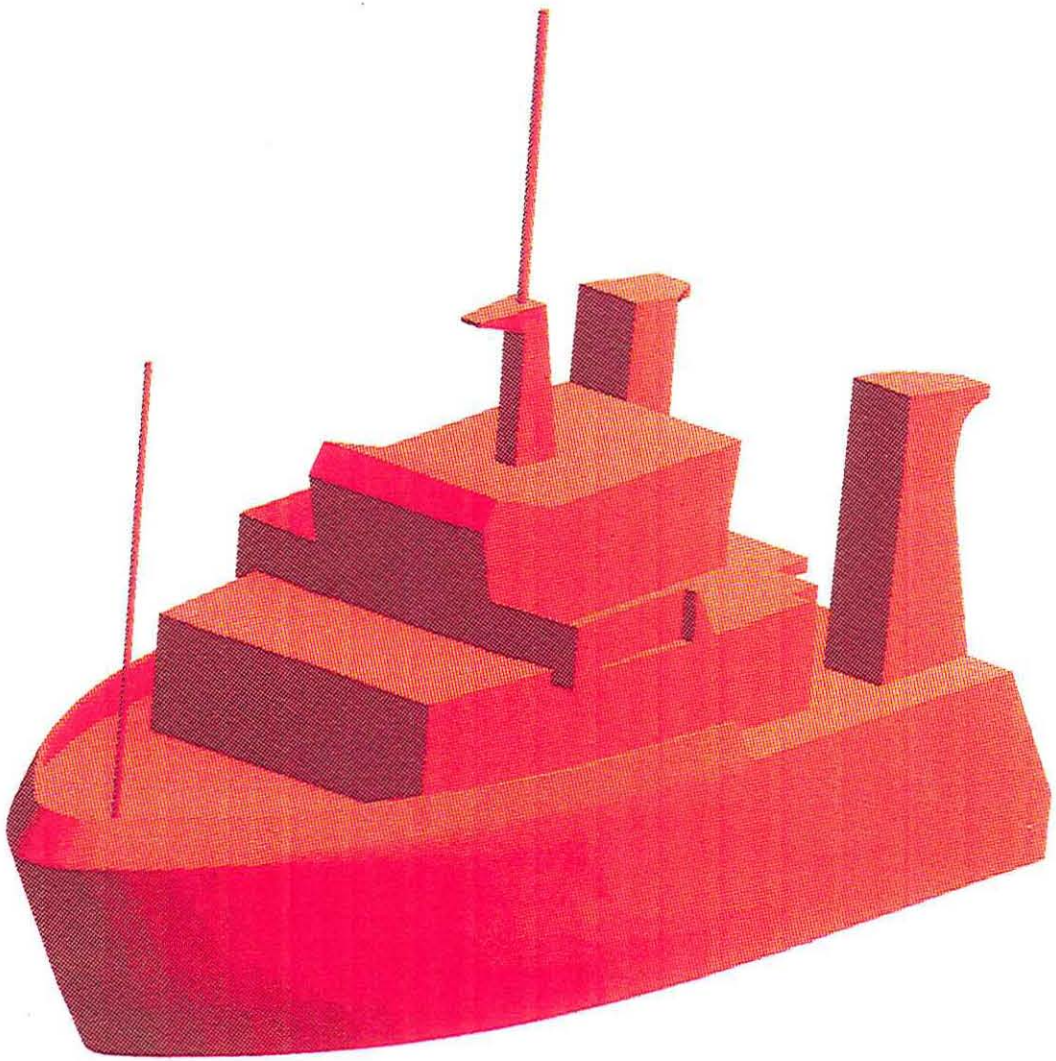

The Warden

13. APPENDIX C - THE ACCURACY OF WIND OBSERVATIONS ON SHIPS

THE ACCURACY OF WIND OBSERVATIONS FROM SHIPS[1]

Peter K. Taylor, Elizabeth Kent, Margaret Yelland, and Ben Moat

James Rennell Centre for Ocean Circulation[2],
Chilworth Research Park,
Southampton, UK

1. Introduction

Wind observations from Voluntary Observing Ships (VOS) are either visual "Beaufort Scale" estimates or obtained by using an anemometer. Although the fraction of reports from each method varies from one ocean area to another, in all areas the percentage of anemometer derived reports has increased with time. Neither method necessarily gives an unbiased estimate of the wind velocity; visual wind estimates depend on calibration against anemometer values, and there are several possible sources of significant, systematic biases in anemometer observations. Given this situation, the aim must be to produce a consistent data set of wind observations in which anemometer and visual derived observations give rise to the same wind speed distributions. Such a data set should eliminate spurious "climatic" trends such as an apparent wind speed increase due to the increased use of anemometers (e.g. Cardone, 1990).

In this paper we will present the results of work at the James Rennell Centre on the accuracy of ship winds, occasionally reviewing other work which, having been published in reports, may not be readily available. Considering sampling issues, we shall briefly review evidence on the percentage mix of visual and anemometer winds (Section 2.1) and comment with regard to the possibility of "fair weather bias" in the VOS wind observations (Section 2.2). Since Ocean Weather Ships have frequently been used as to verify VOS wind estimates we shall report our results from Ocean Weather Station Lima (Section 3). Results from the VOS Special Observing Programme - North Atlantic (VSOP-NA) will be used to compare visual winds (corrected to various Beaufort Scales) to observations from ships equipped with anemometers (Section 4). We will then discuss the accuracy of anemometer wind estimates from ships (Section 5).

2. Sampling Issues

2.1 Percentage of Visual and anemometer winds

Although it is known to contain inaccuracies, Kent et al. (1993) used the List of Selected Ships (WMO, 1990) to estimate that, at about that time, 70% of the global VOS fleet provided visual estimates, 22% used fixed anemometers, and 8% used hand-held anemometers. Which method was used depended principally on which country's meteorological agency had recruited the VOS, for example Germany and the UK advocate visual estimates whereas Japan and the USA use fixed anemometers and France supplies hand-held instruments. Thus, although many VOS operate world-wide, the mix of wind observation methods can be expected to vary from one ocean

---

[1] Prepared for the COADS Winds Workshop, Kiel, 31 May - 2 June 1994.

[2] The James Rennell Centre is a component of the Institute of Oceanographic Sciences Deacon Laboratory

area to another. This is confirmed in the maps of the percentage of anemometer wind reports in the UK Meteorological Office marine data bank. presented by Ive (1987) for each 5 year period from 1960 to 1979; typical values are shown in Figure 1. Cardone et al. (1990) also give the numbers of measured and visual observations for 3 areas, values estimated from their graphs are also shown in Figure 1 together with values from (Ramage, 1987) which, although attributed to the global VOS fleet, are presumed to relate to the S. China Sea.

Several features are apparent from Figure 1. The number of anemometer derived winds has increased more rapidly in the Pacific compared to other ocean areas. Most of the winds from the Atlantic are visual. In the Southern Ocean there are a significant number of anemometer reports, probably from research ships and Antarctic supply vessels. There are problems with the data. Ive (1987) notes that all USA VOS reports for 1975 to 1981 were flagged as visual and this error also appears to be evident in the data of Cardone et al. (1990) for the North Pacific and S. China Sea. The rapid increase in numbers of anemometer winds from the North Atlantic shown by the latter authors also looks suspicious compared to the previous trends.

Figure 1 clearly shows that, unless visual and anemometer winds can be shown to be equivalent, there is the potential for introducing spurious spatial and temporal variations in the calculated wind climate.

2.2 Sampling by Merchant Ships - fair weather bias

The possible existence of fair weather bias must be considered when evaluating visual winds. For example if a Beaufort conversion scale has been derived by comparison of weather ship anemometer and VOS visual wind speed distributions, any fair-weather bias may have been effectively removed from the visual data. Kent and Taylor (1994) noted that the VSOP-NA data set contained fewer observations at high latitudes during the winter months. However this need not have resulted in a bias provided that those observations which were available were randomly distributed with respect to the weather conditions. They tested this possibility by comparing two distributions of wind reports to determine whether the VOS sampled the wind climate at ocean station LIMA (57°N 20°W) in the same way as the weather ship Cumulus which occupies that station. The first distribution was the full set of wind speeds reported by the OWS Cumulus. The second distribution was the subset of OWS Cumulus wind speed reports corresponding to times at which there was a VOS meteorological observation from the 5° by 5° area surrounding LIMA. If more than one VOS report had been received at the same time, the Cumulus report was included in the distribution the appropriate number of times. Figure 2 shows the resulting distributions of wind speed occurrences. Using a χ^2-test the data sets were found to be the same to within 97.5% confidence limits.

Kent and Taylor (1994) therefore concluded that there did not appear to be a significant re-routing of ships during periods of high wind speed in the area around LIMA. Presumably those VSOP-NA ships which travelled further south in winter did so because it was winter rather than because it was rough at the time of their voyage; those that travelled north did so whatever the weather.

3. Accuracy of Ocean Weather Ship wind reports

3.1 Introduction

Wind reports from Ocean Weather Ships have been used for comparison with VOS wind reports by Quayle (1980), Graham (1982) and others, and data from the OWS Cumulus will be used in evaluating the VSOP-NA results (Section 4, below). However the weather ship meteorological observations are generally made to the standard required for weather forecasting rather than climate research. In this section we will therefore report the results of Taylor et al. (1994) which compare research quality wind measurements from the Cumulus with the standard weather ship observations. Both sets of observations were derived from anemometers and may therefore contain some of the errors which will be discussed in more detail in section 5.

3.2 The Data

The *research quality wind data* were obtained during the period April, 1992 to January, 1994, from a sonic anemometer mounted on the port side of the foremast platform. Ten minute averaged "horizontal" wind components and a vector averaged total wind vector were available 4 times per hour. There was negligible difference between these two estimates of the relative wind. The ships motion was recorded from a GPS navigation system. and the ship's head from a flux gate compass, at 2 minute intervals. These data were used to calculate true wind values.

The *standard hourly WMO wind observations* are obtained by a meteorological officer reading an analogue dial. There are two cup-anemometer and wind vanes mounted to either side of the aft mast platform; the windward one is read. The ship speed is obtained from the ship's officer on the bridge, the ship's head from a compass repeater. The true wind is calculated using a hand calculator.

3.3 Ship operating characteristics

Figure 3 illustrates the recorded behaviour of the OWS Cumulus in response to the wind speed climate at Lima. The most likely wind speed is about 10 m/s. For winds up to about 15 m/s the ship usually drifts (sideways with the wind about 10 degrees forward of the port beam) until the edge of the operating area is reached, whereupon the ship steams back to the upwind side of the area. If the wind or sea state is too high (normally above 15 m/s wind speed), the ship heads bow into the wind at slow speed ("hove to"). Note that, while the Met. Office anemometers are well exposed when the ship is drifting, they are situated some distance downwind of the ship's bow when steaming or hove to. The anemometers are, however, at a high level compared to the ships superstructure.

The ship's speed when drifting or hove to is shown in Figure 4. As the wind increases the ship drifts downwind faster. When hove-to the engines are kept at a constant setting; as the wind increases the forward motion decreases.

3.4 Comparison of wind estimates

Wind estimates were compared for relative wind directions from 60° to starboard to 100° to port; this included most of the observations, and ensured that the sonic anemometer had reasonable exposure. Figure 5(a) shows the averaged wind speed difference (Sonic - WMO) as a

function of the true wind speed determined from the sonic data. The sonic and WMO difference was variable but not significantly different from zero when the ship was steaming. The sonic read relatively high when the ship was drifting, and relatively low when the ship was hove-to, compared to the WMO values. This behaviour would be qualitatively explained if the ship's speed were neglected in reporting the true wind. This appears to be confirmed by Figure 5(b) which shows that, when the ship is hove to, the difference between sonic and WMO values corresponds well with the ship speed. When drifting, the difference corresponds to the ship speed plus 0.4 m/s.

3.5 Correction for Cumulus WMO wind observations

Assuming that the sonic anemometer values are correct, Figure 6 shows the correction to be added to the reported winds from Cumulus. Below 10 m/s the reports must be increased by about 0.8 m/s. Above 15 m/s, a decrease of about 0.8 m/s is required. Correcting the data in this way will introduce error into the relatively small number of observations obtained when the ship is steaming.

4. Accuracy of Voluntary Observing Ship visual winds - the VSOP-NA project

4.1 Introduction

Previous studies have compared weather ship data with nearby visual winds (Quayle, 1980, Kaufeld, 1981 and Graham, 1982), compared visual and measured winds from the same ship (Cardone, 1969), or compared wind speed distributions (Quayle, 1980). In analysing the data from the VOS Special Observing Programme - North Atlantic, Kent et al. (1991, 1993) adopted a different method. Each observation from the 46 ships participating in the two year project was matched with the output from a weather forecast model. By using the model as a comparison standard it was not necessary to restrict comparisons to geographically close pairs of observations. Thus it was possible to use all the reports in the VSOP-NA data. The method of wind estimation for each VSOP-NA ship was known, including the position and exposure of any anemometer carried (Kent and Taylor, 1991), and the VSOP-NA ships reported both relative and true wind values.

4.2 Summary of VSOP results

Kent et al. (1993) noted that, for the VSOP-NA ships which used anemometers, the difference of the reported wind from the model value was greater for ships on which the anemometer was situated at a greater height (Figure 7). Having corrected the anemometer winds to 10m, their analysis suggested that the Cumulus winds were biased low at lower wind speeds and also that the model being used as a comparison standard probably underestimated the wind speed by about 1 to 2 m/s (Figure 8). They suggested that visual winds adjusted to the CMM scale are more compatible with anemometer winds than the original estimates based on the Code 1100 scale.

Kent et al., (1991) showed that visual wind observations above 8 m/s were under estimated at night (compared to daytime observations) unless the ship also carried a fixed anemometer. This suggests that the best Beaufort conversion scale would have different values for day and night. However, where a fixed anemometer was carried but visual winds reported, both day and night time values showed similar characteristics to the day time visual winds from ships which did not carry an anemometer. It appeared that the ships officers were not relying solely on the anemometer

at night, but rather using it to ensure consistency in their visual wind estimates. The differences (Figure 9) are of the same order as the difference between the Code 1100 and CMM wind scales.

4.3 Re-analysis of the VSOP-NA results

For this paper the VSOP-NA results have been re-analysed with all wind estimates (anemometer and visual) corrected to the equivalent 10m neutral wind. Height correction was based on the Smith (1988) roughness lengths with the standard Businger-Dyer stability corrections using the observed values of sea surface temperature, air temperature and dew point. For visual winds the Code 1100 estimates represent the 10m wind, the CMM and Kaufeld scales have been corrected from 18m and 25m to 10m respectively. In addition the OWS Cumulus wind estimates have been corrected for the ship motion as discussed in Section 3. Figure 10 shows that the effect of correcting the anemometer wind values was to bring them into closer agreement with the reported Cumulus wind observations. Applying the correction to the Cumulus winds results in close agreement up to about 10 m/s, but increases the difference above about 15 m/s.

The different wind conversion scales are compared to the anemometer wind values in Figure 11a and to the corrected Cumulus reports in Figure 11b. In each case the value is calculated by:

(Average visual wind - model) - (Average anemometer wind - model)

and plotted against model wind speed. In each case the results confirm that, at most wind speeds, the CMM values are to be preferred to the Code 1100 values. For winds below 10 m/s, the CMM scale appears to give better agreement with the anemometer winds than the Kaufeld scale. At higher wind values there is little significant difference between the two scales. Note however that a different conclusion might result if only the night time observations were compared.

5. Errors for anemometer wind measurements on ships

5.1 Introduction

The previous section has shown that, on average, the use of the CMM scale gives better agreement with anemometer wind observations than the use of the Code 1100 scale. However this does not necessarily imply that the CMM scale represents more closely the actual wind speed since anemometer winds may be affected by systematic errors. There are several possible sources of error for anemometer winds measurements. It is not known how well the increasing number of anemometers being deployed have been calibrated or what, if any, measures are taken to ensure that the instruments remain within calibration. In use, the anemometer is exposed to a turbulent flow which fluctuates as the ship rolls and pitches and the anemometer may not be "vertical" with respect to the mean flow. The reported wind is an estimate of the average reading of a fluctuating analogue dial made by the ship's officer. It is not based on 2 minutes, and certainly not on 10 minutes, of observation; 5 seconds seems more likely. Errors are then made in converting to true wind velocity. The following sections will first summarise results from the VSOP-NA experiment concerning anemometer winds (Section 5.2) and then consider the errors likely from ship motion and the airflow disturbance by the ship (Section 5.3). A method of establishing an absolute wind speed calibration will then be suggested (Section 5.4).

5.2 Results from VSOP-NA

Instrument exposure and calibration

The most likely height of an anemometer on a VSOP-NA ship (Figure 12) was about 30m, considerably more than that shown in WMO (1990) for the VOS fleet as a whole. This may be because the VSOP-NA ships carrying anemometers tended to be large container ships. For each ship the anemometer exposure was estimated on a scale from 0 (poorly exposed) to 9 (well exposed) for winds on the bow, beam, and stern. The most likely ship speed at the time of observation was 16 to 18 knots, similar to the most likely wind speed. As a result the relative wind for 73% of observations was from ±45° of the bow and for 97% it was within ±135° from the bow. Thus an anemometer mounted forward of a mast structure would have been shielded for less than 3% of the observations, and 63% of observations achieved the top exposure rating. This does not mean that the anemometer was situated in an undisturbed airflow, for example Figure 13 shows the situation of the anemometer on one of the larger VSOP-NA ships.

It will be shown below that possible mean errors from airflow disturbance by the ship may well be of order 10% or more. In analysing the VSOP-NA results it was not possible to separate these instrument exposure errors from anemometer calibration errors, and the absolute accuracy was difficult to determine. Perhaps the best comparison standard were the OWS Cumulus winds from station Lima. Unfortunately Lima is north of most of the ship routes and it was necessary to assume that the UK Met. Office model was effective in providing a good comparison standard for observations from different areas[1]. With that proviso, and using the wind observations as reported, Kent et al. (1991) found that the VSOP-NA ship reports were about 1 m/s higher than the Cumulus values. Correcting the VSOP-NA ship winds for the height of the anemometer, the observations were on average about 0.8 m/s higher than the reported Cumulus winds (see Figure 10 and discussion above). Correcting the Cumulus reports for the ship's motion resulted in agreement with the anemometer winds up to about 10 m/s; at higher winds the corrected Cumulus values were lower by something under 10%. Thus even with all corrections applied, the VSOP-NA ships appeared to overestimate the winds compared to the Cumulus.

The VSOP-NA results showed that wind speed estimates obtained using hand-held anemometers were different in character to those from fixed instruments. Below about 7m/s, wind speeds from hand-held anemometers gave similar results to the visual wind observations based on the Code 1100 scale. At higher wind speeds few observations were obtained, and these showed large scatter.

Concerning wind direction, the mean differences from the model values were within ±5° for most ships with no obvious bias. Mean difference for ships using wind vanes were similar to and sometimes larger than the values for ships using visual estimates.

Calculation of true wind

The VSOP-NA results showed that a significant and unnecessary error was introduced because officers on ships using anemometers must perform the vector subtraction of the ships

---

[1] This may have not been the case since the OWS Cumulus wind observations would have been given greater weight when assimilated into the model; however tests suggested this was not a significant factor.

velocity from the measured relative wind. Since the most frequently occurring wind speed values were similar to or less than the ships' speeds, large errors could result if this calculation was not performed correctly. The VSOP-NA ships had been requested to report ships speed and head, and the relative wind speed and direction, in addition to the true wind values. Thus this calculation could be tested for about 2500 anemometer based reports. The method used was to calculate the value of the relative wind implied by the true wind report together with the ship's speed and head at the time of observation. This was compared to the relative wind reported. Only about 50% of the reported winds corresponded to calculated relative winds within ±1 m/s of the observed value. A large fraction of the reports (about 25%) were more than ±2.5 m/s different. For wind direction only 70% were within ±10°, and 13% were outside ±50°.

5.3. Errors sources for anemometer winds

Errors due to ship roll and pitch

Ramstorf (1988) assessed the likely anemometer errors due to ships roll because of (i) "anemometer pumping", (ii) the tilt of the anemometer, and (iii) the variation of height in the near surface wind gradient, and demonstrated that only the first of these has the potential to contribute an error significantly above 1%. The wind error due to anemometer pumping is a function of:

$$\frac{\text{(anemometer height above roll axis) x (roll angle)}}{\text{(roll period)}}$$

Thus Figure 15 shows the percentage wind speed error for three cases for which possible combinations of anemometer height, roll angle, and roll period are shown in Table 1. The errors are largest for case (c) which might represent a research vessel with a cup anemometer at 20m rolling through 10° with 5 second period. VOS are perhaps more likely to be represented by cases (a) or (b), for example an anemometer at 40m on a ship with a 20 second roll through 5°. In these cases the errors remain small under most conditions and negligible compared to probable air-flow disturbance effects.

Anemo Ht	Case (a)		Case (b)		Case (c)	
(m)	Roll (°)	Period (sec)	Roll (°)	Period (sec)	Roll (°)	Period (sec)
10	5	5	10	5	16	4
20	5	10	10	10	10	5
40	5	20	10	20	10	10

Table 1. Possible combinations of anemometer height above roll axis (m), roll amplitude (degrees) and roll period (seconds) for the three cases shown in Figure 15.

Errors due to airflow disturbance.

Attempts to determine the wind error at anemometer sites on research ships due to the airflow disturbance due to the ship were summarised by Taylor (1985). Based on comparisons with meteorological buoys (Augstein et al., 1974; Large and Pond, 1982), or with bow boom anemometers (Ching, 1976; Kidwell and Seguin, 1978), he concluded that for relative winds within ±45°of the bow, ±5% was a reasonable accuracy estimate. For winds from other directions

significantly different errors might occur. More recently, wind tunnel studies have been reported by Blanc (1986; 1987) for two naval ships, and Surry et al. (1989) and Thiebaux (1990) for Canadian research ships.

Although referring to a guided missile cruiser, the study of Blanc (1987) is perhaps closest in terms of ship shape and size to a VOS. The errors in speed at the anemometer (Figure 16) show the effects of the main mast which is directly downwind of the anemometer for a relative wind direction of about 100°, and the wake of a smaller obstruction at 90° relative wind. However these effects appear to be super-imposed on an overall wind increase of about 9% which presumably represents the combined effects of the ship's superstructure and of a large radar antenna near the anemometer location. For comparison Figure 17 shows wind errors calculated using the model of Wucknitz, (1977). The wind tunnel results for three Canadian survey ships (Thiebaux, 1990) also show an increased wind speed at the main mast site of typically 5 to 10% for most relative wind directions.

Increased wind speeds of this magnitude at typical anemometer heights above the ships accommodation block have also been predicted by numerical modelling. Kahma and Lepparanta (1981) used a potential flow model to predict errors of about 15% at the mast anemometer site on a small research vessel, the R/V Aranda. Dupuis (1994) has used a two-dimensional turbulent flow model to predict a wind speed increase of about 20% at the main mast anemometer site on the research ship le Suroit. The use of three-dimensional computational fluid dynamics (CFD) to model the airflow over a ship is being evaluated at the James Rennell Centre. Initially the aim is to simulate the wind tunnel results of Thiebaux (1990) (and field results of Anderson, 1993) for the survey ship CSS Dawson. The preliminary results (Ricardo, 1994), Figure 18, have been calculated for winds on the bow and have reproduced the wind tunnel results for two anemometer sites to within about 2%.

In summary, for research ships and similar vessels, most studies show that an anemometer positioned on a mast above the accommodation is likely to over-read to order 10% or so. This applies for all wind directions except where the anemometer is in the wake of the mast. The only studies showing a significant underestimate are comparisons with a bow boom by Ching (1976), and comparisons with a buoy (Augstein et al., 1974), in both cases when the wind was on the beam. The Ching (1976) result could be due to errors in the bow boom data. The Augstein et al. (1974) results seem harder to explain; for the same ship Ramstorf (1988) found an over-estimate of order 10% for beam winds. Whether an anemometer on a VOS (see for example, Figure 13), would under-read or over-read is not known. Numerical simulations of typical VOS shapes would give some indication but we know of no such studies in progress or planned. The evidence presented in section 4.3 (Figure 10) suggests that, after correction for the instrument height, VOS anemometers may read high compared to the OWS Cumulus, at least for wind speeds above 10m/s.

5.4 Toward an absolute wind calibration

Given the difficulty of obtaining accurate wind measurements even from an ocean weather ship or research ship, an alternative standard for wind speed measurements must be sought. Meteorological buoys do not present the air-flow disturbance seen on ships. However it is difficult to ensure that the anemometer remains well calibrated over an extended period of time, and care is necessary in allowing for buoy motion and in the correction for the very low instrument height. If we assume that the quantity that is really required is the wind stress, then an alternative calibration

method is suggested by the results of Yelland et al. (1994). By comparing different anemometers mounted on the foremast of a research ship, they concluded that, whereas wind stress could be estimated to a consistency of about 5% using the inertial dissipation method, stress estimates based on the mean wind and the bulk aerodynamic formula are likely to have errors of order 20 to 30%. By equipping a subset of VOS with instrumentation to make inertial dissipation estimates of the wind stress, a wind velocity climatology could be produced using a specified drag coefficient formulation. Wind observations which were adjusted to be consistent with this climatology would then automatically produce the correct wind stress value. Suitable automatic instrumentation is available for wind stress estimation but the cost of the fast response anemometers and processing systems needed would be large compared to the cost of standard VOS instrumentation.

6. Summary

The percentage of anemometer derived wind reports has increased with time to a varying extent in different ocean areas. To prevent spurious temporal or spatial variations in the marine wind climate it is important that anemometer and visually estimated winds are compatible. Ocean weather ships might be expected to provide an accurate wind velocity estimate with which to calibrate VOS winds. However by operating a sonic anemometer and GPS navigation system on the OWS Cumulus we have detected systematic errors in the wind reports of order 1 m/s. These appear to be caused by the neglect of the correction for the, relatively small, ship speed when drifting or hove to. Using the Cumulus wind observations and the sampling frequency achieved by the VOS, we can detect no fair weather bias in the wind reports from the area around ocean station Lima.

The accuracy of VOS wind reports was examined in the VSOP-NA project. All the visual wind scales examined (Code 1100, CMM IV, and Kaufeld) showed wind difference trends when compared with both OWS Cumulus data and with VOS anemometer data. Code 1100 gives significantly larger wind values at higher wind speeds. The closest agreement between VOS visual wind estimates, and VOS or Ocean Weather Ship anemometer derived winds, was obtained using the CMM IV scale. Visual winds at night under estimated the higher wind speed ranges: this should be investigated further.

For anemometer derived winds from the VSOP-NA ships, significant errors were introduced during the calculation of the true wind speed from the observed relative wind. Correcting for the height of the anemometers improved the consistency of the data set. Having applied all corrections the VOS anemometer derived winds agreed with the OWS Cumulus winds at wind speeds below about 10 m/s; at higher wind speeds the VOS winds appeared to be stronger. The anemometers on the VSOP-NA ships were generally well exposed and it is unlikely that the roll and pitch of the ship resulted in significant error. However field calibrations, wind tunnel studies, and numerical models suggest that, for research ships, an anemometer situated on the main mast is likely to be in error by order 10%. Usually the wind speed is over estimated. The magnitude and sign of this airflow disturbance error for a typical VOS ship is not known. It could be estimated using computer modelling techniques of the sort we are developing for research ships.

At present we have no absolute calibration for marine winds. Estimates of the wind stress using the inertial dissipation method could be used to calibrate marine winds. However the cost of the instrumentation systems would be significant.

7. References

Anderson, R. J., 1993: A study of wind stress and heat flux over the open ocean by the inertial dissipation method. *J. Phys. Oceanogr.*, 23(10), 2153 - 2161.

Augstein, E., H. Hoeber and L. Kruegermeyer, 1974: *Fehler bei Temperatur-, Feuchte- und Windmessungen auf Schiffen in tropischen Breiten.* Meteor Forschungsergebnisse B9, 1 - 10.

Blanc, T. V., 1986: *Superstructure flow distortion corrections for wind speed and direction measurements made from Tarawa Class (LHA1-LHA5) ships.* NRL Report 9005, Naval Research Laboratory, Washington, D.C., 20 pp.

Blanc, T. V., 1987: *Superstructure flow distortion corrections for wind speed and direction measurements made from Virginia Class (CGN38-CGN41) ships.* Report 9026, Naval Research Laboratory, Washington, D.C., 24 pp.

Cardone, V. J., 1969: *Specification of the wind distribution in the marine boundary layer for wave forecasting.* , New York University.

Cardone, V. J., J. G. Greenwood and M. A. Cane, 1990: On trends in historical marine wind data. *Journal of Climate*, 3, 113 - 127.

Ching, J. K. S., 1976: Ship's influence on wind measurements determined from BOMEX mast and boom data. *J. Appl. Meteorol.*, 15(1), 102 - 106.

Dupuis, H., 1994: *Wind speed errors for the research ship le Suroit.* (personal communication).

Graham, A. E., 1982: Winds estimated by the Voluntary Observing Fleet compared with instrumental measurements at fixed positions. *Meteorol. Mag.*, 111, 312-327.

Ive, D. S., 1987: *A comparison of numbers of visually estimated and instrumentally measured wind data, Marine Technical Note No. 2, Revised February 1987,* UK Meteorological Office, Bracknell, 43pp.

Kahma, K. K. and M. Lepparanta, 1981: On errors in wind speed observations on R/V Aranda. *Geophysica*, 17(1-2), 155-165.

Kaufeld, L., 1981: The development of a new Beaufort equivalent scale. *Meteorol. Rundsch.*, 34, 17-23.

Kent, E. C. and P. K. Taylor, 1991: *Ships observing marine climate - a catalogue of the Voluntary Observing Ships Participating in the VSOP-NA.* Marine Meteorology and Related Oceanographic Activities 25, World Meteorological Organisation, Geneva, 123 pp.

Kent, E. C. and P. K. Taylor, 1993: A comparison of heat flux estimates for the North Atlantic ocean. *J. Phys. Oceanogr.*, (submitted).

Kent, E. C., P. K. Taylor, B. S. Truscott and J. A. Hopkins, 1993: The accuracy of Voluntary Observing Ship's Meteorological Observations. *J. Atmos. & Oceanic Tech.*, 10(4), 591 - 608.

Kent, E. C., B. S. Truscott, J. S. Hopkins and P. K. Taylor, 1991: *The accuracy of ship's meteorological observation - results of the VSOP-NA.* Marine Meteorology and Related Oceanographic Activities 26, World Meteorological Organisation, Geneva, 86 pp.

Kidwell, K. B. and W. R. Seguin, 1978: *Comparison of mast and boom wind speed and direction measurements on US GATE B-Scale Ships.* NOAA Tech. Rep. EDS 28, CEDDA, Washington, D.C., .

Large, W. G. and S. Pond, 1982: Sensible and Latent Heat Flux Measurements over the Ocean. *J. Phys. Oceanogr.*, 12, 464-482.

Quayle, R. G., 1980: Climatic Comparisons of Estimated and Measured Winds from Ships. *J. Appl. Meteorol.*, 19, 142-156.

Ramstorf, S., 1988: *Wind observations from RV Rapuhia.* Physics Section report (Internal Report 88/2), Division of Marine & Freshwater Science, DSIR, Wellington, New Zealand. 12 pp.

Ricardo, 1994: *CFD analysis of airflow over the CSS Dawson.* (unpublished report) , Ricardo Consulting Engineers Ltd., Shoreham, U.K .

Smith, S. D., 1988: Coefficients for Sea Surface Wind Stress, Heat Flux and Wind Profiles as a Function of Wind Speed and Temperature. *J. Geophys. Res.*, 93, 15467-15474.

Surry, D., R. T. Edey and I. S. Murley, 1989: *Speed and direction correction factors for shipborne anemometers.* Engineering Science Research Report BLWT-SS9-89, Univ. of Western Ontario, London, Ontario, 83 pp.

Taylor, P. K., 1985: TOGA surface fluxes of sensible and latent heat by in situ measurement and microwave radiometry. *Third session of the JSC/CCCO TOGA Scientific Steering Group.* Scripps Institution of Oceanography, La Jolla, Ca., WMO, Geneva, 30pp. & figs.

Taylor, P.K., Kent, E.C. and Yelland, M.J. (1994) The accuracy of meteorological measurements from an ocean weather ship (in preparation)

Thiebaux, M. L., 1990: *Wind tunnel experiments to determine correction functions for shipborne anemometers.* Canadian Contractor Report of Hydrography and Ocean sciences 36, Bedford Inst. Oceanography, Dartmouth, Nova Scotia, 57 pp.

WMO, 1990: *International list of selected, supplementary and auxiliary ships.* , World Meteorological Organisation, Geneva.

Wucknitz, J., 1977: Flow distortion by supporting structures. : *Air-sea interaction: Instruments and methods*, F. Dobson, L. Hasse and R. Davis, Ed., Plenum Press, 605 - 621.

Yelland, M. J., P. K. Taylor, I. E. Consterdine and M. H. Smith, 1994: The use of the inertial dissipation technique for shipboard wind stress determination. *(accepted by J.Atmospheric Ocean Technology)*

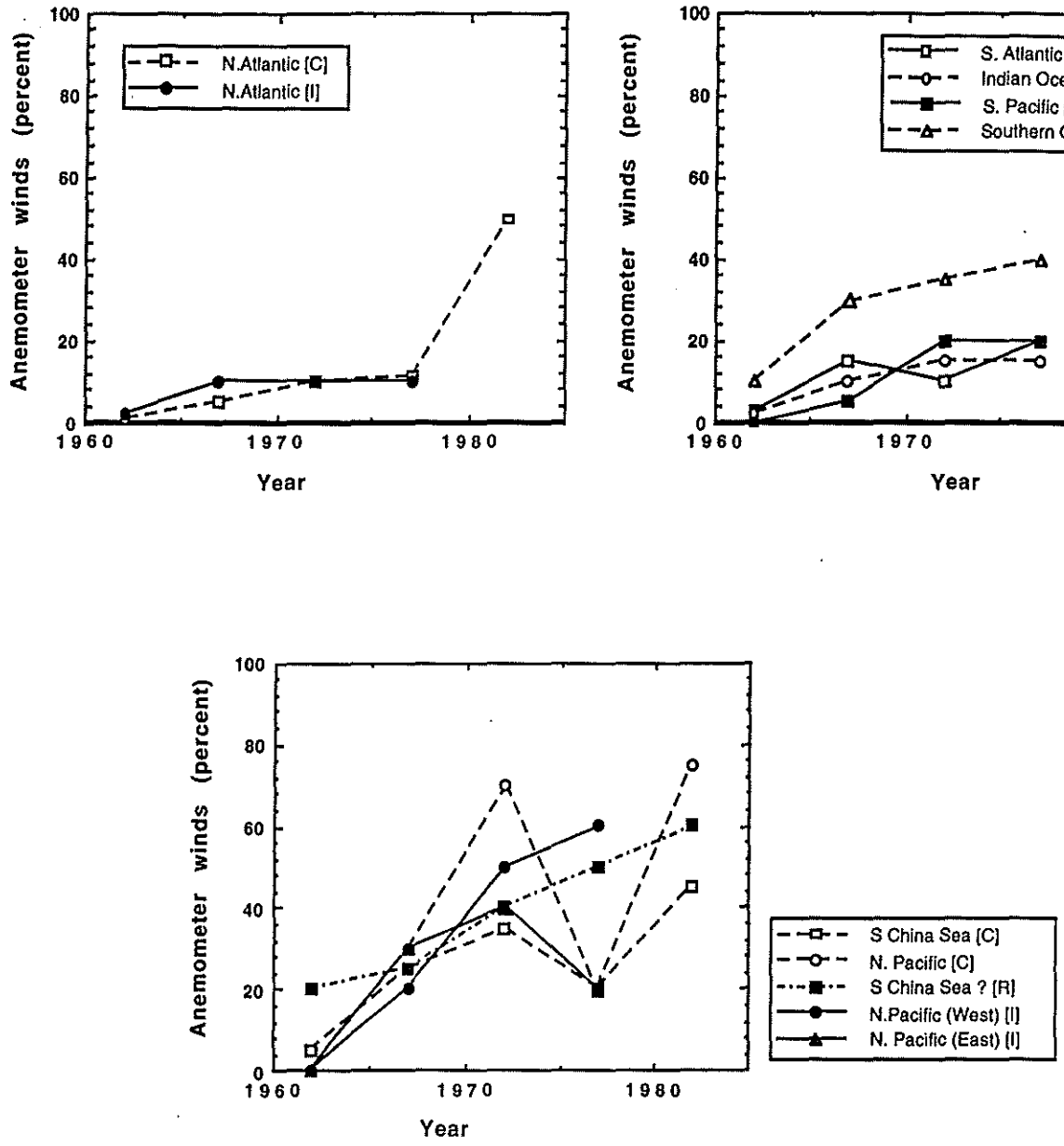

Figure 1. Percentage of anemometer wind reports for different ocean areas for 5 year periods from 1960 to 1985. The values have been roughly estimated from [C] Cardone et al., (1990), [I] Ive, (1987), [R] Ramage, (1987). The areas shown are (a) N. Atlantic, (b) Indian and southern hemisphere oceans, (c) N. Pacific regions.

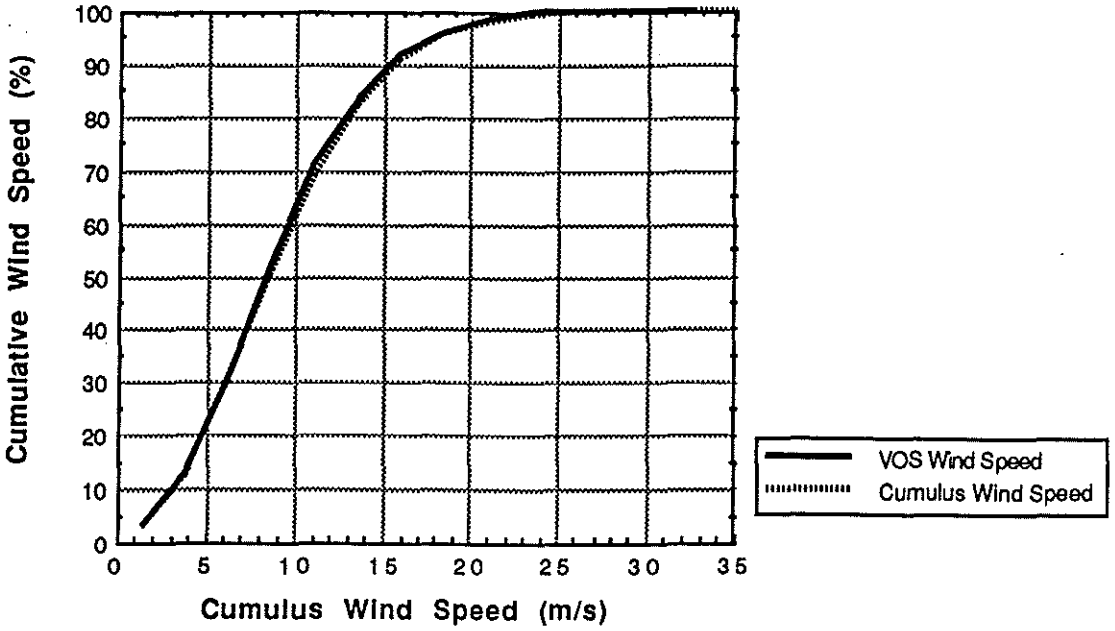

Figure 2. Cumulative percentage distribution of OWS Cumulus wind data and VOS wind data as a function of OWS Cumulus wind speed (m/s) at the time of the VOS observation.

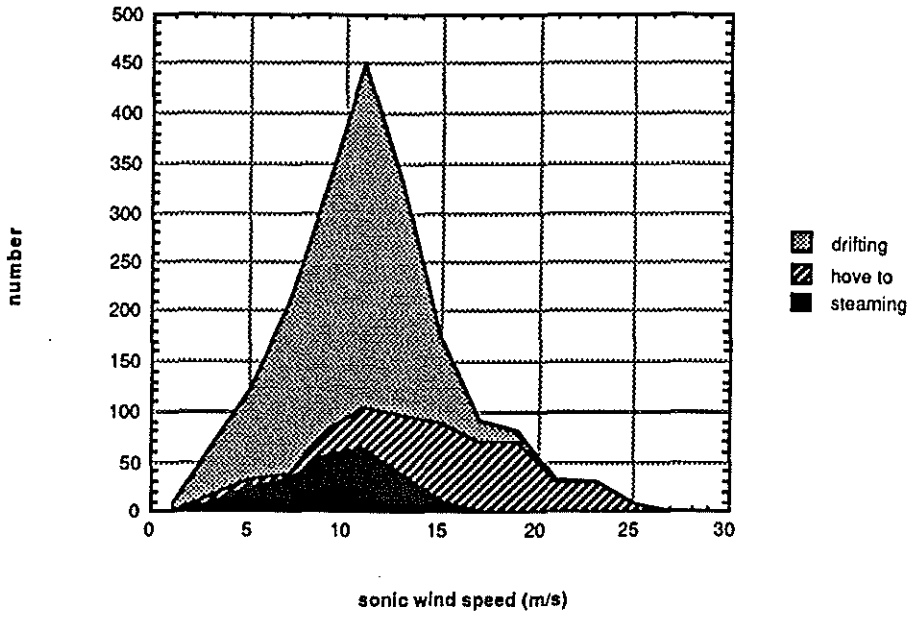

Figure 3. Area plot of wind speed occurrences from the Sonic anemometer data from OWS Cumulus. The number of occurrences is shown for each 2 m/s interval. The shaded area represents the contribution to the total number of cases obtained at each wind speed when the ship was drifting, steaming, or hove to.

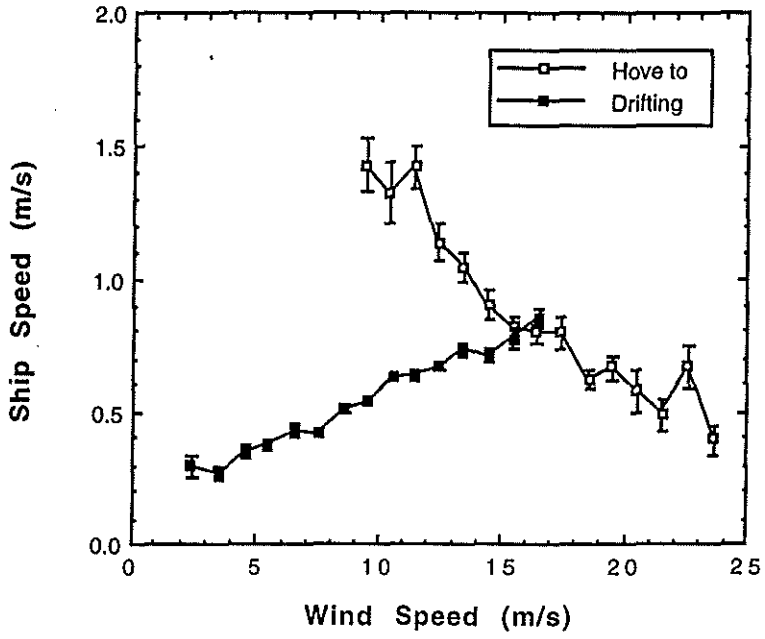

Figure 4. Mean ship speed (m/s) when drifting or hove-to plotted against the true wind speed derived from the sonic anemometer and GPS data.

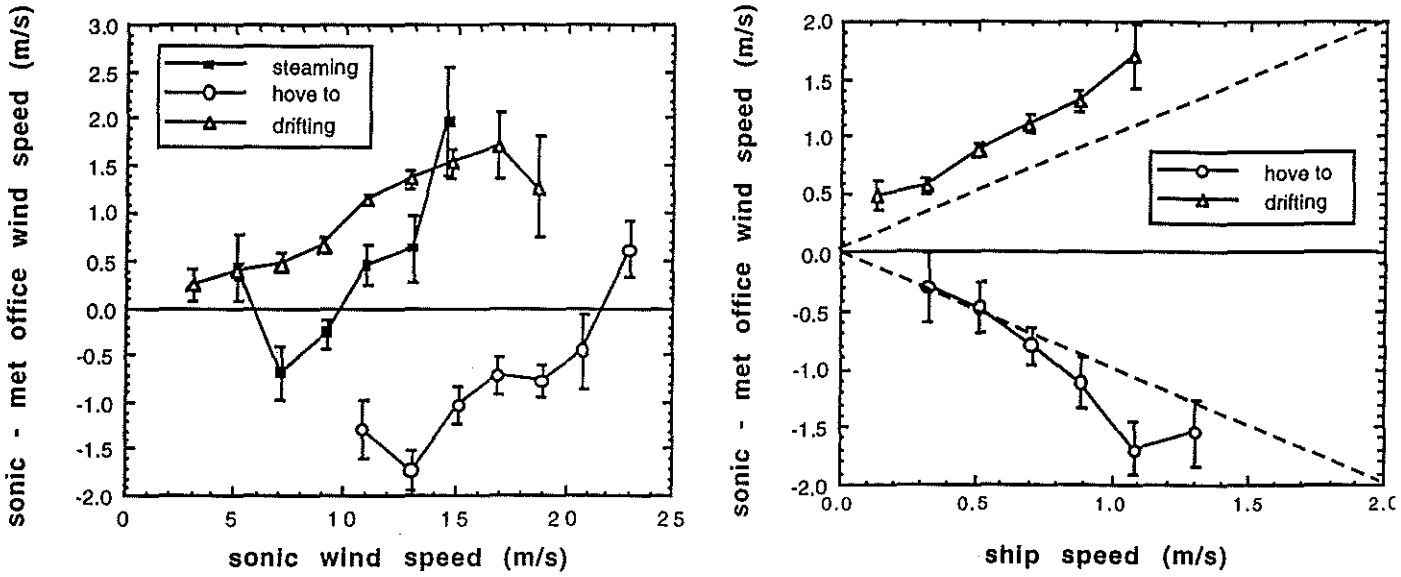

Figure 5 (a). Averaged difference between the wind speed reports, (Sonic - WMO), plotted against the true wind speed derived from the sonic anemometer and GPS data.

(b) Averaged difference between the wind speed reports , (Sonic - WMO), when the ship is hove-to or drifting plotted against the ship speed.

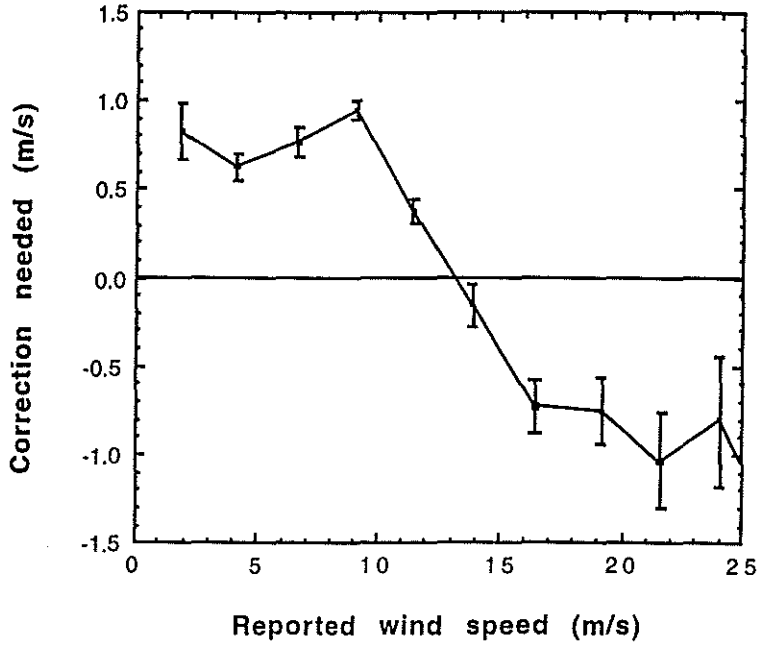

Figure 6. Correction to be added to Cumulus WMO wind observations calculated as a function of the uncorrected WMO observation.

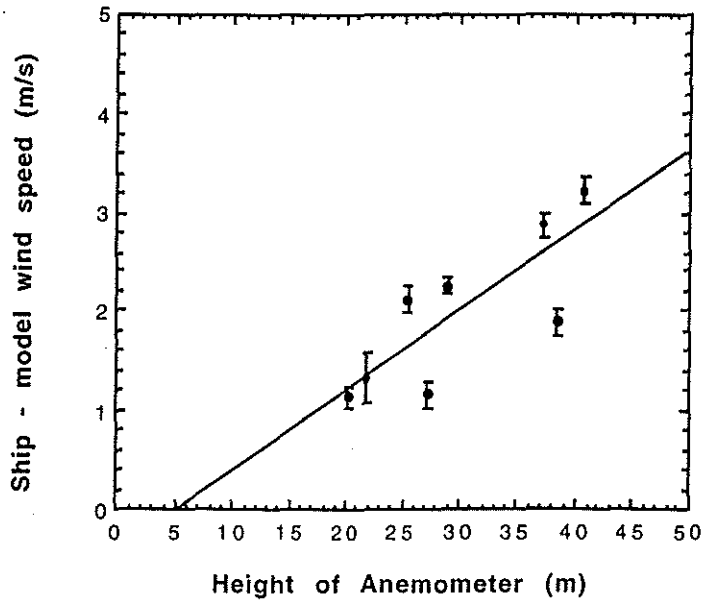

Figure 7. Average difference between the reported wind and the model value for VSOP-NA ships which used fixed anemometers plotted against the height of the anemometer (adapted from Kent et al., 1993).

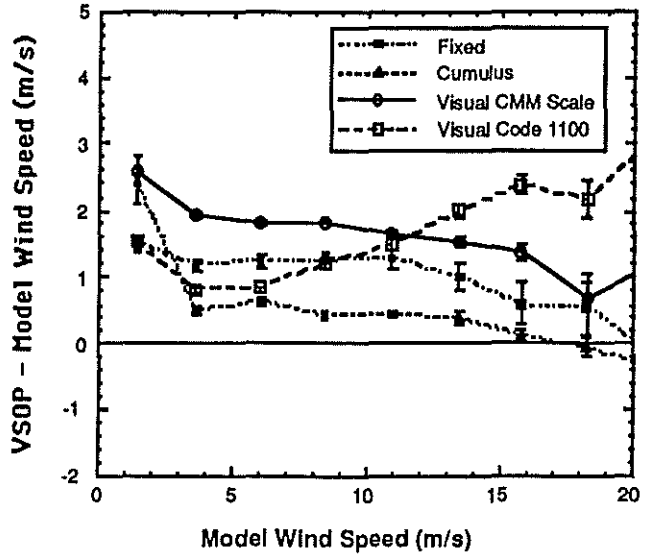

Figure 8 The mean difference in wind speed measurements (VSOP-NA ship minus model value, m/s) plotted against the model wind speed value. The results from fixed anemometers have been corrected for the anemometer height. The visual estimates have been corrected to the CMM Beaufort scale. (The dashed line represents the visual values using the Code 1100 scale). Also shown are the anemometer data for the Ocean Weather Ship Cumulus. (From Kent et al., 1993))

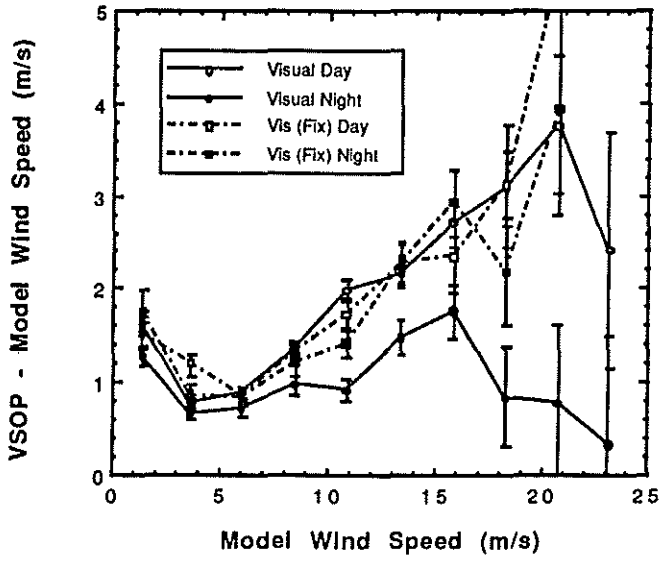

Figure 9. VSOP measured wind speed (m/s) binned on model wind speed (m/s) separately for visual winds reported on ships with and without fixed anemometers and for day and night observations. (From Kent et al., 1991)

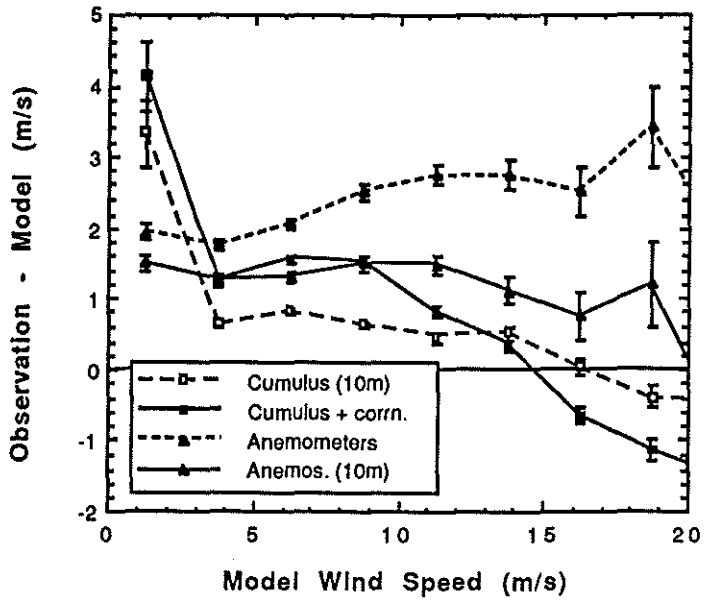

Figure 10. Average difference between the reported wind and the model value for VSOP-NA ships which used anemometers both before and after correcting to the 10m neutral wind values. Also shown are the difference for the Cumulus, corrected to 10m height, both before and after correction for ship motion. Uncorrected values are joined by broken lines, corrected values by full lines.

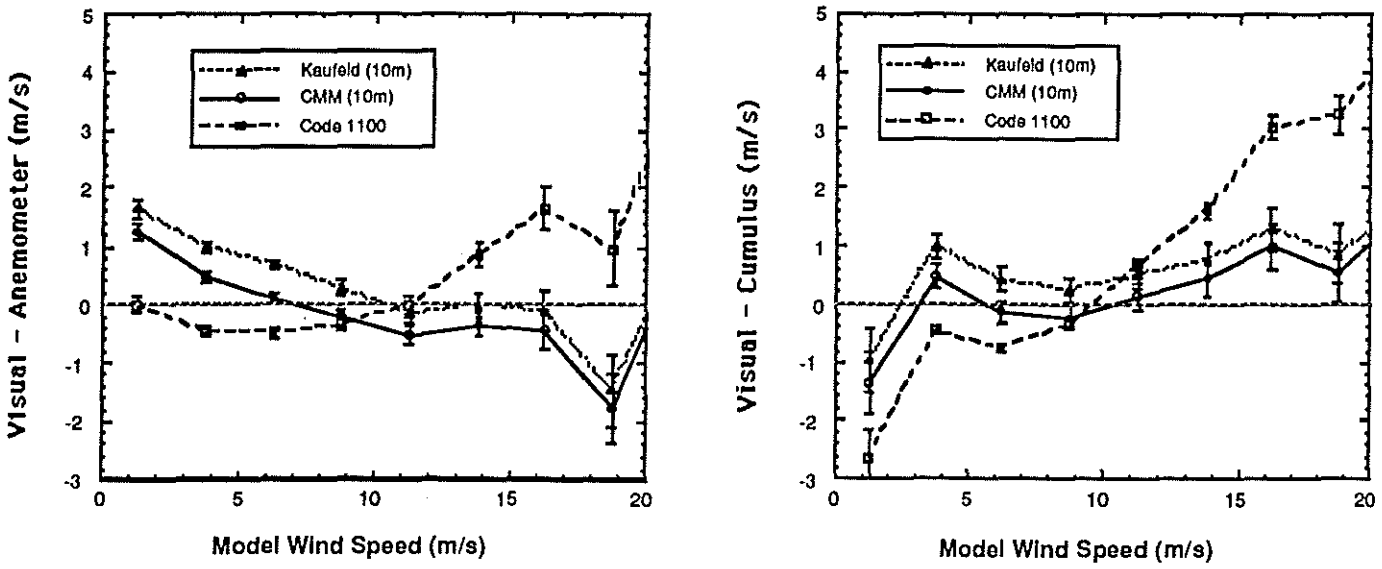

Figure 11. Average difference between 10m neutral values for visual winds corrected to different conversion scales and anemometer derived values. (a) Anemometer values from the VSOP-NA ships. (b) Anemometer wind estimates from the OWS Cumulus (corrected for ship motion).

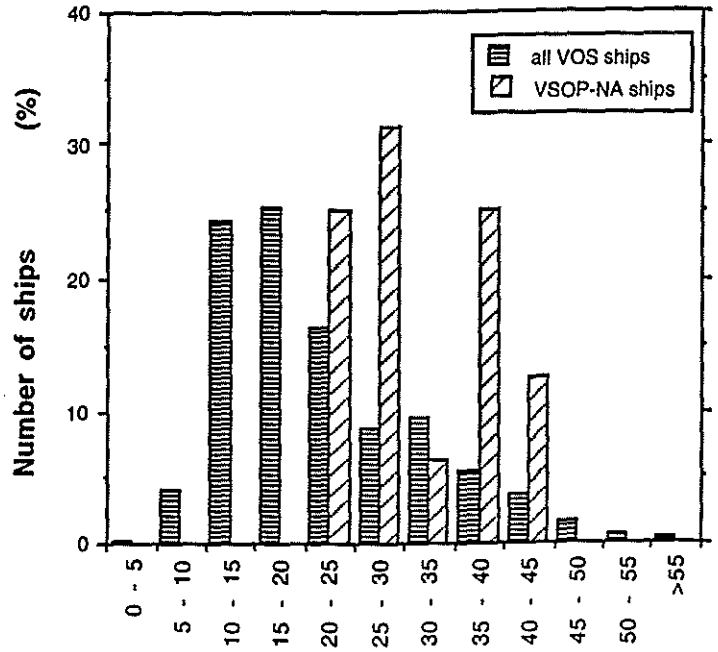

Figure 12. Anemometer heights for the VSOP-NA ships and for the whole of the VOS fleet (from Kent and Taylor, 1991)

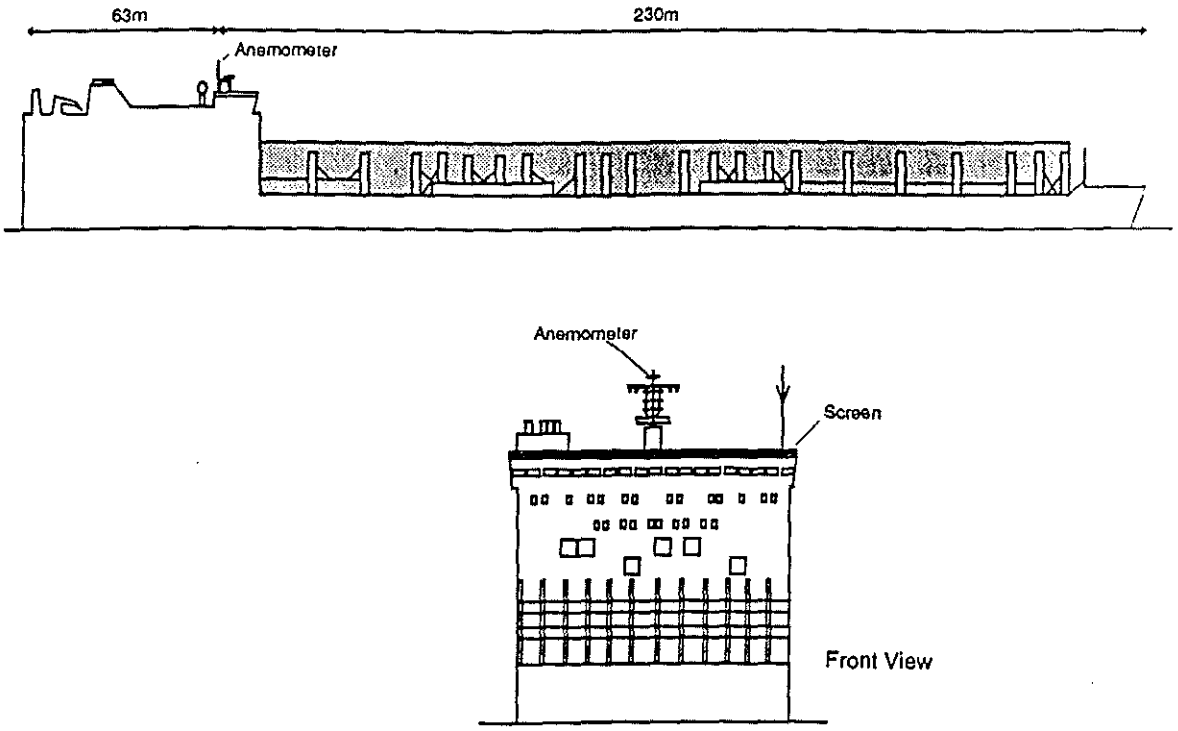

Figure 13. Situation of the anemometer on one of the VSOP-NA ships, the Atlantic Cartier. The anemometer was about 40m above sea level.

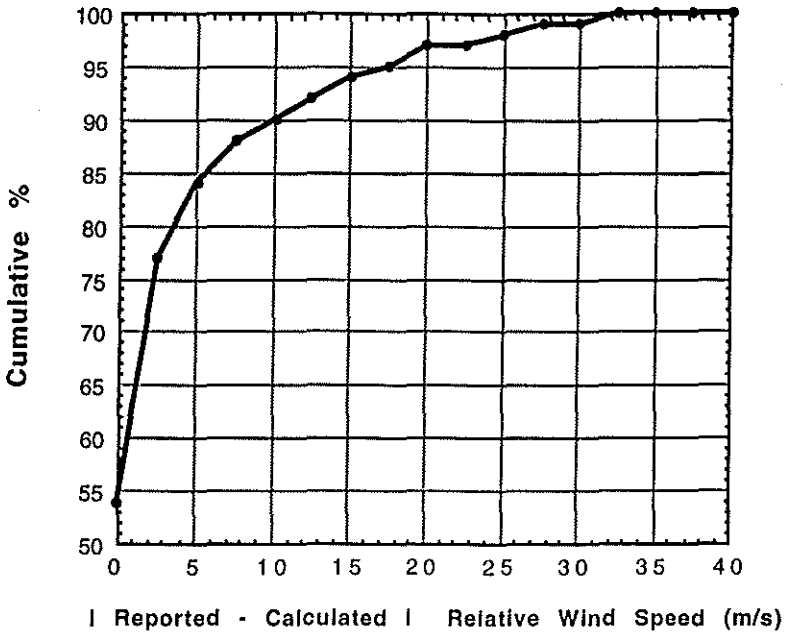

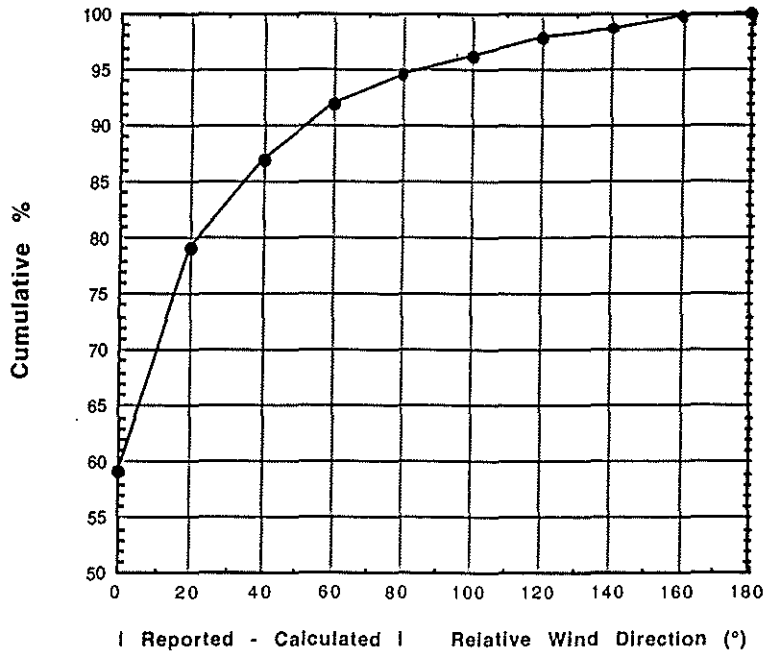

Figure 14 Cumulative percentage plot of the difference in the relative wind reported by the VSOP-NA ship and the relative wind calculated from the reported true wind velocity together with the ship's heading and speed at the time of the observation. (a) wind speed; (b) wind direction.

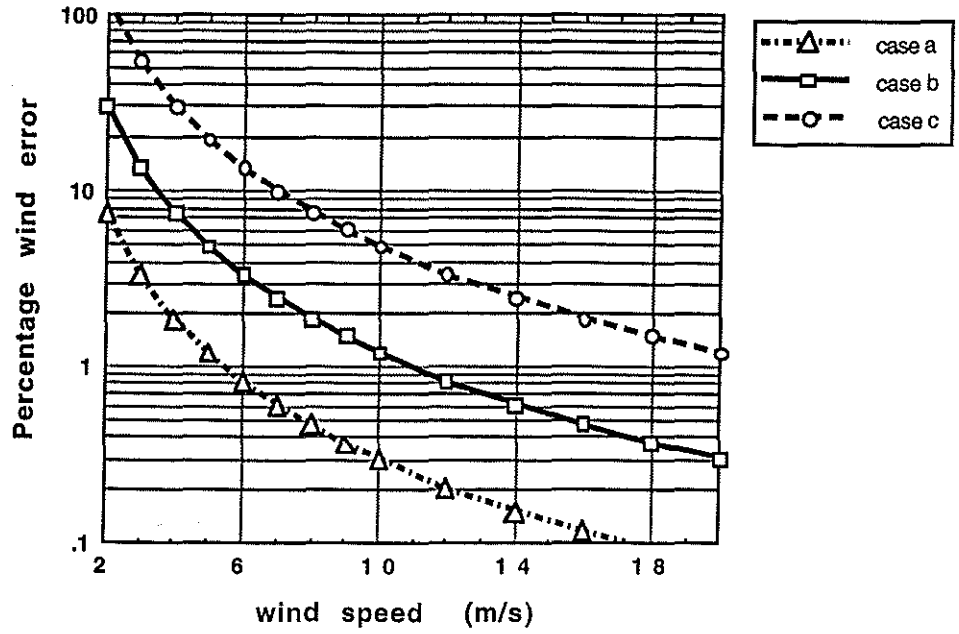

Figure 15 Percentage wind speed error due to anemometer pumping by the ship's roll for three cases (see text).

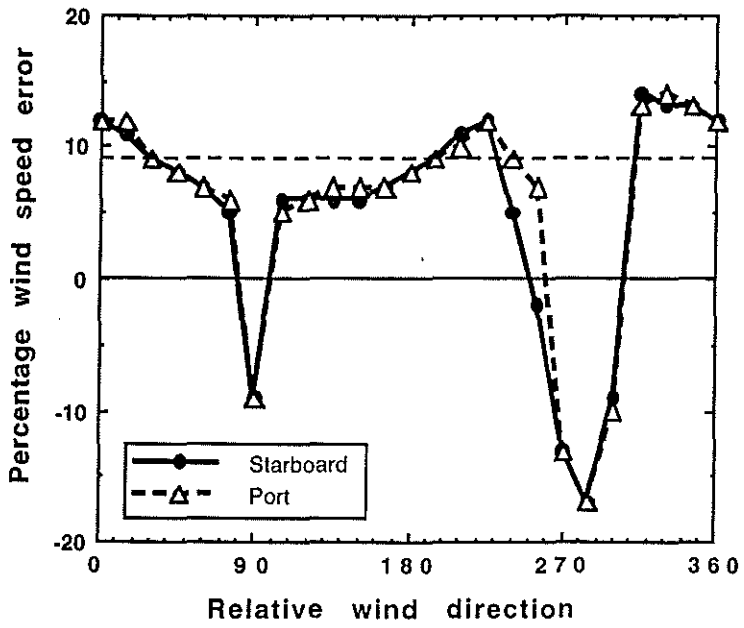

Figure 16. Percentage wind error from the wind tunnel study of Blanc (1987). The data from the port anemometer has been plotted as if the anemometer were situated in the starboard anemometer position.

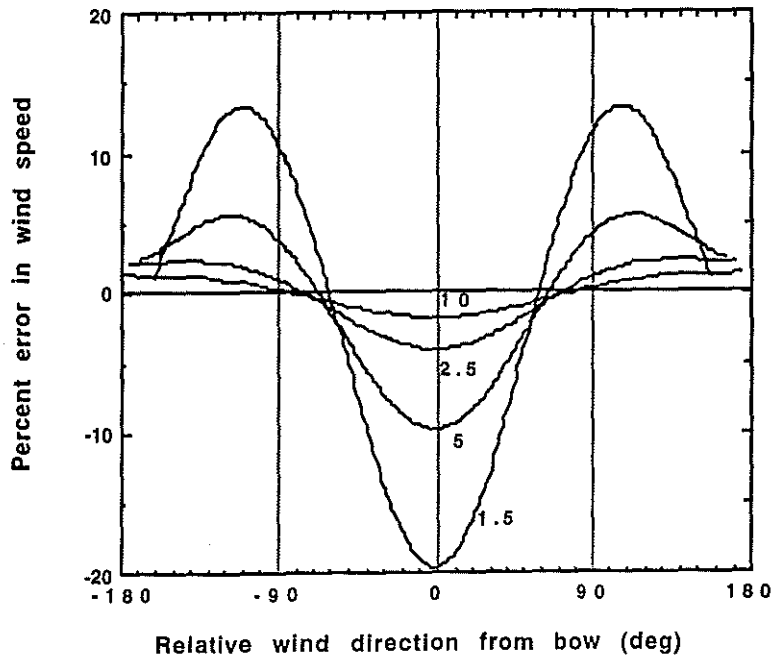

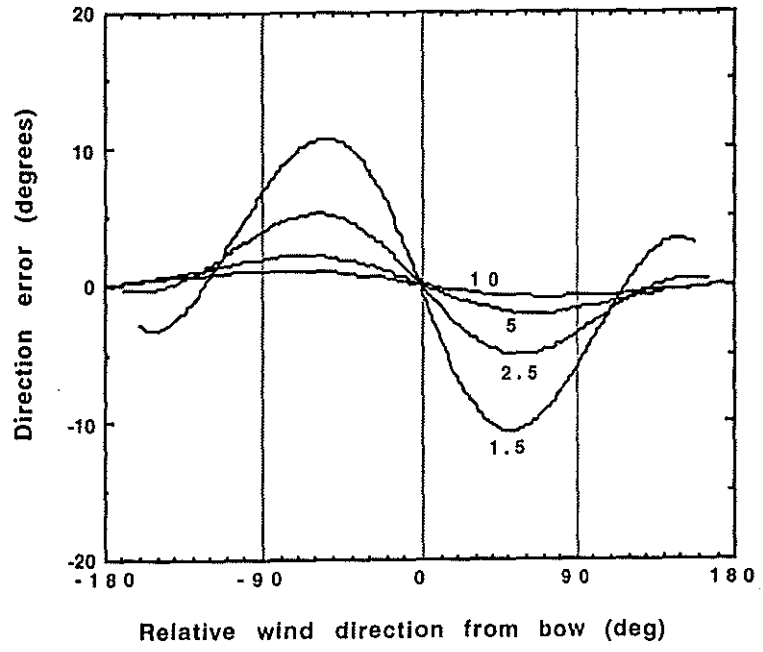

Figure 17. Errors in (a) wind speed (%) and (b) wind direction (degrees) at a positions 1.5, 2.5, 5, and 10 mast diameters away from a circular mast, calculated using the model of Wucknitz, (1977)

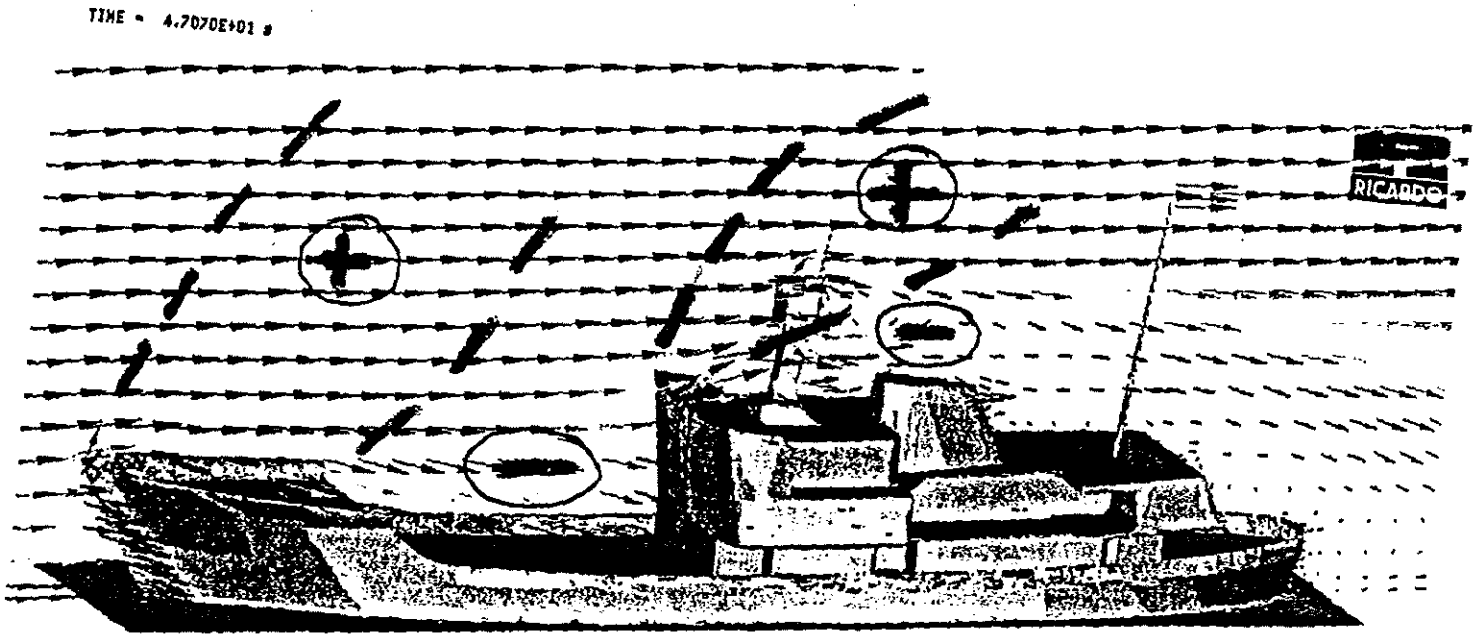

Figure 18 Flow over the CSS Dawson determined by CFD modelling (Ricardo, 1994). Regions of positive and negative wind speed error are marked.